Light-controlled micron-scale molecular motion

By

Mario Samperi,[1,2,§] Bilel Bdiri,[2] Charlotte D. Sleet,[2] Robert Markus,[3] Ajith R. Mallia,[2] Lluïsa Pérez-García[1,4,5] & David B. Amabilino*[2]

1 School of Pharmacy, University of Nottingham, University Park, NG7 2RD, United Kingdom.

2 School of Chemistry, GSK Carbon Neutral Laboratories for Sustainable Chemistry, University of Nottingham, Triumph Road, NG7 2TU, United Kingdom.

3 SLIM Imaging Unit, School of Life Sciences, University of Nottingham. NG7 2RD, United Kingdom

4 Departament de Farmacologia, Toxicologia i Química Terapèutica, Universitat de Barcelona, Av. Joan XXIII, 27-31, 08028 Barcelona, Spain

5 Institut de Nanociència i Nanotecnologia IN2UB, Universitat de Barcelona, 08028 Barcelona, Spain

§ Present address: CNR-ITAE, Via Salita Santa Lucia Sopra Contesse 5, 98126 Messina, Italy

ORCID accounts: Mario Samperi 0000-0003-4362-2574 Robert Markus 0000-0003-4535-303x Lluïsa Pérez-García 0000-0003-2031-4405 David B. Amabilino 0000-0003-1674-8462

*Correspondence to: david.amabilino@nottingham.ac.uk

Abstract

The micron-scale movement of biomolecules along supramolecular pathways – mastered by nature – is a remarkable system requiring strong yet reversible interactions between components under action of a suitable stimulus. Responsive microscopic systems using a variety of stimuli have demonstrated impressive relative molecular motion. However, locating the position of a movable object that travels along self-assembled fibres under an irresistible force has yet to be achieved. Here, we describe a purely supramolecular system where a molecular "traveller" moves along a "path" over several microns when irradiated with visible light. Real time imaging of the motion in the solvated state using total internal reflection fluorescence microscopy shows that anionic porphyrin molecules move along the fibres of a bis-imidazolium gel upon irradiation. Slight solvent changes mean movement and restructuring of the fibres giving microtoroids, indicating control of motion by fibre mechanics with solvent composition. 'The insight provided here may lead to the development of artificial travellers that can perform catalytic and other functions.

Main article text

The controlled movement of molecules along a specific path over distances larger than their scale is mastered biochemically in cells.[1] Totally artificial molecular machines of increasing sophistication and elegance have shown work at nanometres scale.[2-4] These systems can also instigate hierarchical movement in materials at a much larger distance than their own size when provided with a suitable stimulus.[5,6] Regarding translational movement, interface-based Brownian motion of molecules along preferred inorganic axes[7,8] and electrically stimulated directional drive of a single molecule[9] have been shown, and DNA has been used as a building block for nanoscale path and walker-type systems.[10] However, controlled molecular motion along a purely synthetic molecular pathway to emulate natural processes has not been addressed.

In this paper we describe a supramolecular system (Fig. 1) where a fluorescent molecule – a "traveller" – upon irradiation moves along a "path" comprising gemini amphiphiles when a molecular switch is incorporated into the gel material. The supramolecular system makes use of electrostatic interactions between oppositely charged fibrous cationic scaffold – the path – and the two anionic chromophores – the switch and the traveller (Fig. 1). The switch is an essential third component that facilitates movement, with photothermal effects and switching taking place upon excitation to enable the phenomena that occur when irradiated. The path is made of a gemini imidazolium-based amphiphile (**1**·2Br, Fig. 1A) that self-assembles in mixtures of water and ethanol leading to supramolecular gels,[11] and incorporates the 5,10,15,20-tetrakis(4-carboxyphenyl)porphyrin tetra-anion (TCPP).[12] This hybrid gel has TCPP-containing fibres that are robust and not dynamic when irradiated (under identical conditions to those we describe below),[12] because of the electrostatic interaction between the components and high degree of order in the fibres. The system is made responsive by incorporating an azobenzene derivative (4-(phenylazo)benzoate, Azo) that can be photoisomerised between *trans* and *cis* states[13] (Fig. 1A) and *vice-versa*, and in general is part of a family of compounds used to push systems away from equilibrium.[14,15]

Results and Discussion

Multicomponent Gel Preparation and Characterisation

The three-component gel was prepared by mixing an aqueous solution containing the sodium salt TCPP and sufficient excess base to deprotonate Azo with **1**·2Br and Azo in ethanol. The amount of the components in the stock solutions were adjusted to give gels with 5:5 or 7:3 water:ethanol volume ratio and final concentrations of 8 mM **1**·2Br, 60 μM TCPP and 2 mM Azo. The Azo comprised a mixture of *trans* and *cis* isomers at a ratio of 90:10, the photostationary state under ambient lighting. The resulting materials have the morphological characteristics of supramolecular gels (Extended Data Fig. 1, Supplementary Information Fig. S1) and have the viscoelastic properties typical of this kind of soft matter with crossing of storage and loss moduli between 2 and 20% strain (Extended Data Fig.2 and Supplementary Information Table S1).

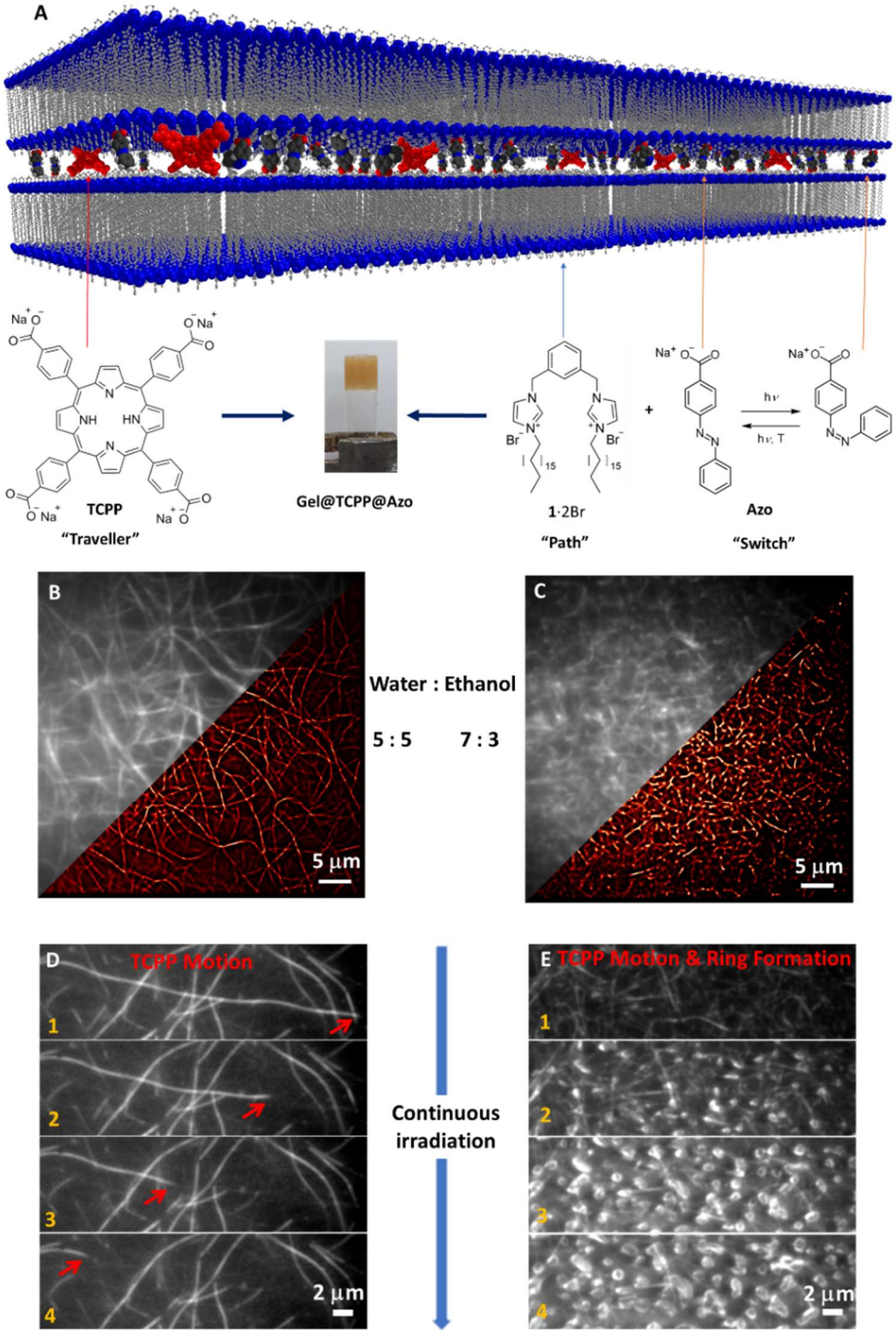

Fig. 1. Gel formation and photoactivated molecular movement. (A) Addition of aqueous solutions of the sodium salt TCPP to ethanolic solutions of **1**·2Br and Azo leads to the formation of supramolecular gels that incorporate TCPP and Azo within the fibrillar network, with a cartoon structure of part of a single fibre shown. TIRF microscopy (B,C) shows the incorporation of the TCPP into the fibres (in greyscale), highlighting the influence of the solvent ratio on the morphology of the network for the two different solvent mixtures, 5:5 (B) and 7:3 (C). The coloured sections of these images show super resolution radial fluctuation (SRRF) data that highlight the differences seen by TIRF. Upon continuous laser irradiation at 405 nm (total irradiation time 8.3 minutes), TIRF images show the result of photoactivated TCPP molecules moving along the gel fibres obtained in water:ethanol 5:5 (D, give times 1,2,3,4, see also Movie S1), whereas using the solvent mixture 7:3, the movement of TCPP induces morphological changes of the network which convert porphyrin-containing fibres into rings (E, give times 1,2,3,4, see also Movie S2). Scale bars on the TIRF micrographs correspond to 5 µm in B and C and 2 µm in D and E.

The location of the TCPP in the solvated gel networks reported here is revealed by total internal reflection fluorescence (TIRF) microscopy,[16] that shows the three-dimensional fibre shape and connectivity of the multicomponent supramolecular gels Gel@TCPP@Azo (Fig. 1B and 1C, respectively). The technique takes advantage of an evanescent field existing at the interface of two materials with different refractive index, in this case the glass slide (at the bottom of the sample) and the gel sample (that is introduced in the liquid state very shortly after mixing). The focal plane is thin and selective to the region close to the interface, avoiding the strong background fluorescence and high laser intensity associated with other high resolution optical microscopy techniques. The gelator molecules are not imaged (**1**.2Br contains no chromophore that absorbs in the region probed using the microscope). There is a significant difference in the apparent morphologies observed by TIRF as a function of the solvent composition (water-ethanol ratio 5:5 and 7:3). The interconnections between fibres in the network also vary (and confirmed by scanning electron microscopy (SEM) of the corresponding xerogels, Supporting Information Fig. S1). Fibres in the 5:5 mixture are more well-defined and straighter than those in the 7:3 mixture. Powder X-ray diffraction shows that the supramolecular structures are similar (Extended Data Fig. 3) and consistent with incorporation of the organic anions between the layers of cationic amphiphile (Fig. 1) as we reported previously for Gel@TCPP,[11] although some of the organic anions may reside on the outer surface of the fibres. The rheological properties of these multicomponent gels also reflect the morphological changes. The 5:5 solvent ratio shows that incorporation of TCPP and/or Azo in the gels gives heightened storage and loss moduli and higher critical stress values (Table S1) compared with pure **1**.2Br. The increased resistance to deformation and rupture compared with the pure gel is less obvious in the gels formed from the 7:3 water:ethanol, which are significantly more robust than the gels made in 5:5 solvent, though. The solvent composition is clearly a determining factor[17] influencing the behaviour of these gels because of the fibre morphology.

Dynamic Effects in Multicomponent Gels

Continued irradiation in the TIRF experiments show very contrasting dynamic effects in the Gel@TCPP@Azo materials made in either 5:5 or 7:3 water:ethanol. For the 5:5 solvent mixture, prolonged irradiation at 405 nm (but also at different wavelengths, *vide infra*) results in movement of the TCPP molecules along the fibres (Fig. 1D, and even more evident in Movie S1). This movement is witnessed by a clear fluorescence reduction in some of the fibres, with the most intensely fluorescent parts of these objects moving to the area outside of the frame. To prove this effect (Fig. 2), a selected area of a sample was irradiated continuously for 8.3 minutes (Fig. 2C, see also video of the irradiation, Movie S3), and a larger area was measured before and after light exposure. Comparison of the TIRF micrographs reveals that the fluorescence intensity of the fibres exposed to the light becomes very significantly decreased (Fig. 2B). This effect was confirmed by measuring the relative fluorescence intensity of background, irradiated fibres, and fibres outside the irradiated region (50 of each, see Supplementary Information Fig. S2). The magnified TIRF images in Figs. 2D and 2E show a closer view of a fibre that partially crossed the irradiated zone and ran into the area that was left in the dark. The fluorescence signal along this fibre has clearly changed after

irradiation, with a significant increase in intensity in the part of the fibre that is farther from the centre (Fig. 2F) and confirming the movement of TCPP molecules along the path.

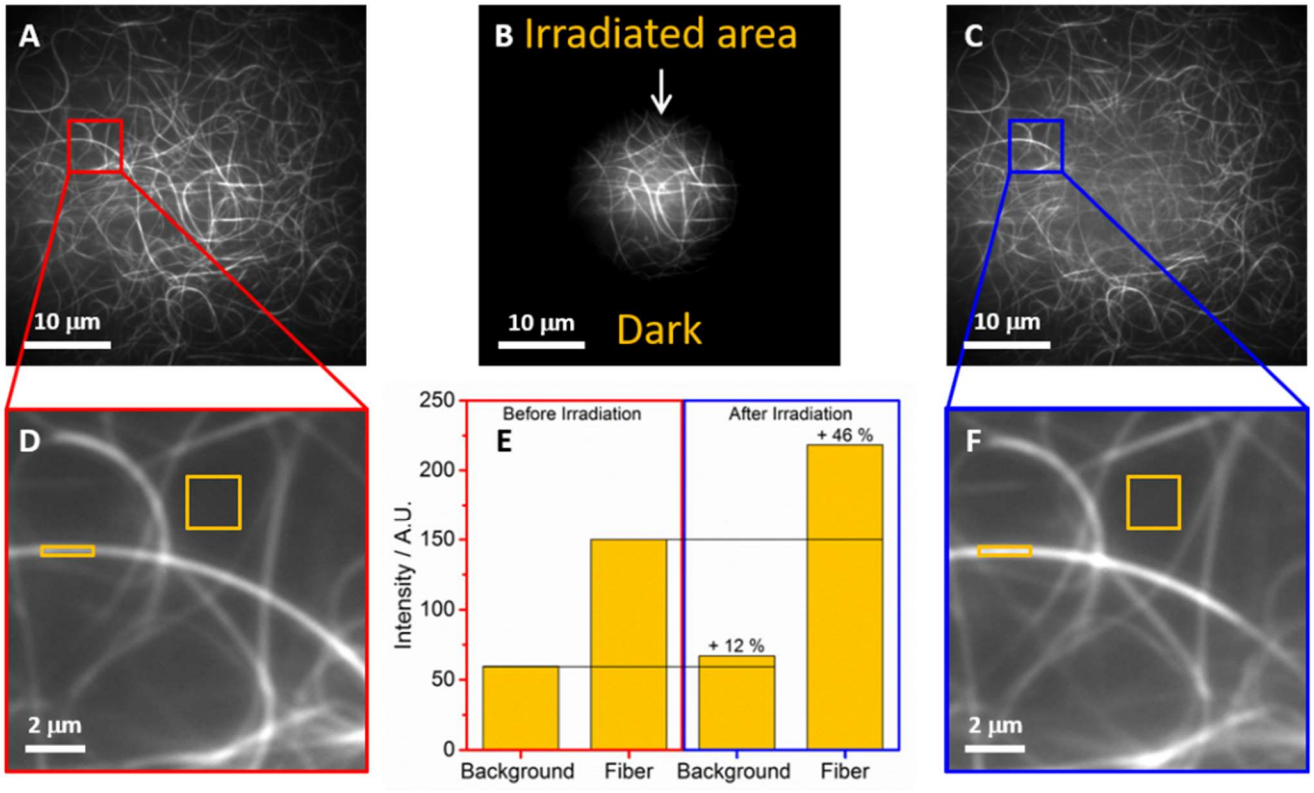

Fig. 2. TIRF images of Gel@TCPP@Azo in water:ethanol 5:5 before (A) and after (C) irradiation at 405 nm (for a total of 8.3 minutes) performed only in the central area of the sample, leaving the outer part in the dark (B). Magnifications of a specific area of the sample (indicated by red and blue squares) showing the difference in fluorescence along the fibre before (D) and after (F) irradiation. (E) Evaluation of the total intensity of the fluorescence signal in the two areas indicated in yellow, clearly shows a significant increment of fluorescence intensity on the fibre (+46%) and a minor increase in the background.

The movement of TCPP travellers along fibre paths (Fig. 3A) can be monitored using the relative fluorescence intensity in the TIRF experiment over time (Fig. 3B). The intensity at any given point on a fibre that displays traveller motion can decrease, or increase and then decrease rapidly, an effect that is consistent with movement along the supramolecular path, and the changes observed are consistent with stochastic movement, whose direction varies for different fibres. The accumulation of porphyrin in the fibres outside the irradiated region is shown in the intensity difference plot in Fig. 3C, that shows a clear decrease of porphyrin in the irradiated region and an increase in the area adjacent to it. In the dark, the TCPP does not move significantly (Fig S3). Attempts to irradiate the enriched TCPP region and induce motion back to the depleted region have so far been unsuccessful (Fig. S4). It is possible for the TCPP to leave the focal plane of the measurement, that is very close to the bottom of the sample well in the slide used for the experiments. Those molecules that move into the bulk of the sample in this way cannot be imaged readily using this technique (although they can be detected in the difference maps in Extended Fig. 5). The stochastic nature of the measurement and the inherent inhomogeneities in the material mean that a number

of behaviours are observed, but the movement out of the irradiated area is the single main dynamic effect we observe.

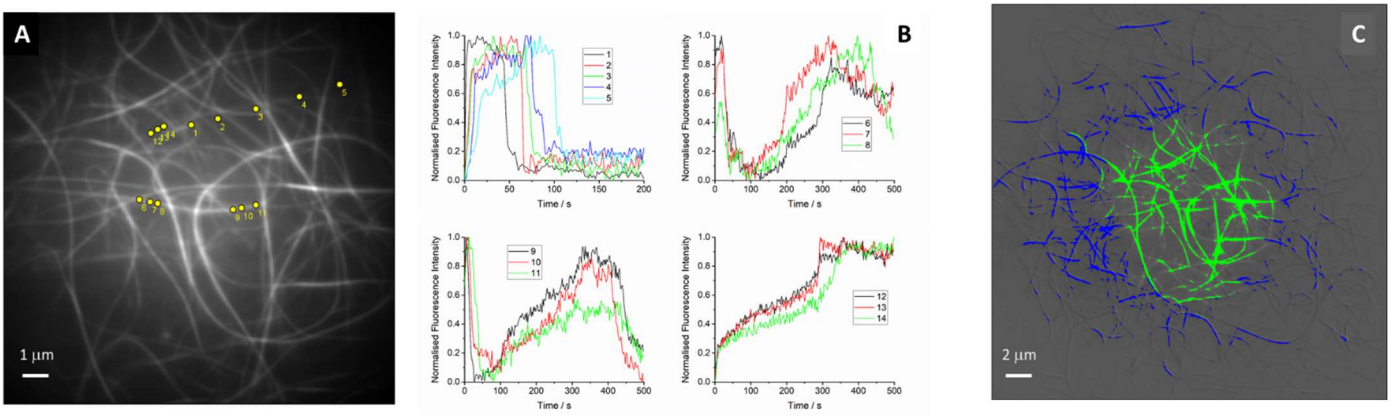

Fig. 3. Evidence for traveller movement. TIRF image A of Gel@TCPP@Azo in water:ethanol 5:5 shows the region irradiated at 405 nm (for a total of 8.3 minutes) also shown in Fig.2. Dots mark points on fibres whose intensity over time was monitored and is plotted in the graphs shown in B, where it can be seen that the intensity increases and decreases for areas 2-5, 6-8 and 9-11, which plots the direction of travel of TCPP. Image C is a start-minus-end subtraction with threshold selection (2.3% above and below the total signal) highlighting the increase of fluorescence outside (highest intensity gain values in blue) and decrease inside the irradiated area (highest intensity loss values in green).

The material formed in the same solvent mixture without Azo, Gel@TCPP,[12] does not show this dynamic behaviour. When Gel@TCPP is irradiated under identical TIRF conditions to the Azo-containing gel there is a quenching of fluorescence (see Movies S10 and S11), but no significant change in the location of the porphyrin or the fibre morphology, regardless of the solvent compositions (over the same range used for the dynamic experiments described above). These observations show that the presence of Azo causes the apparent dynamic effects upon irradiation. In addition, to explore the effect of possible release of the TCPP from the fibres, we prepared a gel where no additional base was added to deprotonate AzoH, meaning that an equilibrium between protonated TCPP and Azo exists. A TIRF experiment on this sample (Movie S12) shows rapid dynamics but also a pronounced "fogging" of the image over time (Fig. S5), indicative of destruction of the gel fibres and release of TCPP that had diffused across the whole area being imaged. The expulsion of the porphyrin is presumably a result of the weakened interactions between the traveller and the path, and confirms the importance of electrostatic forces between path and traveller in order for the porphyrin to remain on the supramolecular fibres.

Fibre and Traveller Imaging

In the Gel@TCPP@Azo, the porphyrin remains in many of the fibres that are relatively unaffected by the irradiation, and the intrinsic heterogeneity of the sample (the concentration of TCPP, Azo and bromide counter-ions and the thickness of the fibres varies) surely contributes to determining whether the porphyrin moves upon irradiation. To confirm that the path remains after TCPP travel, we prepared an analogue of **1**.2Br (see SI for details) containing a fluorophore that could be imaged at a different wavelength to TCPP.

Compound **2**.2Br (Fig. 4A) was used (at 1% in moles compared with the main gelator) to prepare the four-component composite gel Gel@**2**@TCPP@Azo in 5:5 water:ethanol. The overlaid image from TIRF micrographs (Fig. S6) and SRRF analysis recorded at different wavelengths prove the incorporation of both **2**.2Br and TCPP into the fibres of **1**.2Br (Fig. 4). Irradiation of this sample again causes the TCPP to travel along the fibres, as shown by the decrease in TCPP fluorescence intensity in the centre of the image in Fig. 4E, as seen more clearly in the difference map. (Fig. 4G-H)

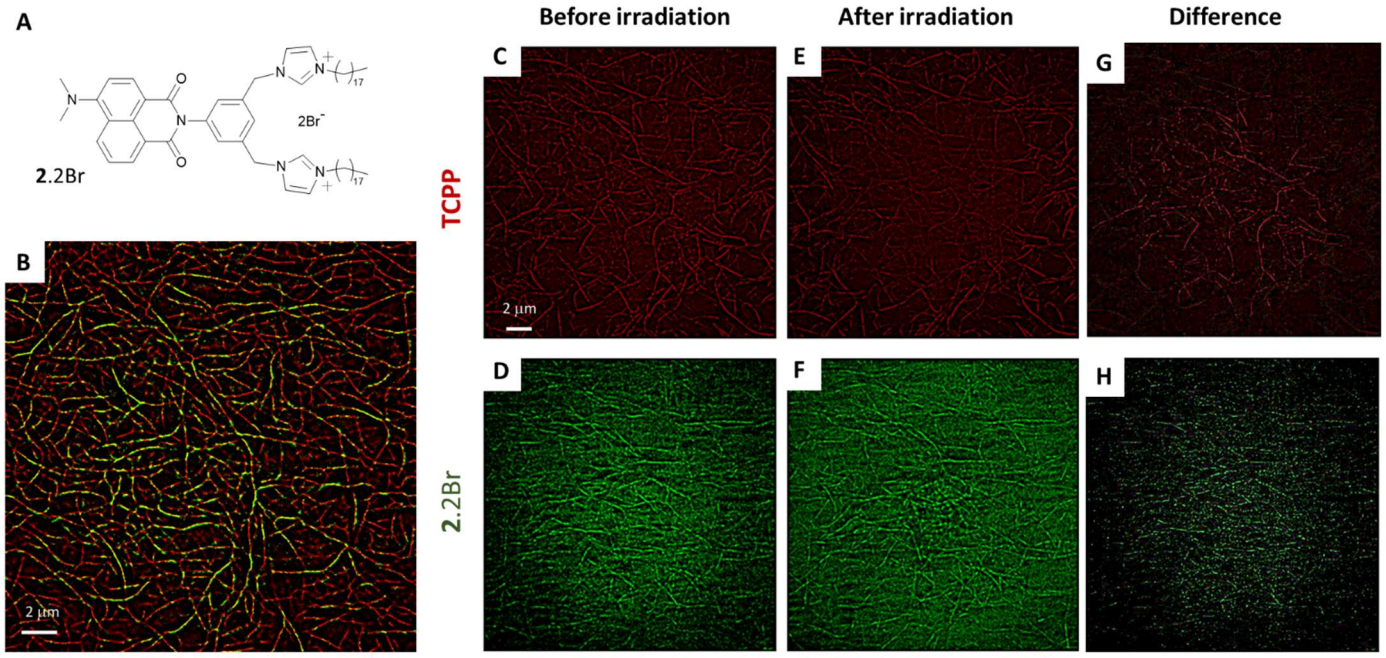

Fig. 4. Imaging path and traveller. A shows the chemical structure of the fluorescent co-gelator **2**.2Br used to trace the gel fibres, and B the superposed SRRF images of Gel@2@TCPP@Azo in water:ethanol 5:5 with emission coloured red showing the location of TCPP and green where **2**.2Br is situated. Images C and D show the separate channels corresponding to TCPP and **2**.2Br, respectively, and E and F the same regions after irradiation at 405 nm for a total of 8.3 minutes performed only in the central area of the sample, leaving the outer part in the dark. In image E, the central region is clearly darker than image C, while image F shows essentially no change in overall fluorescence when compared with image D. The change in TCPP content is shown in the difference map between C and E presented in image G. Some of the gelator fibres in F are clearly shorter than the original state (D), changes that can be seen by the bright patches in the difference image in H. Imaging details: laser 405 nm, emission filter LP 650 for TCPP, and BP 495-550 for **2**.2Br.

Multicomponent Gel Fibre Reorganisation

In the gel made in 7:3 water:ethanol (Fig. 1), irradiation in the TIRF experiments also leads to movement of TCPP, but now the fibres containing the porphyrin are transformed into circular shapes. Closer inspection of the series of TIRF images (Fig. 5 A-E taken from the continuous sequence in Movie S2) shows that the TCPP molecules are clearly redistributed into toroidal-shaped objects. The TCPP is no longer distributed evenly in linear fibres but are confined to micrometre scale rings. It is apparent that these rings are formed by breakage and bending of the fibres which rearrange within the network, generating new interconnections between adjacent strands and finally evolving into circular ribbons.[18,19] Upon continued irradiation, the

dynamics of the system do not arrest completely once the rings have formed, but continue, altering the morphology of these circular ribbons which become larger and merge together to form bigger rings with relatively different shape as observed in the TIRF images.

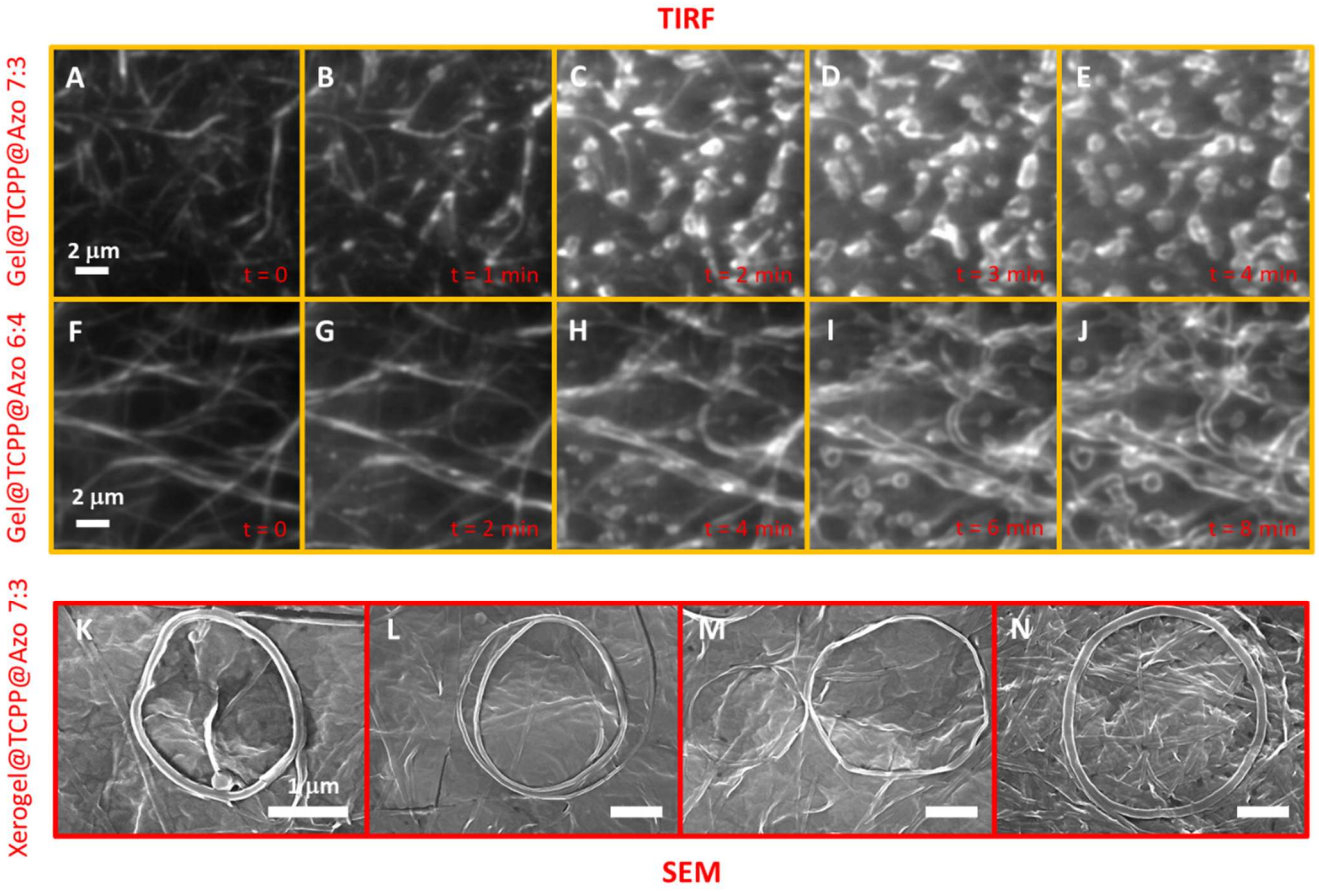

Fig. 5. Light-induced toroid formation. Consecutive TIRF images of Gel@TCPP@Azo in water:ethanol 7:3 at 1 minute intervals of irradiation at 405 nm in the microscope (A-E) showing the conversion of fibres into rings, and the equivalent experiment with the same gel component composition in water:ethanol 6:4 (F-J) with images taken 2 minutes apart showing the formation of rings and reorganization of the fibres (images extracted from Movies S2 and S4, respectively). The SEM micrographs show rings formed after irradiation with a xenon lamp of a solar simulator of the hydrated Gel@TCPP@Azo 7:3 on the SEM stub (K- N, see experimental section for preparative details). Scale bars in TIRF images represent 2 µm and in SEM micrographs 1 µm.

The morphological reorganisation of the fibres to rings allowed observation of the effect with a more general light source and over a wider area: Irradiation of the bulk gel using a xenon lamp of a solar simulator gave a xerogel with several rings of slightly different form and size and, more importantly, highlights their multi-strand morphology (Fig. 5 K-N). The rings are never completely isolated from the rest of the fibres, but rather are linked with the gel network by a fibre strand that extends outside the ring, an observation that is in line with what observed in the hydrated gel by TIRF imaging and SRRF analysis (Movie S9 and Extended data Fig. 6). The diameter of the rings in this bulk experiment is slightly bigger than in the TIRF conditions, that is likely caused by the different nature light source.

An intermediate solvent ratio between the cases that show linear motion of TCPP and fibre rearrangement leads to an intermediate morphological outcome: Rings as well as separated tapes are formed when irradiating the gel with a 6:4 water:ethanol ratio (Fig. 5 F-J and Movie S4). This observation indicates that the structural mechanism of rearrangement in the samples with greater proportion of water (the 6:4 and 7:3) involves the relatively thin fibres splitting and subsequently bending and rearranging to form rings (Figs. S7 and S8). It is clear here that the TCPP anions are concentrated in the rings compared with the uncoiled fibres and the Azo anions could be exchanged out during toroid formation (through isomerisation[20]) in an analogous way to that seen upon drug release resulting stress in the gelator lamellae caused by non-uniform distribution of anions.[21] We have confirmed that the isomerisation is important in this process using biphenyl-4-carboxylic acid in place of Azo (see below).

Origins of Molecular Motion in the Multicomponent Gels

The presence of the Azo is essential to efficient molecular movement, so that the photoisomerization between *trans* (more stable) and *cis* (less stable) isomers is responsible. Irradiation of Azo with UV light (at 365 nm) promotes the *trans*→*cis* conversion, and heat and/or visible light ($\lambda > 400$ nm) move the distribution to the *trans* form.[22] However, an equilibrium exists, and the n→π* transition of both the *cis* and *trans* isomers absorbs at 405 nm where the TIRF irradiation is used, and it is known that the photoisomerization quantum yields for azobenzene at slightly higher wavelength are both appreciable (with the *cis*→*trans* being favoured and having the higher extinction coefficient).[23] Therefore, theoretically, isomerisation in both directions can take place under irradiation in the microscopy experiments. UV-Vis absorption spectroscopy shows that the photostationary state of Azo at equilibrium (at room temperature and under daylight exposure, the experimental conditions used for gel formation) comprises a *trans*:*cis* isomer ratio of 90:10 (Extended data Fig. 4). In solution, irradiation at 365 nm shifts the equilibrium to the *cis* isomer. Similar effects are seen in the gel and in presence of TCPP (Extended data Fig. 4.), showing that the photoisomerization does occur in the gel state.

Therefore, the porphyrin motion observed is facilitated by Azo's isomerisation under irradiation at 405 nm, which can produce local deformations within the fibre's structure allowing TCPP to diffuse along the gelator path. The wavelength dependence in the TIRF experiments supports this hypothesis: TIRF using light at 405, 488, 561 and 642 nm show that while the movement of TCPP molecules along the fibres occurs with all wavelengths studied, light at 405 nm is clearly the most effective in promoting the movement of TCPP (Extended data Fig. 5 and Movies S5-8). This effect appears to arise from an overlap of the 405 nm light with the Azo absorption band in that region, as all three other light wavelengths do coincide with absorption bands of the porphyrin and not with Azo. Ex situ experiments on samples with and without TCPP prove this point (Tables S2 and S3, Figs. S9-S12), where light at 561 and 642 nm does not perturb the photostationary state of Azo (both alone in solution and in presence of TCPP). However, when a xenon lamp of solar simulator was used, and only in the presence of TCPP, the equilibrium of azobenzene moves towards the *trans* isomer, from the initial *trans*:*cis* ratio of 90:10 to a 98:2 distribution indicating a mechanism of

favouring the *trans* form. The variable wavelength studies (Extended data Fig. 5 and Movies S5-8) also show that the TCPP is essentially static on the length and time-scales of the experiment (several minutes) unless the system is excited with light of appropriate energy.

If the *cis*-*trans* reversible isomerisation is important for traveller motion, we reasoned that enriching the Azo sample with the metastable cis isomer would enhance motion, and that is exactly what happens. Irradiating the ethanolic stock solution of Azo at 365 nm prior to mixing of components gave a 35:65 *trans*:*cis* ratio that was used to form the Gel@TCPP@Azo in 5:5 water:ethanol. The TIRF experiment on this material (Movie S13) showed extremely fast dynamics. Stills from the experiment (Extended data Fig. 8) show that the fibres apparently disappear, and, unlike the experiment with the 90:10 isomer ratio, no bright streaks are seen. The experiment confirms the importance of the *cis*→*trans* isomerisation in the dynamics of these gel systems.

Analysis of the rate of loss of fluorescence in the areas occupied by the fibres incorporating TCPP gives an idea of the dynamics taking place in the gel systems. The fluorescence intensity in the TIRF measurements of fibres in Gel@TCPP, Gel@TCPP@Azo (*trans*:*cis* 90:10) and Gel@TCPP@Azo (*trans*:*cis* 35:65) was monitored over time and the intensity loss fitted to an exponential decay function to provide an approximate rate (see Supplementary information Figures S13-S17, Table S5). In the case of Gel@TCPP this effect arises from bleaching, the other samples have porphyrin movement. The data show that while Gel@TCPP@Azo (*trans*:*cis* 90:10) has on average three times faster fluorescence loss compared with Gel@TCPP, the sample containing the enriched *cis* isomer of Azo has dynamics that are an order of magnitude faster, and confirm the acceleration by this form of the switch that is responsible for the molecular movement seen in the TIRF experiments.

These findings suggest that photoisomerization of the *cis*-Azo accompanied by a local photothermal effect could give rise to the motion. The heating of the samples under irradiation has been measured when the gels are irradiated with white light, where the gels incorporating all components show the largest effect at the macroscopic level (Table S4, Figs. S18). Therefore, the photothermal effect surely contributes to the motion of the porphyrin, and that heat arises from absorption by the TCPP as well as by Azo. The photothermal effect is important in deformation of soft materials of different kinds,[24,25] and in the case we describe here contributes to the formation of the rings but in the first instance clearly gives rise to molecular motion of the TCPP along the gelator fibres.

Combining TCPP and Azo in the gel leads to energy transfer from the porphyrin to the switch, as shown by steady state fluorescence spectroscopy of the gels (see Extended data Fig. 7). Azobenzenes are known to accept energy from triplet energy donors.[23] The fluorescence spectra of the gels show a higher emission from Gel@TCPP than Gel@TCPP@Azo in either 5:5 or 7:3 water:ethanol mixtures, although the situation is modulated under continued irradiation. As the Gel@TCPP@Azo materials are irradiated at 405 nm, the fluorescence intensity of the 5:5 sample decreases steadily. In contrast, the fluorescence of the TCPP in the sample in 7:3 water:ethanol increases after irradiation, eventually reaching the same fluorescence as the

Gel@TCPP sample in the same solvent under the same conditions. This observation, in accord with the TIRF measurements where the sample appears brighter after toroid formation, indicates that the Azo is expelled from the fibres (and are therefore no longer able to quench TCPP fluorescence) upon rearrangement of the fibres. It corresponds to a light activated release of a component that leads to fibre ring formation similar to spontaneous release of other guests in the gel.[20]

In principle, the heat released from TCPP could be enough for movement to occur by breaking electrostatic interactions between the porphyrin and the gelator, and when the organisation of the gel is different to that of Gel@TCPP (where no significant motion is seen). To explore if a purely structural effect could be responsible, using biphenyl-4-carboxylic acid (Biph) instead of the azobenzene we made a new gel composite and studied the material with TIRF. We replaced directly Azo for Biph in the preparation of the composite gel made in 7:3 water:ethanol. The TIRF experiments of this sample – carried out under the same conditions as Gel@TCPP@Azo - show a slow rearrangement to toroids (see Supplementary Information Movie S14 and Figure S19). Therefore, the Biph counterion apparently generates enough space to allow partial movement when the TCPP is irradiated and the transferred thermal energy induces motion.

Conclusions

We have established that the minimalist, yet structurally and phenomenologically very complicated, systems reported here have five key aspects that are central to their behaviour upon light absorption and mechanism of action; (i) strong electrostatic interactions that keep the traveller on the path; (ii) the isomerisation of the switch that facilitates traveller movement; (iii) heat release from the traveller and switch after irradiation that provides the energy to promote motion; (iv) energy transfer from the porphyrin to the switch, (v) structural features of the gel – fibre dimensions and mechanical characteristics – that determine whether micron scale travel or toroid formation occur.

A mechanism consistent with our observations involves light absorption by switch and traveller, release of heat upon relaxation and isomerisation, giving energy to the traveller to disrupt the local electrostatic interactions and structural disturbance of the path that allow the traveller to move.

The controlled movement of TCPP along the path of a gelator where Azo isomerizes and gives photothermal effects facilitating the functioning of the system apparently contrasts with other systems showing disassembly upon isomerisation.[26] The reorganization of the fibres in certain solvent conditions is facilitated here as a result of similar effects, where the movement of the traveller is accompanied by path change. The possibilities of changing the supramolecular fibre nature through controlled mixing in these systems[11,27] and others opens a myriad of possibilities to modulate the dynamic nature of the systems.

The large difference in behaviour observed in the dynamic response of the composite gels results from the morphology of the fibres. The thicker fibres in 5:5 water:ethanol allow movement over several microns and the gel superstructure remains intact on the whole. The 7:3 mixture contains much narrower fibres, that clearly rearrange in all likelihood because of splintering of layers of gelator accompanied by porphyrin that

then curve and form the circular objects. These phenomena correspond to weaker and stronger gels, respectively (as indicated by rheological experiments), where the property is a result of the whole network of interconnected fibres rather than individual gelator superstructures. The Gel@TCPP@Azo gel in 5:5 water:ethanol shows movement away from an irradiated area, that motion is not reversible in our hands for now (Fig. S4); we believe that a back-and-forth motion along the fibres will require significant path redesign. The high-resolution optical microscopes permit remarkable insight into supramolecular composition in soft materials in solvents,[28] and lend themselves to light-induced molecular translation.[29] This kind of system is therefore interesting for the study of synthetic supramolecular machines,[30] that may lead to the movement of complementary travellers that can perform catalytic or other functions.[31,32]

Acknowledgements. All the authors thank the School of Life Sciences Imaging (SLIM) in Nottingham for access to the optical microscope, and the Nanoscale and Microscale Research Centre (nmRC) for facilitating access to electron microscopes. DBA thanks the Telluride Conference on Molecular Rotors, Motors, and Switches for inspiring this research. We warmly thank Mònica Amabilino i Pérez for assistance with graphics (DBA). ARM acknowledges funding from European Union's Horizon 2020 research and innovation program under the Marie- Skłodowska -Curie grant agreement No:793424. The microscope facility was established using BB/L013827/1 fund. This work was supported by the Engineering and Physical Sciences Research Council (EPSRC) [under grants EP/M005178/1 and EP/N024818/1] (DBA), EU ERDF (FEDER) funds and the Spanish Government grant TEC2017-85059-C3-2-R (LPG), and the University of Nottingham (BB, MS) including work under the Propulsion Futures Beacon of Excellence (DBA).

Author contributions Author contributions are defined based on the CRediT (Contributor Roles Taxonomy) and listed alphabetically. Conceptualization: D.B.A. and L.P-G. Data curation: M.S. Formal analysis: M.S., D.B.A. and L.P-G. Funding acquisition: D.B.A. and L.P-G. Investigation: M.S., B.B., A.R.M., R.M. and C.D.S. Methodology: D.B.A., M.S., R.M. and L.P-G. Project administration: D.B.A. and L.P-G. Supervision: D.B.A. and L.P-G. Validation: D.B.A. and L.P-G. Writing original draft: M.S., D.B.A. and L.P-G. Writing review and editing: M.S., L.P-G and D.B.A.

Competing interests. The authors declare no competing interests.

References

1. Sasaki, K., Kaya, M. & Higuchi, H. A unified walking model for dimeric motor proteins. *Biophys. J.* **115**, 1981-1992 (2018).

2. Kassem, S., van Leeuwen, T., Lubbe, A.S., Wilson, M.R., Feringa, B.L. & Leigh, D.A. Artificial molecular motors. *Chem. Soc. Rev.* **46**, 2592-2621 (2017).

3. Baroncini, M., Silvi, S. & Credi, A. Photo- and redox-driven artificial molecular motors. *Chem. Rev.* **120**, 200-268 (2020).

4. Pezzato, C., Cheng, C., Stoddart, J. F. & Astumian, R. D. Mastering the non-equilibrium assembly and operation of molecular machines. *Chem. Soc. Rev.* **46**, 5491–5507 (2017).

5. García-López, V., Chen, F., Nilewski, L.G., Duret, G., Aliyan, A., Kolomeisky, A.B., Robinson, J.T., Wang, G., Pal, R. & Tour, J.M. Molecular machines open cell membranes. *Nature* 548, 567–572 (2017)

6. Dattler, D., Fuks, G., Heiser, J., Moulin, E., Perrot, A., Yao, X. & Giuseppone, N. Design of collective motions from synthetic molecular switches, rotors, and motors. *Chem. Rev.* **120**, 310–433 (2020).

7. Haq, S., Wit, B., Sang, H., Floris, A., Wang, Y., Wang, J., Pérez-García, L., Kantorovitch, L., Amabilino, D.B. & Raval, R. A small molecule walks along a surface between porphyrin fences that are assembled in situ. *Angew. Chem. Int. Ed.* **54**, 7101-7105 (2015).

8. Abbasi-Pérez, D., Sang, H., Pérez-García, L., Floris, A., Amabilino, D.B., Raval, R., Recio, J.M. & Kantorovich, L. Controlling the preferential motion of chiral molecular walkers on a surface. *Chem. Sci.* **10**, 5864-5874 (2019).

9. Kudernac, T., Ruangsupapichat, N., Parschau, M., Maciá, B., Katsonis, N., Harutyunyan, S. R., Ernst, K.-H. & Feringa, B. L. Electrically driven directional motion of a four-wheeled molecule on a metal surface. *Nature* **479**, 208–211 (2011).

10. Xing, Y., Liu, B., Chao, J. & Wang L. DNA-based nanoscale walking devices and their applications. *RSC Adv.* **7**, 47425–47434 (2017).

11. Samperi, M., Pérez-García, L. & D.B. Amabilino, Quantification of energy of activation to supramolecular nanofibre formation reveals enthalpic and entropic effects and morphological consequence. *Chem. Sci.* **10**, 10256-10266 (2019).

12. Samperi, M., Limón, D., Amabilino, D.B. & Pérez-García, L. Enhancing singlet oxygen generation by self-assembly of a porphyrin entrapped in supramolecular fibres. *Cell Rep. Phys. Sci.* **1**, 100030 (2020).

13. Bandara H.M.D. & Burdette, S.C. Photoisomerization in different classes of azobenzene. *Chem. Soc. Rev.* **41**, 1809–1825 (2012).

14. Kathan, M. & Hecht, S. Photoswitchable molecules as key ingredients to drive systems away from the global thermodynamic minimum. *Chem. Soc. Rev.* **46**, 5536-5550 (2017).

15. Tecilla, P. & Bonifazi, D. Configurational Selection in Azobenzene-Based Supramolecular Systems Through Dual-Stimuli Processes. *Chemistry Open* 9, 538-553 (2020).

16. Mattheyses, A.L., Simon, S.M. & Rappoport, J.Z. Imaging with total internal reflection fluorescence microscopy for the cell biologist. *J. Cell Sci.* **123**, 3621-3628 (2010).

17. Canevet, D., del Pino, A.P.; Amabilino, D.B. and Salle, M. Varied nanostructures from a single multifunctional molecular material. *J. Mater. Chem.* **21**, 1428-1437 (2011).

18. Kim, Y., Li, W. Shin, S. & Lee, M. Development of Toroidal Nanostructures by Self-Assembly: Rational Designs and Applications. *Acc. Chem. Res.* **46**, 2888–2897 (2013).

19. Datta, S., Kato, Y., Higashiharaguchi, S., Aratsu, K., Isobe, A., Saito, T., Prabhu, D.D., Kitamoto, Y., Hollamby, M.J., Smith, A.J., Dagleish, R., Mahmoudi, N., Pesce, L., Perego, C., Pavan, G.M. & Yagai S. Self-assembled poly-catenanes from supramolecular toroidal building blocks. *Nature* **583**, 400–405 (2020).

20. Carl, N., Müller, W., Schweins, R. & Huber, K. Controlling self-assembly with light and temperature. *Langmuir* **36**, 223–231 (2020).

21. Limón, D., Jiménez-Newman, C., Calpena, A. C., González-Campo, A., Amabilino, D.B. & Pérez-García, L. Microscale coiling in bis-imidazolium supramolecular hydrogel fibres induced by the release of a cationic serine protease inhibitor. *Chem. Commun.* **3**, 4509-4512 (2017).

22. Cao, H., Jiang, J., Zhu, X., Duan, P. & Liu, M. Hierarchical co-assembly of chiral lipid nanotubes with an azobenzene derivative: optical and chiroptical switching. *Soft Matter* 7, 4654–4660 (2011).

23. Bortolus P. & Monti S. Cis-trans photoisomerization of azobenzene. Solvent and triplet donors effects. *J. Phys. Chem.* **83**, 648–652 (1979)

24. Nath, N.K., Panda, M.K., Sahoo, S.C. & Naumov, P. Thermally induced and photoinduced mechanical effects in molecular single crystals—a revival. *CrystEngComm* **16**, 1850–1858 (2014).

25. Pilz da Cunha, M., van Thoor, E.A.J., Debije, M.G., Broer, D.J. & Schenning, A.P.H.J. Unravelling the photothermal and photomechanical contributions to actuation of azobenzene-doped liquid crystal polymers in air and water. *J. Mater. Chem. C* **7**, 13502—13509 (2019).

26. Fredy, J.W., Méndez-Ardoya, A., Kwangmettatama, S., Bochicchioc, D., Matt, B., Stuart, M.C.A., Huskens, J., Katsonis, N., Pavanc, G.M. & Kudernac, T. Molecular photoswitches mediating the strain-driven disassembly of supramolecular tubules, *PNAS* **114**, 11850–11855 (2017).

27. G. Sathyanarayanan, M. Rodrigues, D. Limón, R. Rodriguez-Trujillo, J. Puigmartí-Luis, L. Pérez-García and D.B. Amabilino, Drug-Loaded Supramolecular Gels Prepared in a Microfluidic Platform: Distinctive Rheology and Delivery through Controlled Far-from-Equilibrium Mixing. *ACS Omega* **2**, 8849–8858 (2017).

28. Kubota, R., Nakamura, K., Torigoe, S. & Hamachi, I. The power of confocal laser scanning microscopy in supramolecular chemistry: In situ real-time imaging of stimuli-responsive multicomponent supramolecular hydrogels, *ChemistryOpen* **9**, 67–79 (2020).

29. Kageyama, Y. Light-Powered Self-Sustainable Macroscopic Motion for the Active Locomotion of Materials. *ChemPhotoChem* **3**, 327-336 (2019).

30. Aprahamian, I. The future of molecular machines, *ACS Cent. Sci.* 6, 347−358 (2020).

31. Zheng, L., Zhao, H., Han, Y., Qian, H., Vukovic, L., Mecinović, J., Král, P. & Huck W.T.S. Catalytic transport of molecular cargo using diffusive binding along a polymer track. *Nature Chem.* **11**, 359–366 (2019).

32. Muller-Deku, A., Meiring, J.C.M., Loy, K., Kraus, Y., Heise, C., Bingham, R., Jansen, K.I., Qu, X.Y., Bartolini, F., Kapitein, L.C. Akhmanova, A., Ahlfeld, J., Trauner, D. & Thorn-Seshold, O. Photoswitchable paclitaxel-based microtubule stabilisers allow optical control over the microtubule cytoskeleton, *Nature Communications* **11**, 4640 (2020).

METHODS

Materials and methods

All solvents and reagents employed for synthesis in this work were of analytical grade. Absolute ethanol came from Fisher Scientific (99.8 % HPLC Grade). MilliQ water (Milli-Q plus system from Millipore) was used for all sample preparation. Sodium hydroxide (NaOH) was purchased from Merck (Germany), 4-(phenylazo)benzoic acid and biphenyl-4-carboxylic acid from Sigma-Aldrich. Compound 1,3-bis[(3-octadecyl-1-imidazolio)methyl]benzene dibromide (**1**·2Br) was synthesized as previously reported in literature.[33] 5,10,15,20-Tetrakis(4-carboxyphenyl)porphyrin (TCPP) was synthesized adopting the reported synthetic protocol.[34] The synthesis of the naphthalimide gelator (**2**·2Br) is detailed in the supplementary information.

Gel preparation

Gel samples were always prepared by addition of MilliQ water to an ethanolic solution of **1**·2Br, giving a final amphiphile concentration of 8 mM and the desired water-ethanol ratio (5:5 or 7:3). Generally, samples were made to total volume of 1mL in 3mL vials, sealed after gentle mixing (with a micropipette) and letting them stand undisturbed at room temperature to allow the gel formation. Gels were deemed to have formed when no flow was observed upon vial-inversion test. For TCPP-containing gels, aqueous solutions of the TCPP sodium salt were prepared by dispersing the desired amount of solid TCPP in water followed by the addition of 4 equivalents of sodium hydroxide (from a 0.1 M stock solution). For Azo-containing gels, an ethanolic solution of 4-(phenylazo)benzoic acid (Azo)was premixed with **1**·2Br, and the equimolar equivalent of sodium hydroxide was added in water in order to incorporate the Azo as its sodium salt. The final concentration of TCPP and Azo within the gels was always 60 μM and 2 mM, respectively.

Gel characterization

Fluorescence imaging was performed on a Zeiss Elyra PS1 super resolution microscope equipped with Zen 2012 acquisition and processing software, fitted with an alpha Plan-Apochromat 100×/1.46 Oil DIC M27 Elyra objective lens operating in TIRF (Total internal reflection fluorescence), using either lasers at 405 nm (50 mW), 488 nm (200 mW), 561 nm (200 mW), or 642nm (150 mW), and emission filters LP 650 (for TCPP) and BP 495-550 (for **2**.2Br). A droplet of 30°C oil (Zeiss, Immersol™ 518F/30°) was cast on the objective before imaging. Automatic focusing was always adopted to keep constant the desired focal plane during the acquisition. Image acquisition was performed in two different modalities, named TIRF and SRRF. For TIRF, images were acquired with a pco.edge sCMOS camera using the '16 Avg' option, at 0.05-0.5 laser power for observation and camera exposure time 200 ms. The laser power is 4.3 $mWcm^{-2}$ for the 405 nm laser using a 10x lens 0.3NA. Videos recorded in TIRF were obtained acquiring 2500 frames (zero gap between frames, total acquisition time 8.3 minutes) with camera exposure 200 ms, grouped by 10 with applied averaging intensity to obtain 250 frames, with video conversion at 20 frames per second in the main.

For SRRF mode, images were obtained acquiring 100 image frames using 0.1-0.5 % laser power, recorded with an EM-CCD (Andor EM-CCD camera iXon Du 897) with 200 gain and 25 ms exposure time per frame. Video recorded in SRRF was obtained acquiring 20000 frames (zero gap between frames, total acquisition time 2 minutes) with camera exposure 25 ms, grouped by 100 with applied averaging intensity to obtain 50 frames, with video conversion at 10 frames per second.

Samples were prepared directly into CELLview™ Microscopic Slides with Glass Bottoms by Greiner Bio-One GmbH that have a 10-well compartmentalization block allowing to form the gel in situ and perform the imaging directly without any further sample manipulation. Image processing was carried out with Fiji image analysis software[35] and SRRF analysis was performed using the open-source NanoJ-SRRF software package.[36] Temporal radiality pairwise product mean (TRPPM) was used as algorithm, with ring radius of 0.5, radiality magnification of 10, 6 axes in a ring, intensity weighting and gradient smoothing. Central irradiation experiments were performed using the TIRF/μHP filter in order to reduce the irradiated area of the sample.

Scanning Electron Microscopy (SEM) was performed on a JEOL 7100F FEG-SEM instrument on samples casted on aluminum stubs, dried under vacuum (fast drying achieved within 5-10 seconds after deposition to minimize possible drying effects) and coated with a 5-nm thick layer of Iridium using a Quorum Q150TES sputter coater. Image acquisition was carried out using a working distance of 6 mm and 5 kV accelerating voltage. For the imaging of the rings, the sample were deposited on the stub and irradiated before being dried using a xenon lamp equipped with a long-pass filter at 455 nm, a 10 cm thick water filter to remove the IR portion of the spectrum, at 3 sun (300 mW/cm^2) for 10 minutes. The sample was sealed using blue tag and a glass slide to prevent solvent evaporation during irradiation.

Powder X-Ray diffraction (XRD) patterns were acquired with a PANalytical MPD X-Ray Powder Diffractometer in Bragg–Brentano geometry, using Cu-Kα radiation ($K\alpha_1$ = 1.540560 Å and $K\alpha_2$ = 1.544390 Å) with a voltage and current of 40 kV and 40 mA, respectively. 3 mL of gel were prepared for each sample analyzed, which were dried under reduced pressure to obtain xerogels. The powder was collected and placed on brass sample holder for data acquisition in 2-Theta scale between 2-30°, with a step size of 0.013°.

The rheological characterization was carried out using an Anton Paar MCR 302 rheometer equipped with temperature controller and parallel plate geometry setup (PP50 stainless steel, 50 mm diameter, 1 mm gap between plates). All the measurements were carried out at 298 K. Samples were prepared as 10 mL total volume in 7 cm diameter Petri dishes, sealed to prevent solvent evaporation and kept at room temperature for two days before study. Samples were gently transferred on the rheometer plate without breakage and the extra material was removed to suit the working geometry. Resistance to deformation and resistance to rupture were evaluated performing oscillation amplitude tests at a deformation frequency of 1 Hz.

UV-Vis extinction spectroscopy was performed using a Cary 5000 UV-Vis spectrophotometer (Agilent). Fluorescence spectroscopy was measured using a FLS 980 spectrometer (Edinburgh Instruments) equipped

with a front face sample holder. The measurements were carried out using quart cuvettes having 2- or 10-mm path length.

References

33 Casal-Dujat, L., Rodrigues, M., Yagüe, A., Calpena, A. C., Amabilino, D. B., González-Linares, J., Borràs M. & Pérez-García, L. Gemini imidazolium amphiphiles for the synthesis, stabilization, and drug delivery from gold nanoparticles. *Langmuir* **28**, 2368-2381 (2012).

34 Datta-Gupta N. and Bardos, T.J. Synthetic Porphyrins. I. Synthesis and spectra of some para-substituted meso-tetraphenylporphines. *J. Heterocyc. Chem.* ***3***, 495-502 (1966).

35 Schindelin, J., Arganda-Carreras, I., Frise, E., Kaynig, V., Longair, M., Pietzsch, T., Preibisch, S., Rueden, C., Saalfeld, S., Schmid, B., Tinevez, J.-Y., White, D.J., Hartenstein, V., Eliceiri, K., Tomancak P. & Cardona, A. Fiji: an open-source platform for biological-image analysis, *Nature Methods* **9**, 676-682 (2012).

36 Laine, R.F., Tosheva,, K.L., Gustafsson, N., Gray, R.D.M., Almada, P., Albrecht, D., Risa, G.T., Hurtig, F., Lindås, A.-C., Baum, B., Mercer, J., Leterrier, C., Pereira, P.M., Culley S. & Henriques, R. NanoJ: a high-performance open-source super-resolution microscopy toolbox. *J. Phys. D-Appl. Phys.* ***52***, 163001 (2019).

Data availability

All data supporting the findings are included in the manuscript and Supplementary Information.

Additional information

Correspondence and requests for materials should be addressed to D.B.A.

Extended Data

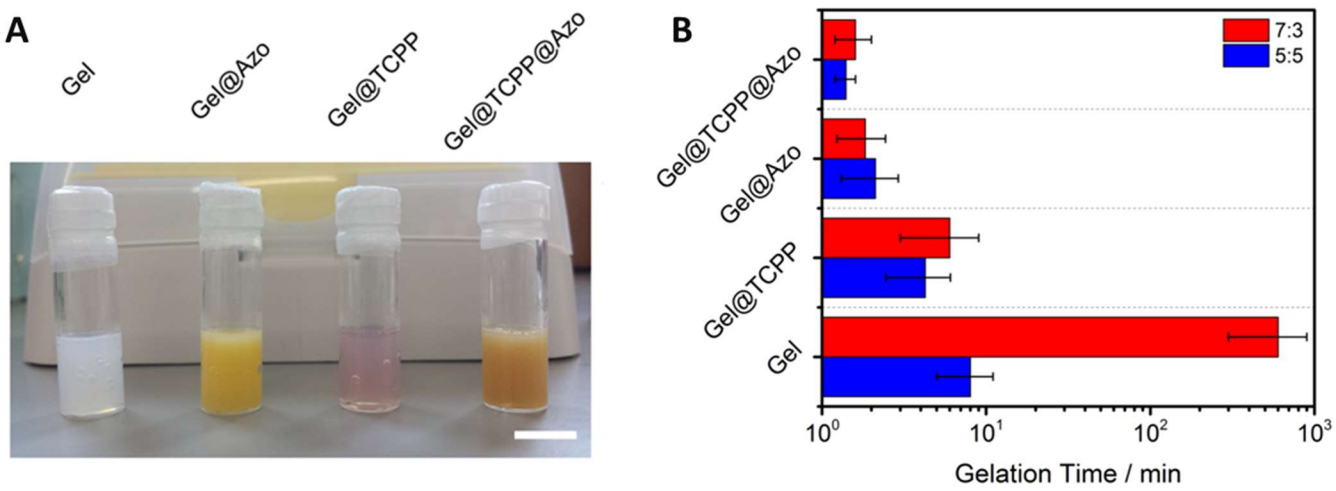

Extended data Fig. 1. Gel formation. (A) A picture of gel samples of **1**·2Br obtained with water:ethanol ratio 5:5 without guest molecules (Gel), with incorporated azobenzene (Gel@Azo), porphyrin (Gel@TCPP) and both (Gel@TCPP@Azo). The scale bar represents 1 cm. (B) Gelation time of the samples at room temperature (approximately 22 °C) obtained with solvent ratio 5:5 (blue bars) and 7:3 (red bars).

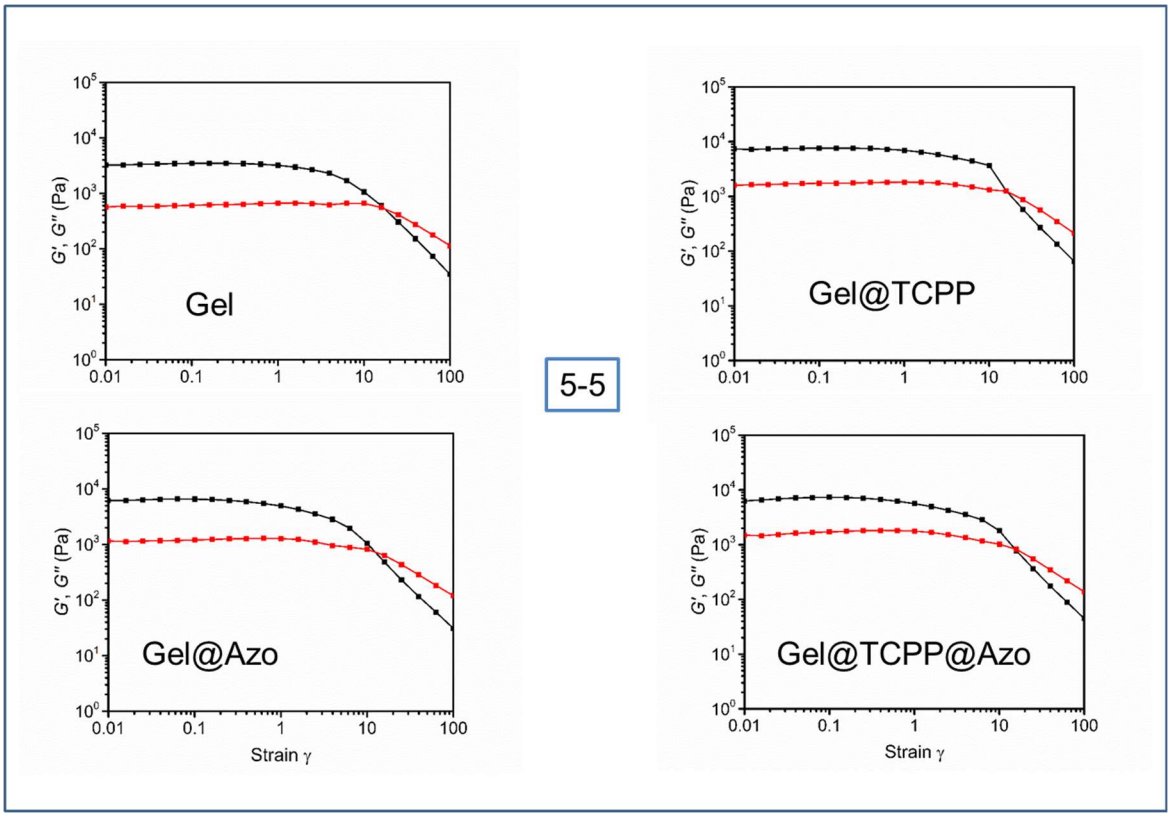

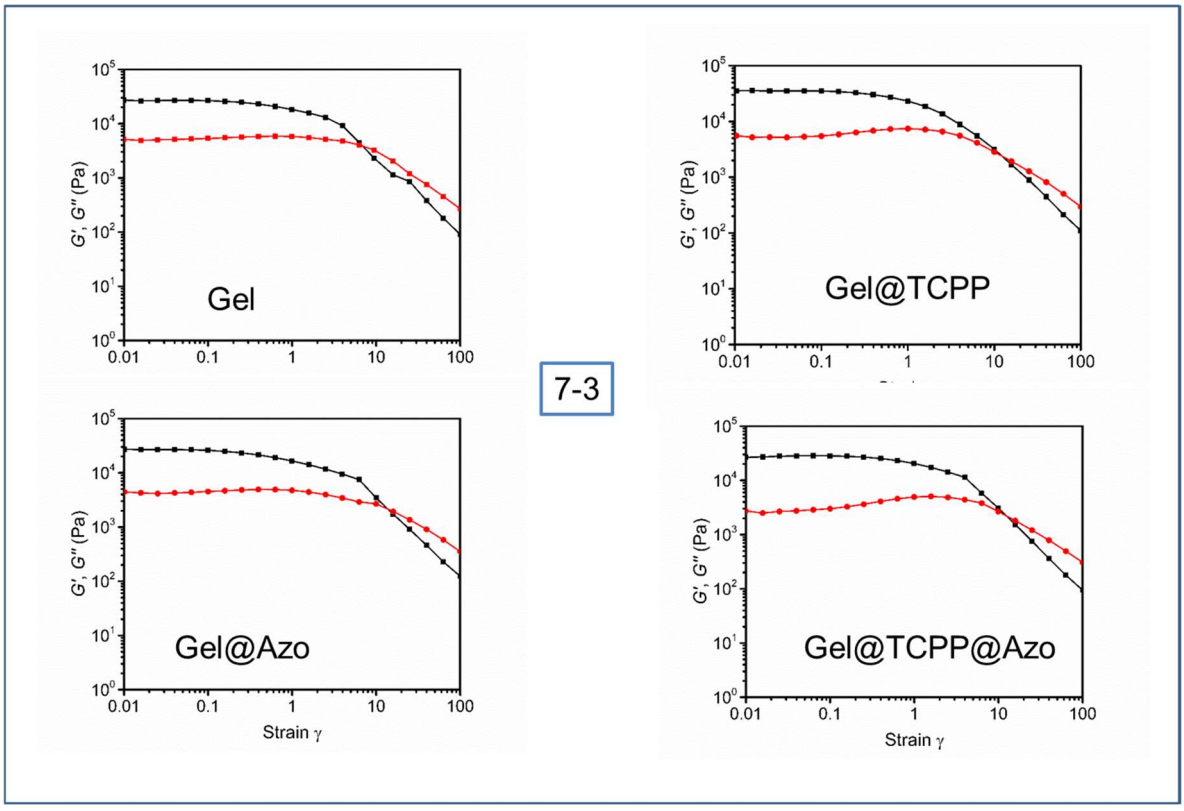

Extended data Fig. 2. Rheology of the multicomponent gels. Shear stress profiles displaying storage (G', black curve) and loss (G", red curve) moduli obtained for gels in water-ethanol ratio 5:5 (top box) and 7:3 (bottom box).

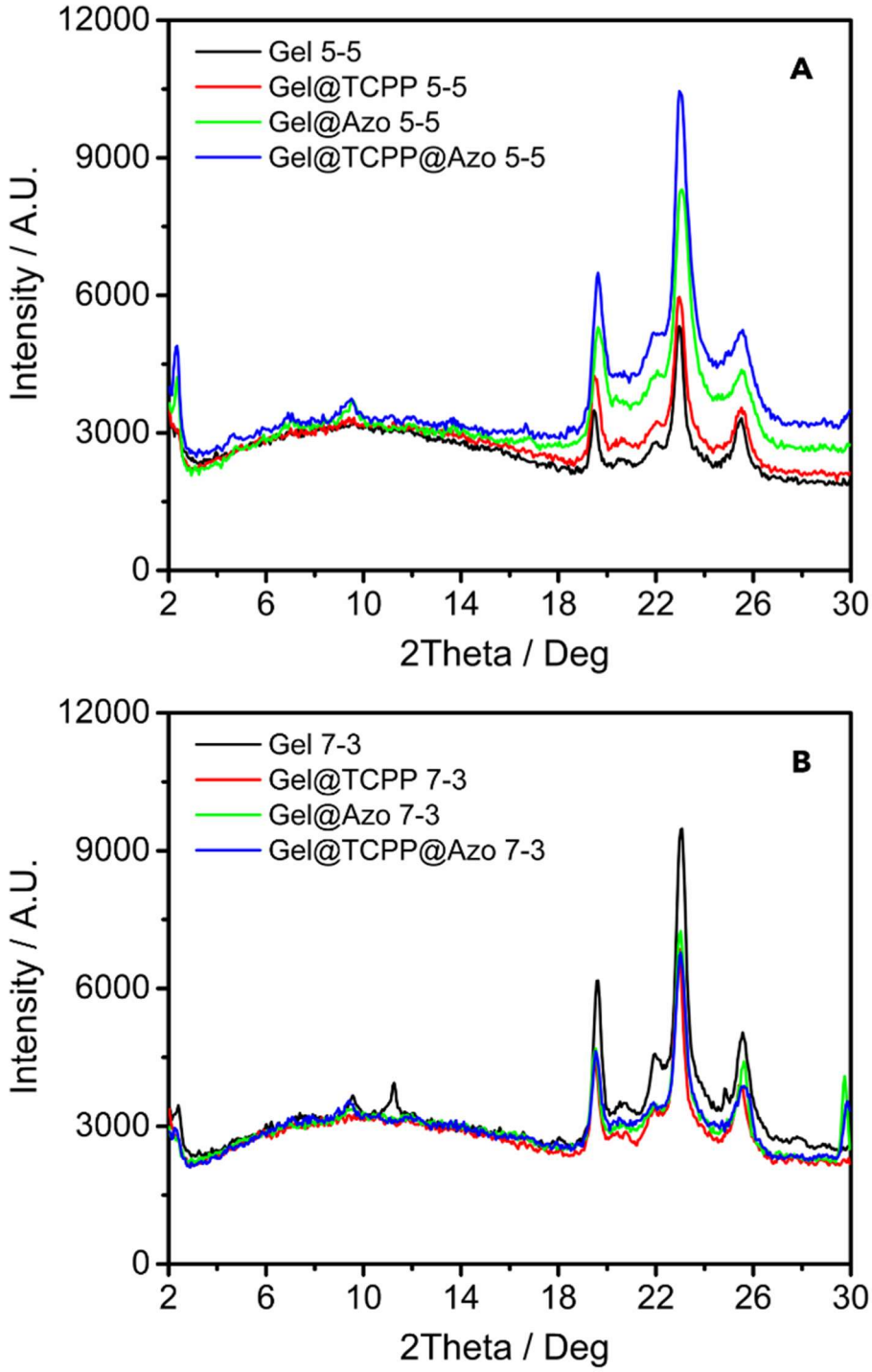

Extended data Fig. 3. X-ray powder diffractograms of xerogels made from gel with no guests (black lines), Gel@TCPP (red lines), Gel@Azo (green lines) and Gel@TCPP@Azo (blue lines) in water-ethanol ratio 5:5 (A) and 7:3 (B).

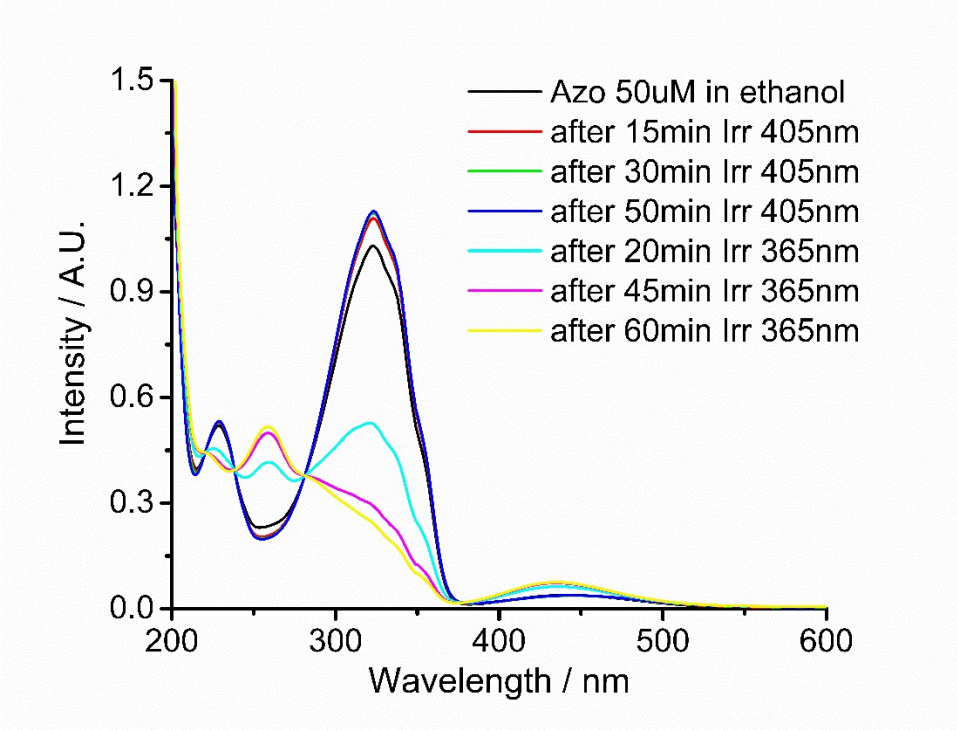

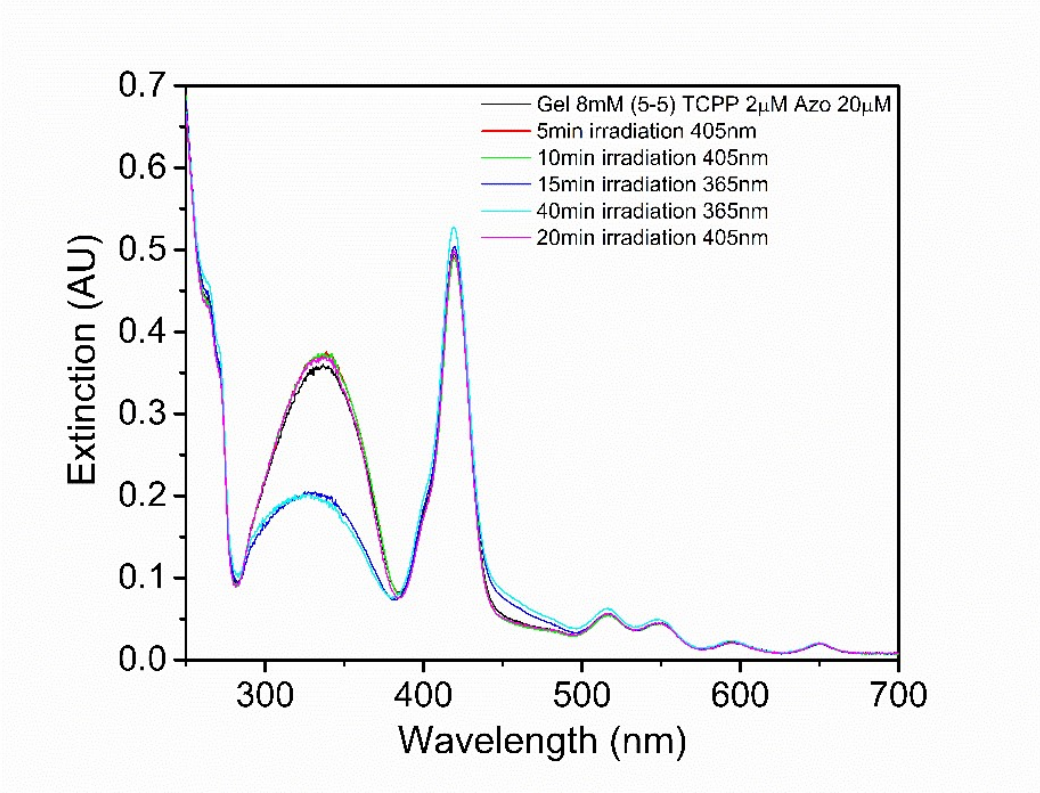

Extended data Fig. 4. Isomerisation of Azo in solution and in the multicomponent gel. UV-Vis absorption spectra of: Top. Azo 50 μM in homogeneous ethanol solution as prepared (black line) and sequential irradiation under light at 405 and 365 nm, and; Below. Gel@TCPP@Azo in 5:5 water:ethanol under light irradiation at 405 and 365 nm.

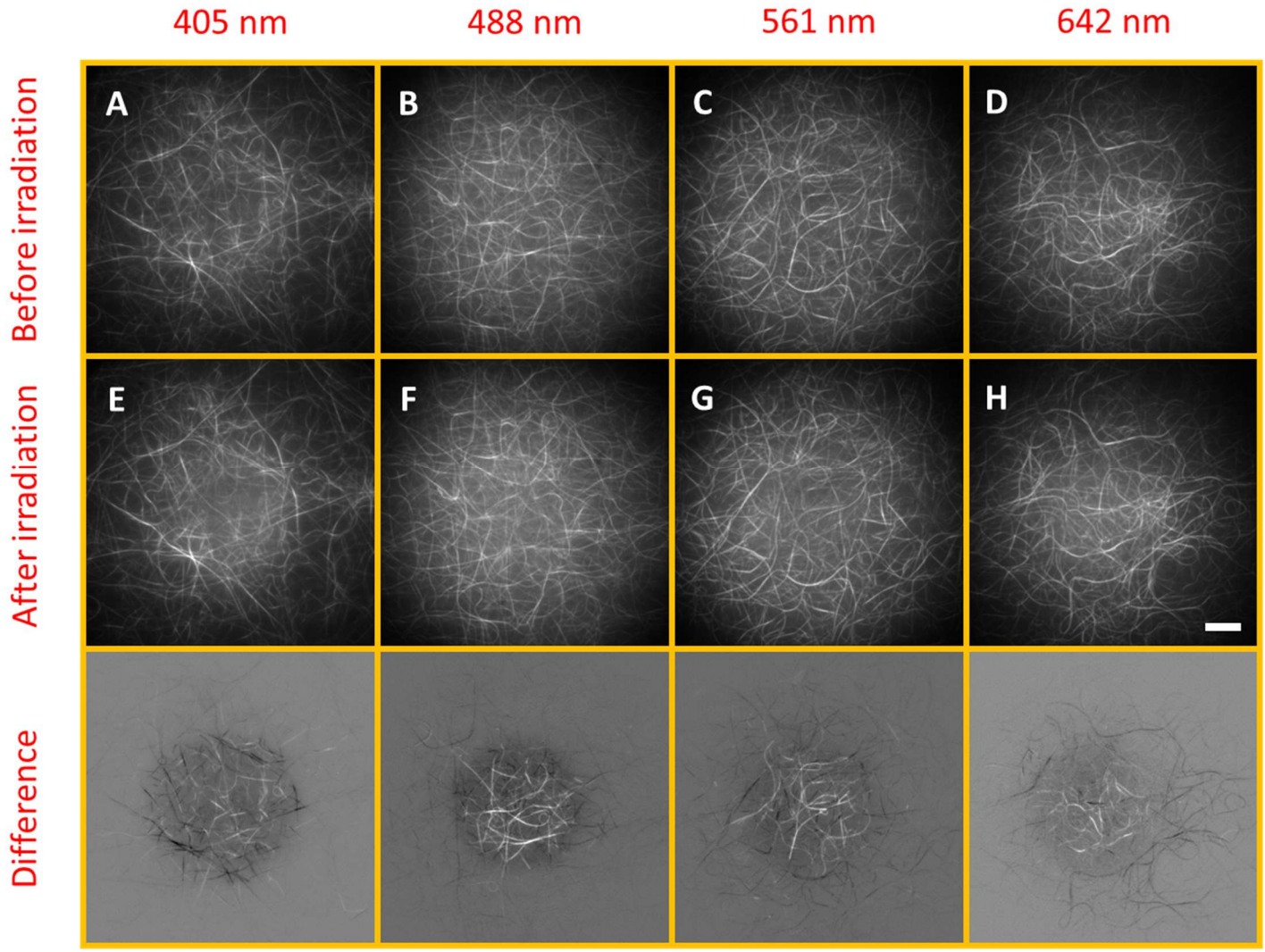

Extended data Fig. 5. Wavelength dependence of molecular motion. TIRF images of Gel@TCPP@Azo in water-ethanol 5:5 before (A-B-C-D) and after (E-F-G-H) irradiation (for a total of 8.3 minutes) with light at 405, 488, 561, 642 nm in the central region. Scale bar represents 10 μm. The difference maps below show the areas where changes of intensity can be appreciated (note that the white and black intensities on the four maps have different intensities and do not indicate amount of change). Some fibres in the irradiated area are darker in the difference map (so there is more porphyrin after irradiation). Those fibres are apparently above the focal plane, deeper into the sample compared with the layer imaged. In principle, this can occur because laser intensity is higher at the slide-sample interface, then decreases as we look deeper into the sample. It is evidence for movement of TCPP into the sample as well as to the sides of the irradiated area.

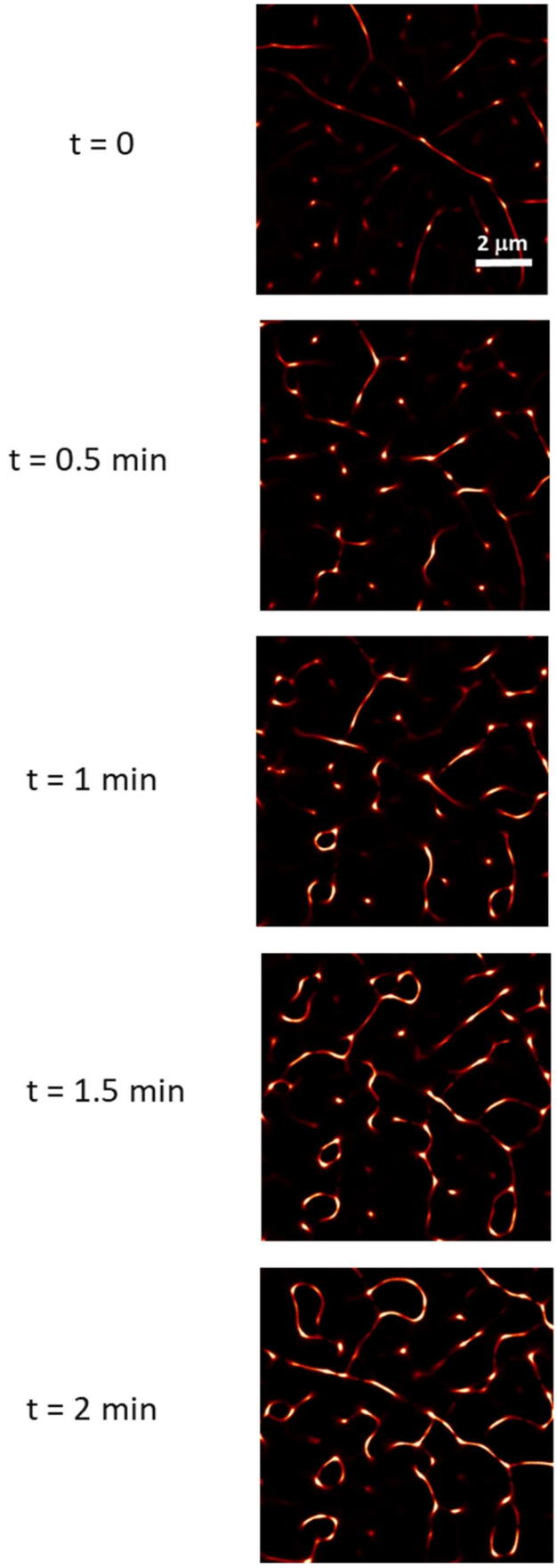

Extended data Fig. 6. Ring formation from fibres. Zoomed SRRF images of Gel@TCPP@Azo in water-ethanol 7:3 during irradiation at 405 nm. The frames are taken from Movie S9. Scale bar represents 2 µm, all images are to the same scale.

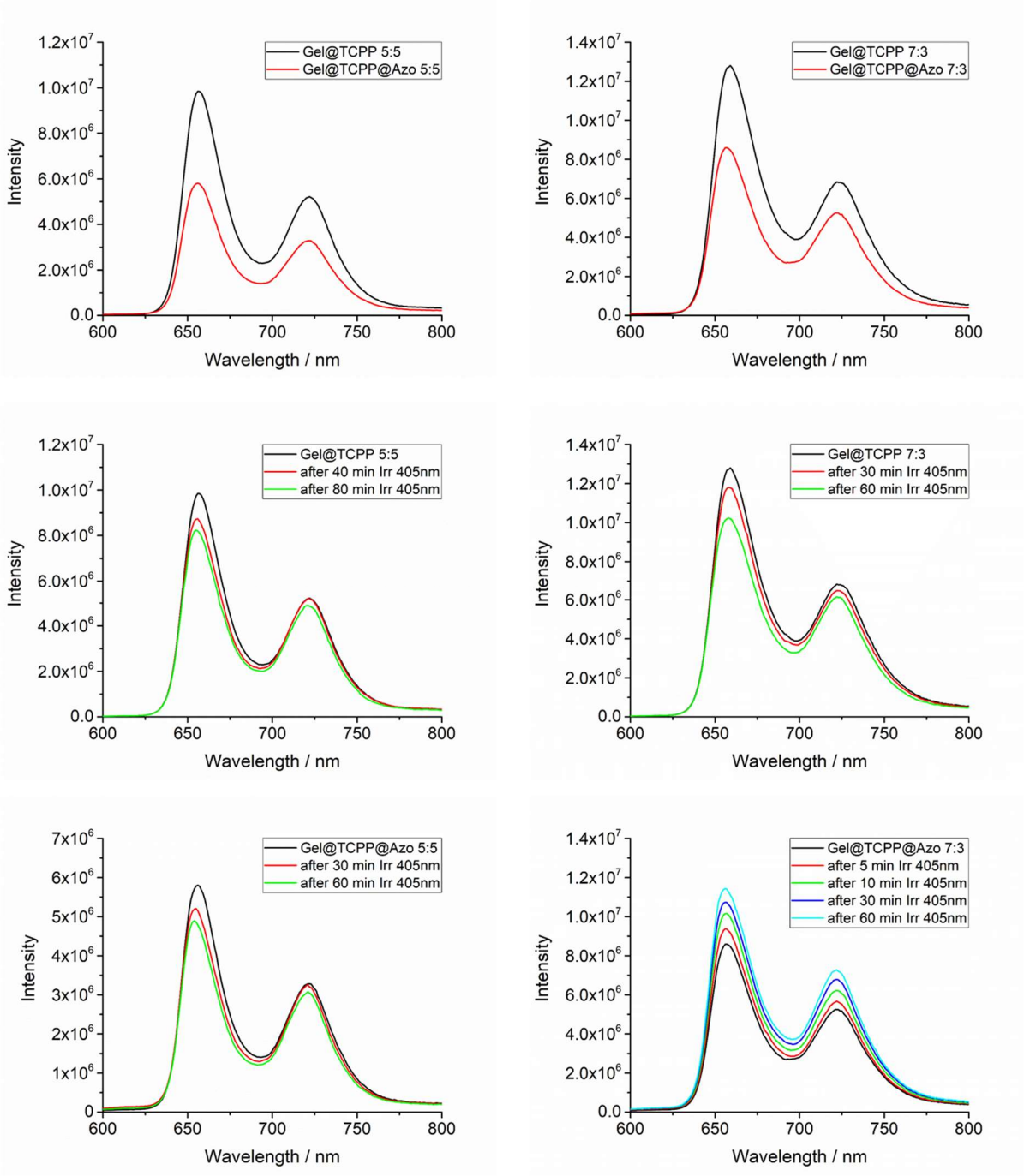

Extended data Fig. 7. TCPP fluorescence in the gels. The steady state fluorescence spectra (excitation wavelength 405 nm) in both 5:5 and 7:3 water:ethanol gels show (top row) that there is a quenching of the porphyrin fluorescence in Gel@TCPP@Azo compared with Gel@TCPP for both solvent mixtures, as a result of energy transfer from the TCPP to the Azo chromophore. The middle row shows the time evolution of the same Gel@TCPP samples under continuous irradiation at 405 nm, where a modest bleaching is observed over time for both solvent systems. The bottom row shows the evolution of the fluorescence of Gel@TCPP@Azo under continuous irradiation, where at 5:5 water:ethanol a slight bleaching is observed (similar to Gel@TCPP), while for the 7:3 mixture an increase in fluorescence is observed, so that after 60 minutes the intensity is actually higher than that for Gel@TCPP after the same time.

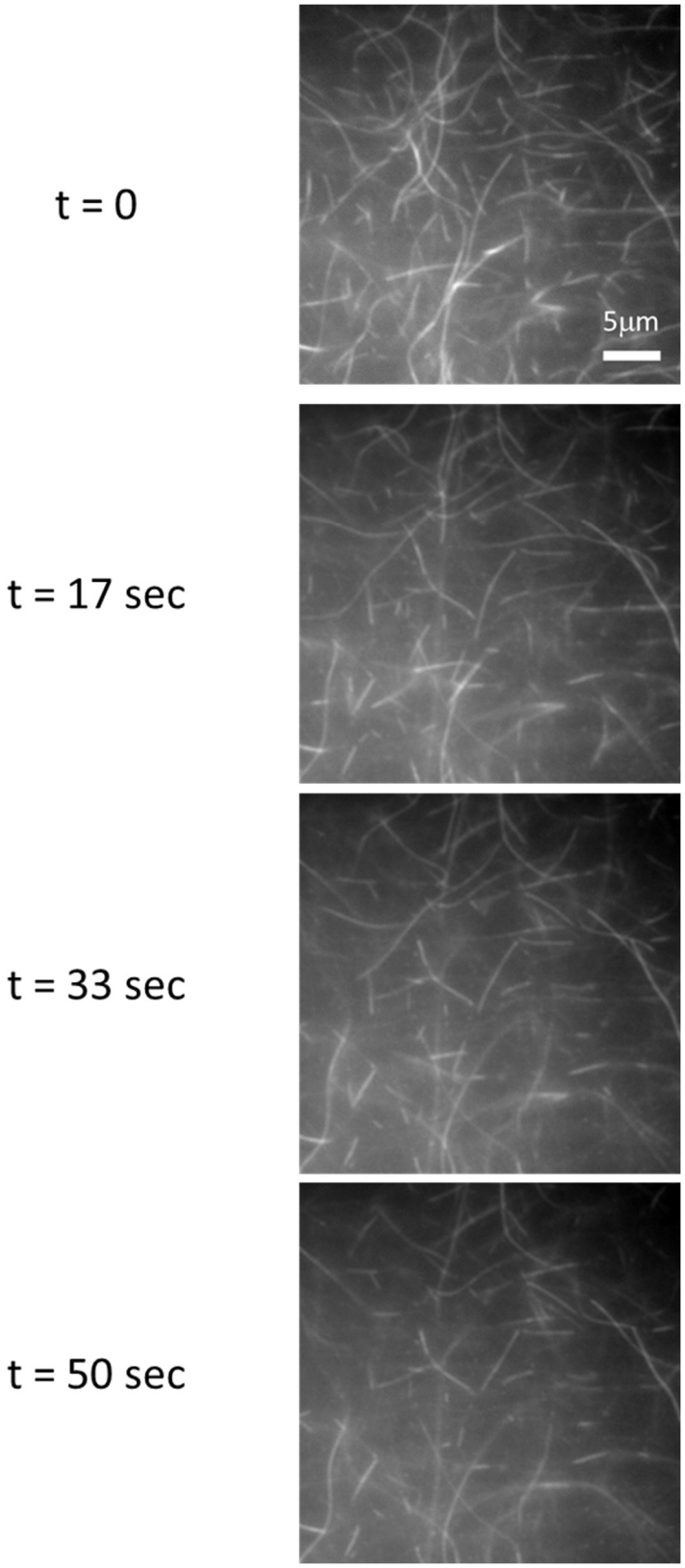

Extended data Fig. 8. Isomerisation of a majority of the cis-Azo enhances motion. TIRF micrographs at time zero with irradiation at 405 nm (top) and after the end of Movie S13 of sample Gel@TCPP@Azo where Azo was enriched in the *cis* isomer by photoisomerization prior to gel preparation. Scale bar represents 5 µm, all images are to the same scale.

Supplementary Information

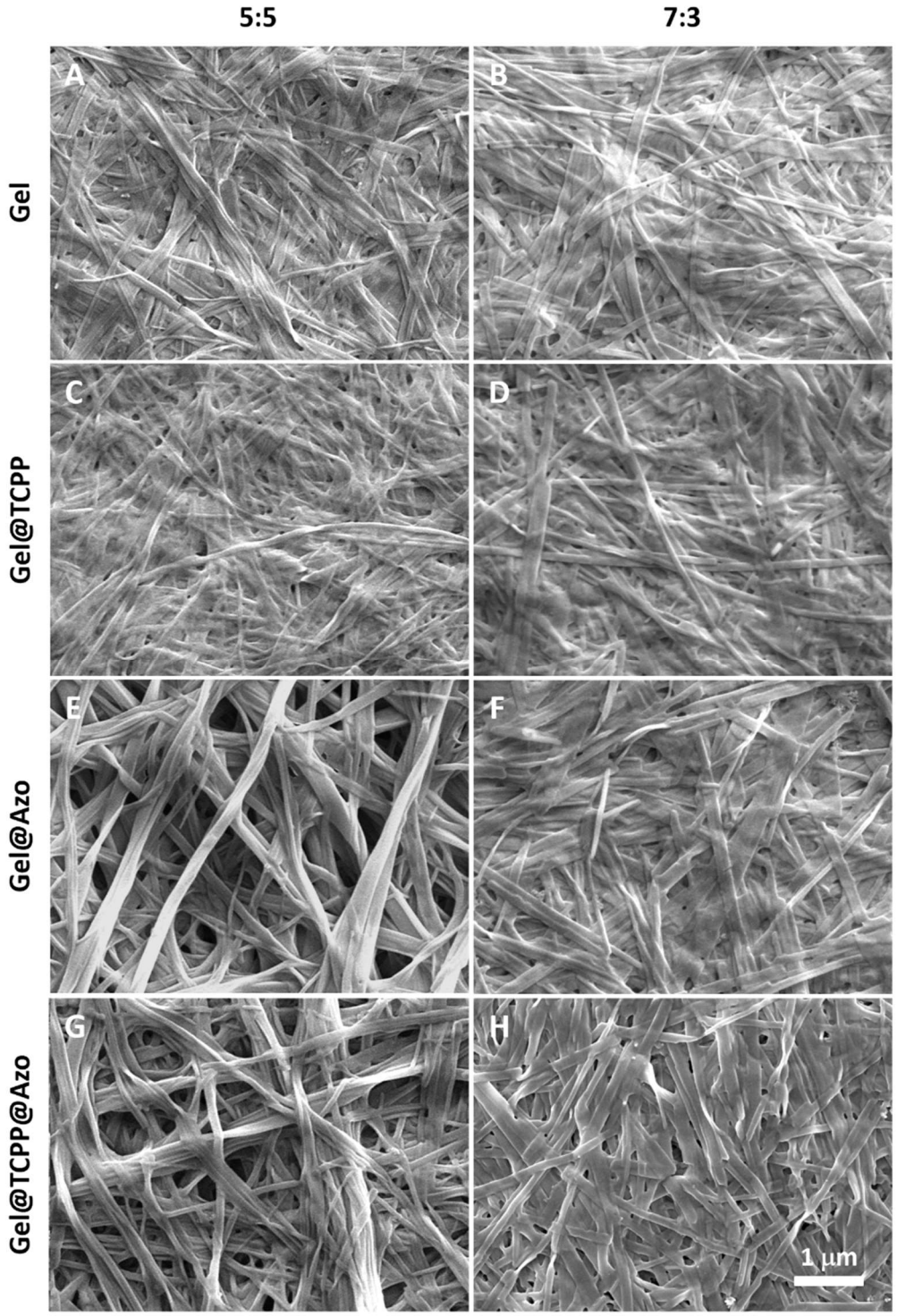

Figure S1. SEM micrographs of xerogels made from gels at 8 mM concentration of **1**·2Br in water-ethanol ratio 5:5 and 7:3, without guest molecules (A-B), with TCPP 60 μM (C-D), with Azo 2 mM (E-F) and with both TCPP and Azo (G-H) prior to irradiation. The scale bar in the micrograph H corresponds to 1 μm, and all micrographs are on the same scale.

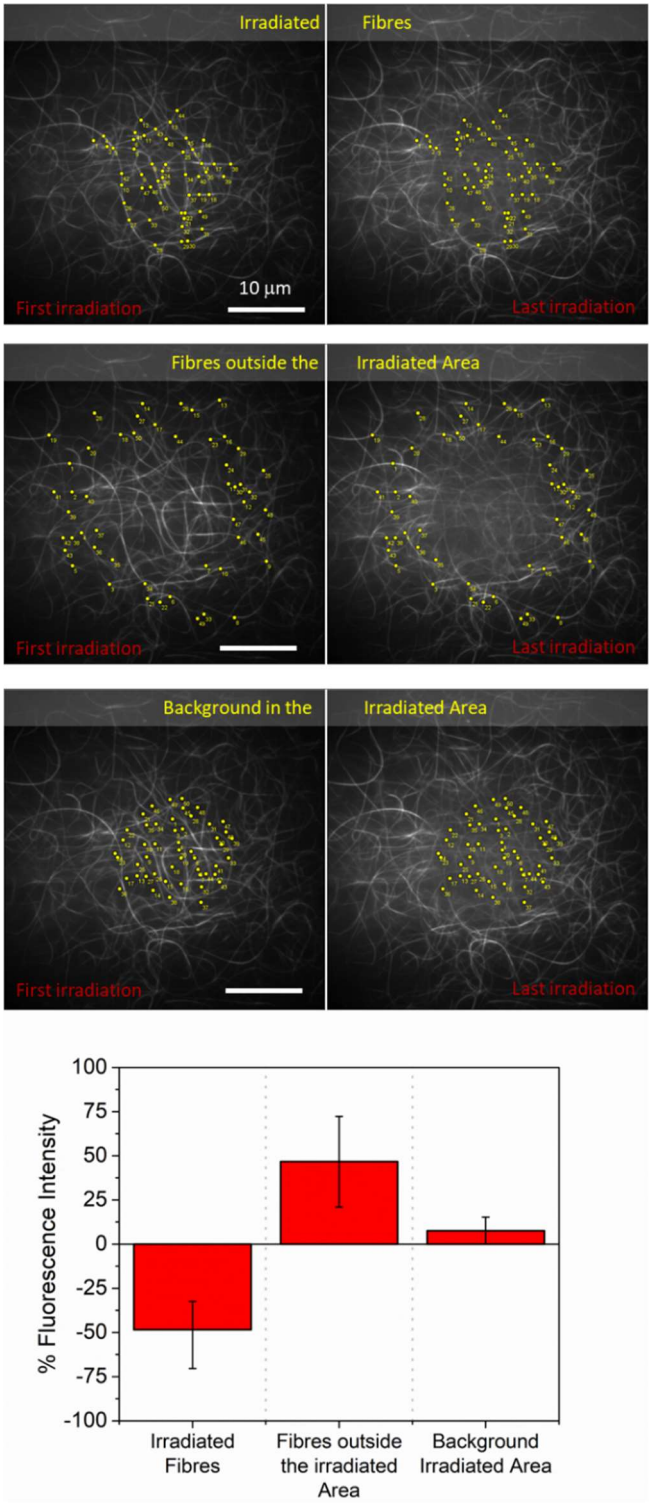

Figure S2. A chart (bottom) showing the changes in fluorescence intensity in the TIRF micrographs shown of sample Gel@TCPP@Azo obtained in water-ethanol ratio 5:5. The points taken for this plot are shown in the images, in the first recorded image in the series and in the last recorded image, for fibres inside and outside the irradiated (405 nm) area as well as for darker areas between the fibres in the irradiated region. Scale bar represents 10mm. See Table S6 for numerical values.

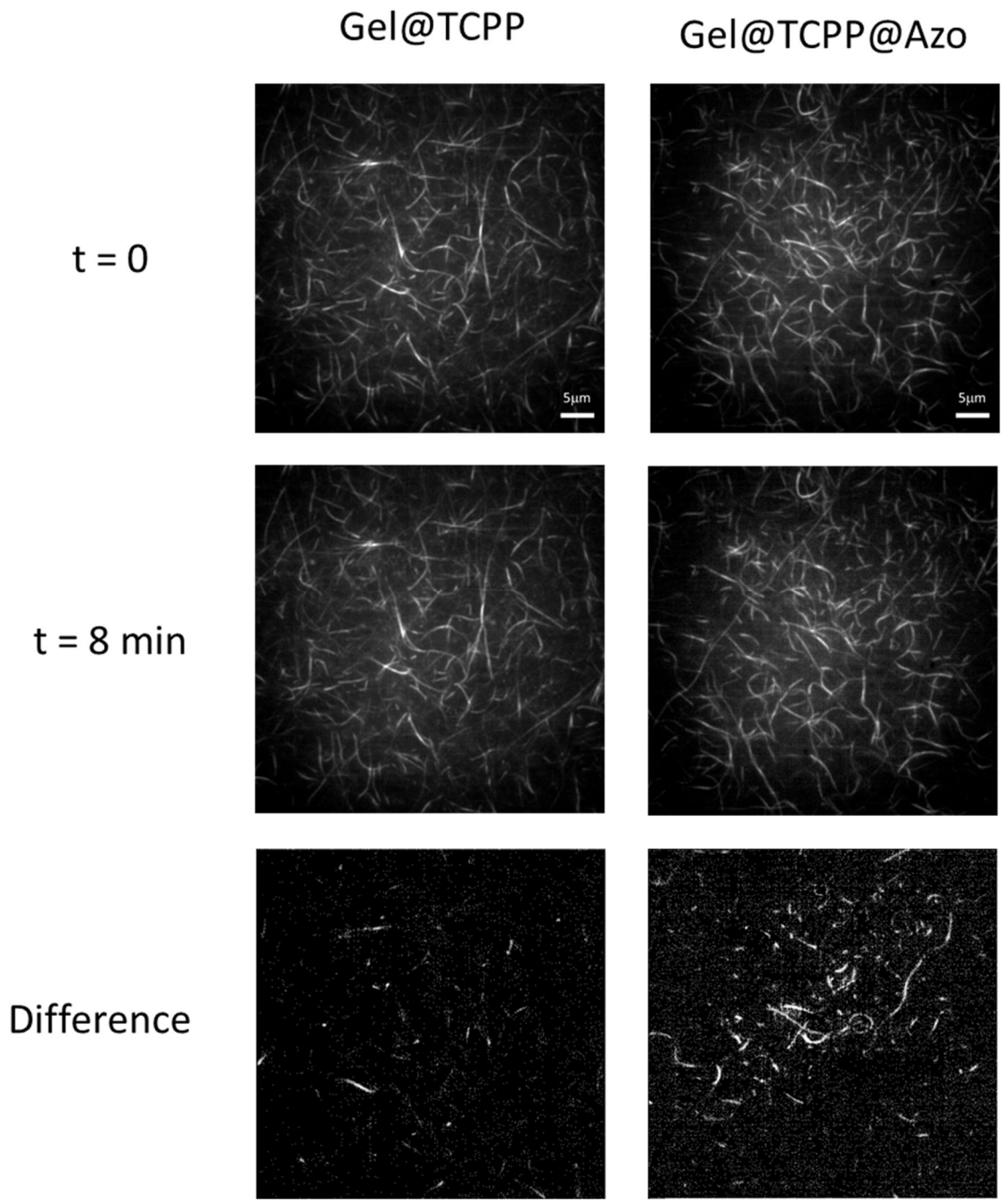

Figure S3. TIRF micrographs with irradiation at 405 nm of sample Gel@TCPP and Gel@TCPP@Azo obtained in water-ethanol ratio 5:5 showing the first micrograph and a third micrograph taken 8 minutes later (with a total irradiation corresponding to the capture of three images) and the difference map for the two samples. The results show the small change in the sample without Azo (there are often movement of a small number of fibres during measurements) and the relatively much larger movement in the sample with Azo. It should be noted that the sample was in the dark between the micrographs, and therefore correspond to the very early stages of motion in the Gel@TCPP@Azo sample where the videos are recorded under continuous irradiation. Scale bar represents 5□m.

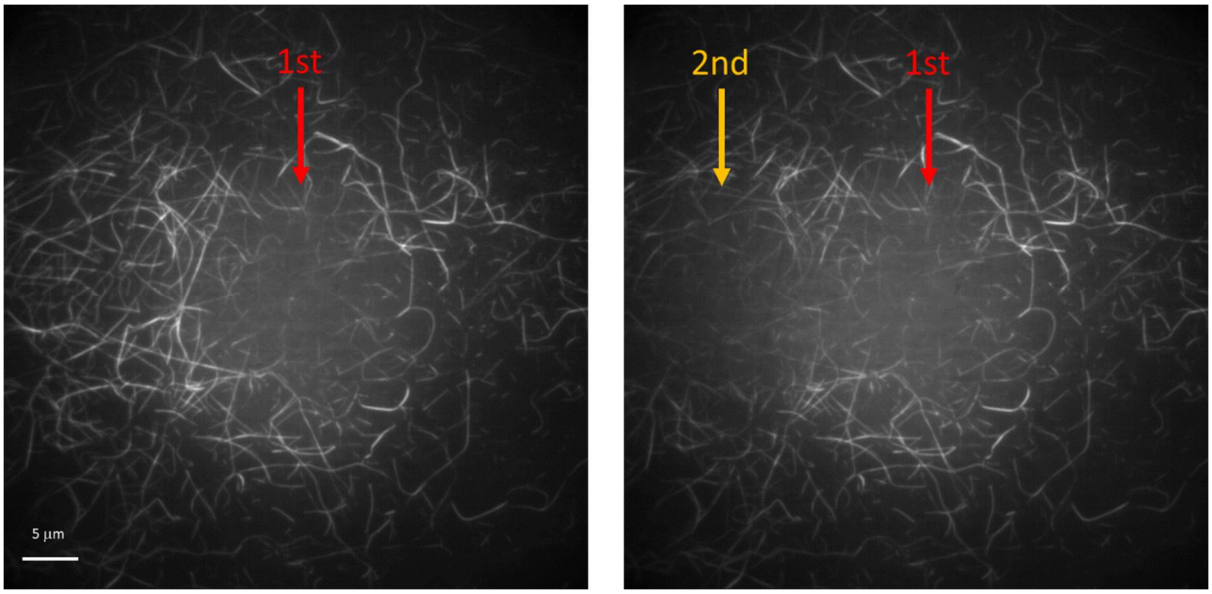

Figure S4. TIRF micrographs of Gel@TCPP@Azo formed in 7:3 water:ethanol showing an area irradiated at 405 nm to cause movement (1st) followed by a subsequent irradiation (2nd) in an attempt to move the TCPP back to the original (1st) area. No recovery could be detected in this or other similar experiments, indicating that the motion is not reversible in the system as it stands.

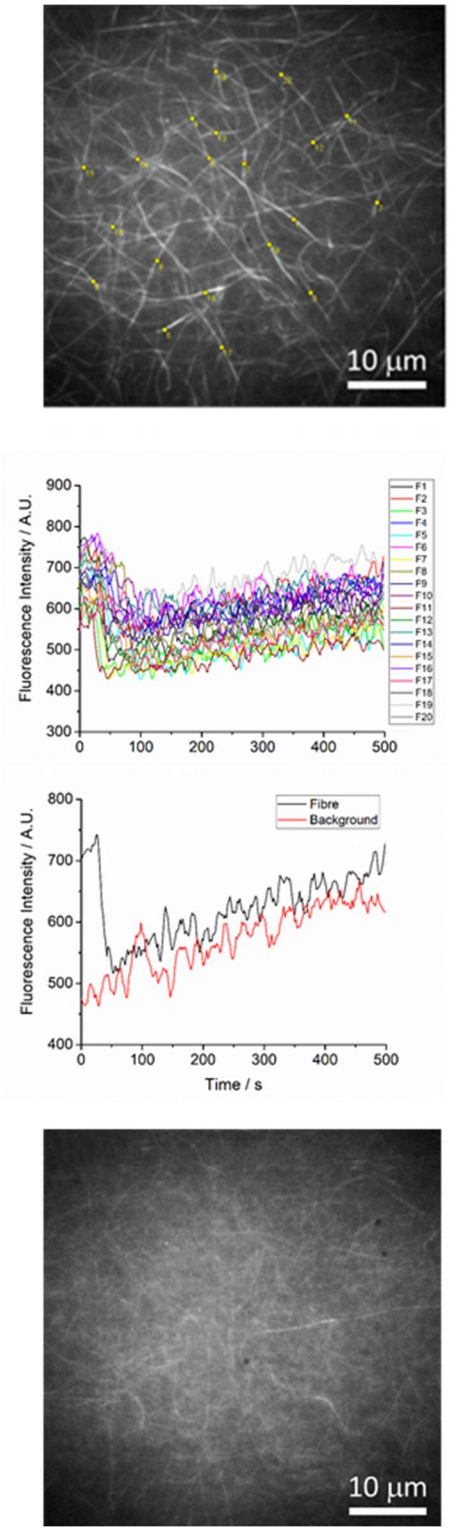

Figure S5. TIRF micrographs of Gel@TCPP@AzoH formed in 7:3 water:ethanol showing how the background fluorescence rises – indicative of general porphyrin distribution after irradiation at 405 nm. The top image shows initial TIRF micrograph and the points where kinetic traces have been monitored using the fluorescence intensity (top graph) and the bottom graph shows a typical fluorescence intensity signal for the background and over a region where a fibre was originally present. The bottom TIRF image is at the end of the irradiation. Scale bars represents 10 mm.

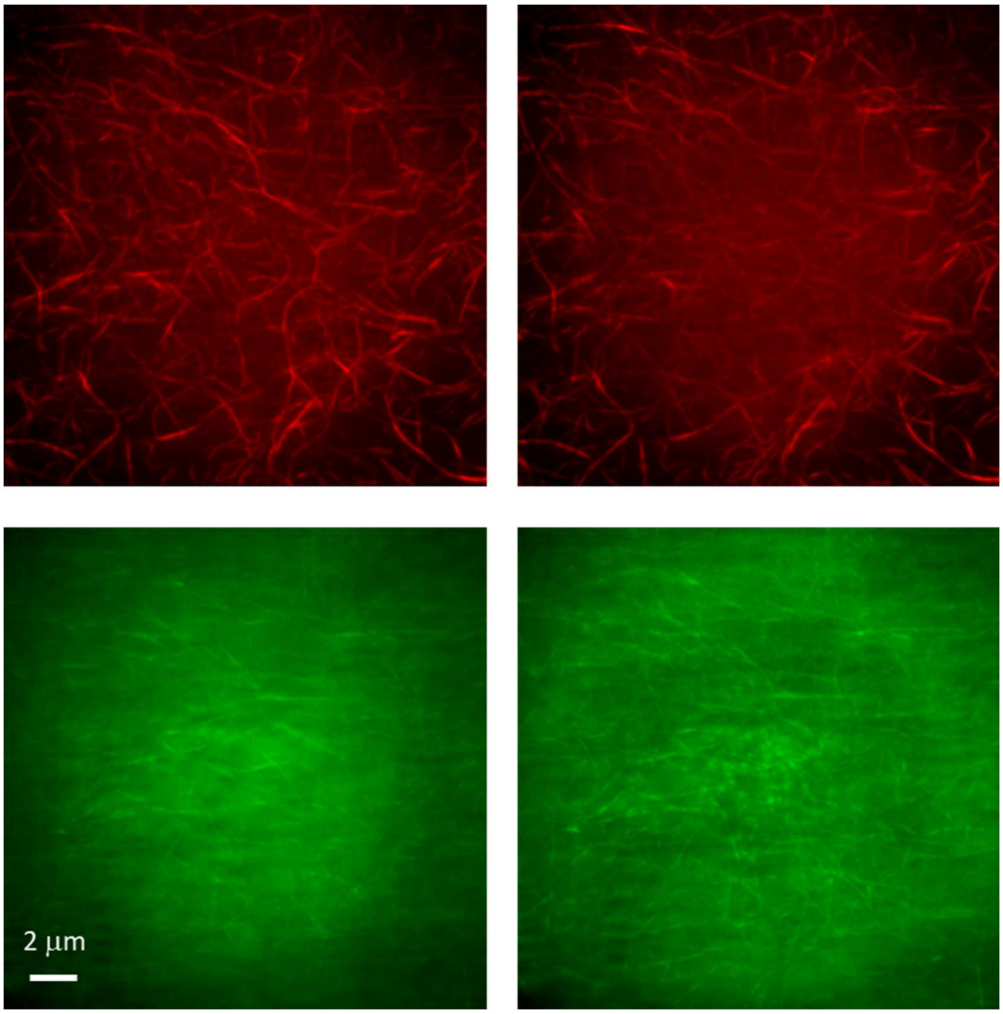

Figure S6. TIRF micrographs of Gel@TCPP@Azo@2.2Br formed in 7:3 water:ethanol at the beginning (left) of irradiation at 405 nm and at the end (right) of the experiment, after 8.3 minutes. Emission coloured red showing the location of TCPP and green where **2**.2Br is situated.

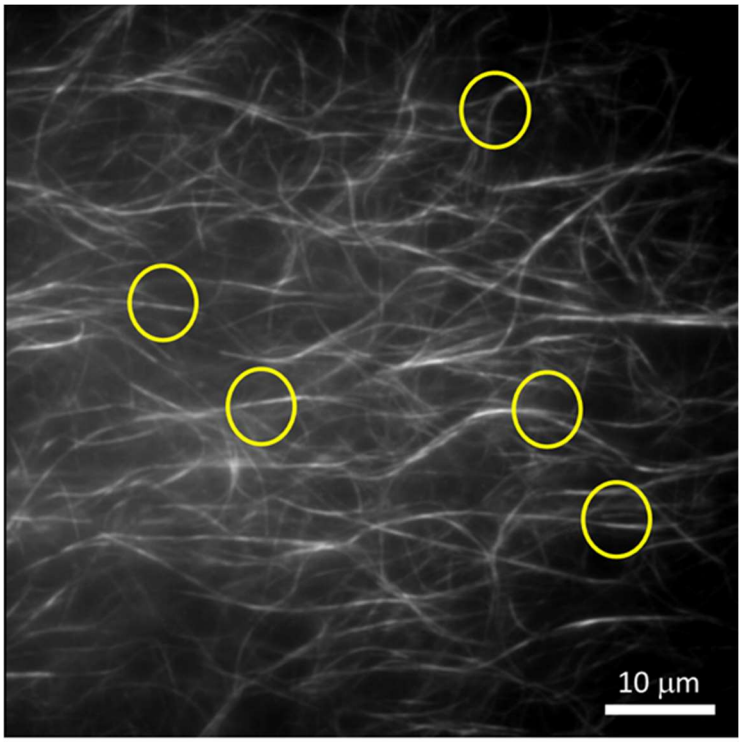

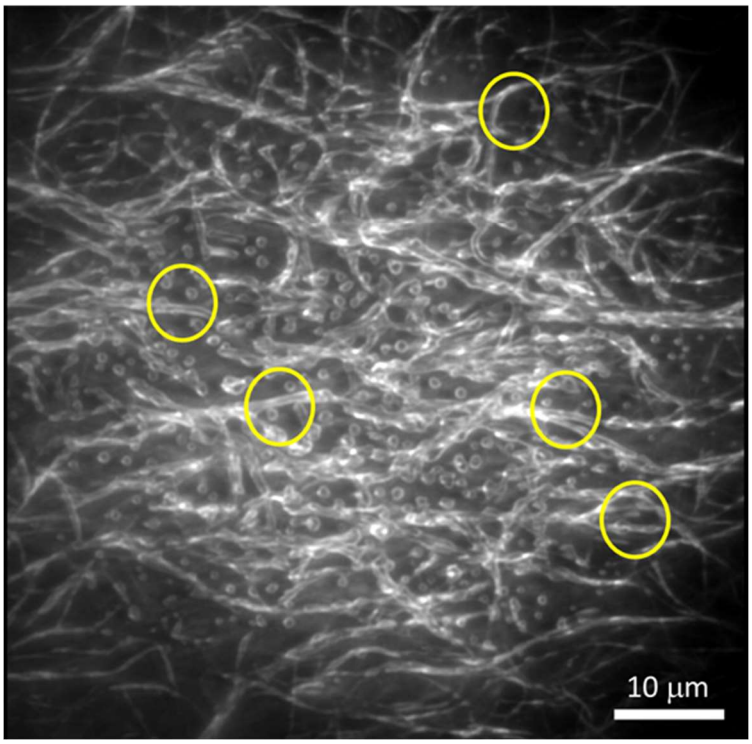

Figure S7. TIRF micrographs at time zero with irradiation at 405 nm (top) and after the end of Movie S4 of sample Gel@TCPP@Azo obtained in water-ethanol ratio 6:4 with some of the areas where the original fibres separate highlighted. Scale bar represents 10 mm.

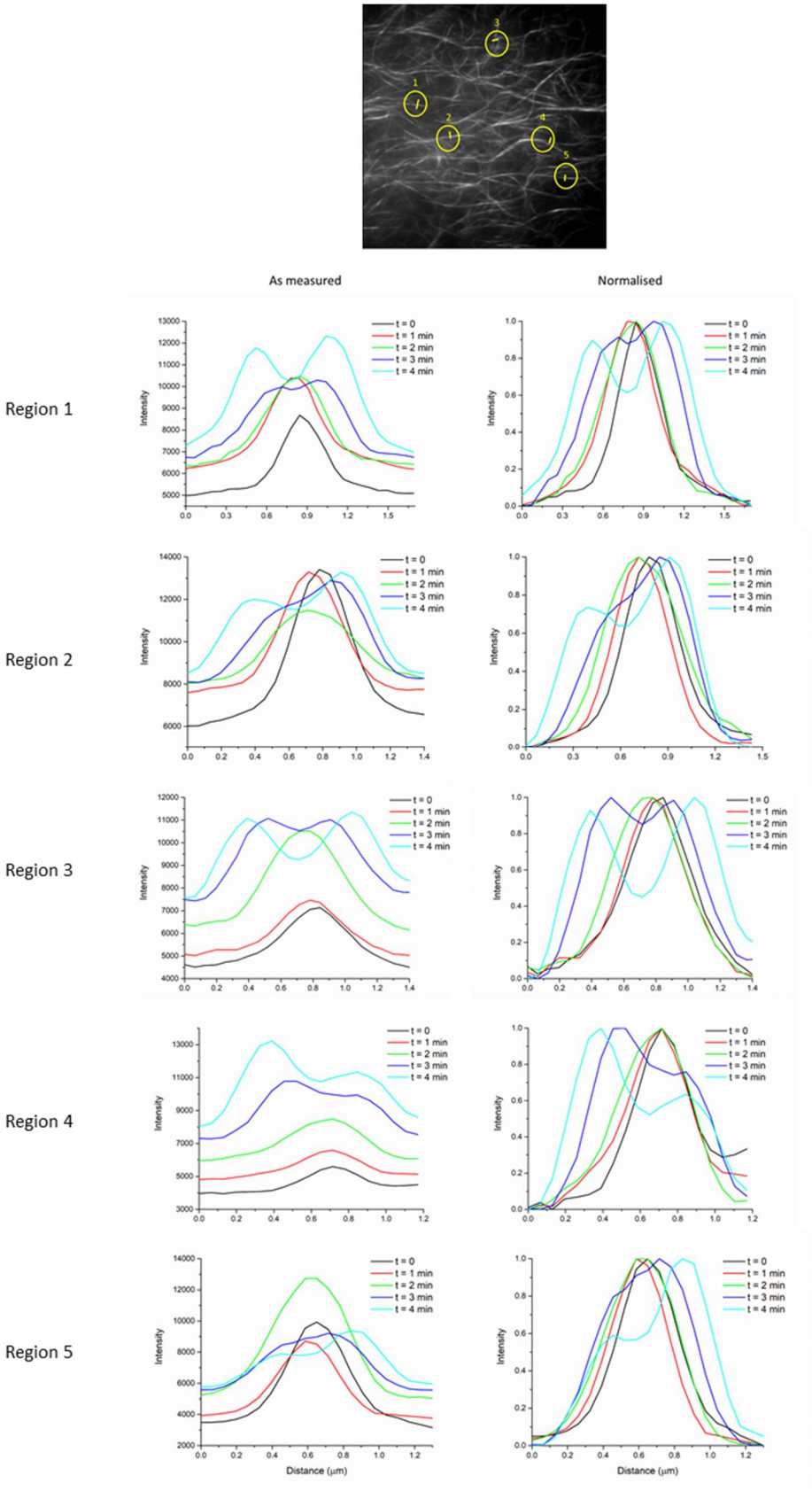

Figure S8. A TIRF micrograph with irradiation at 405 nm (top) of sample Gel@TCPP@Azo obtained in water-ethanol ratio 6:4 with profiles of five regions where fibres separate, shown as-measured and after normalising for highest intensity.

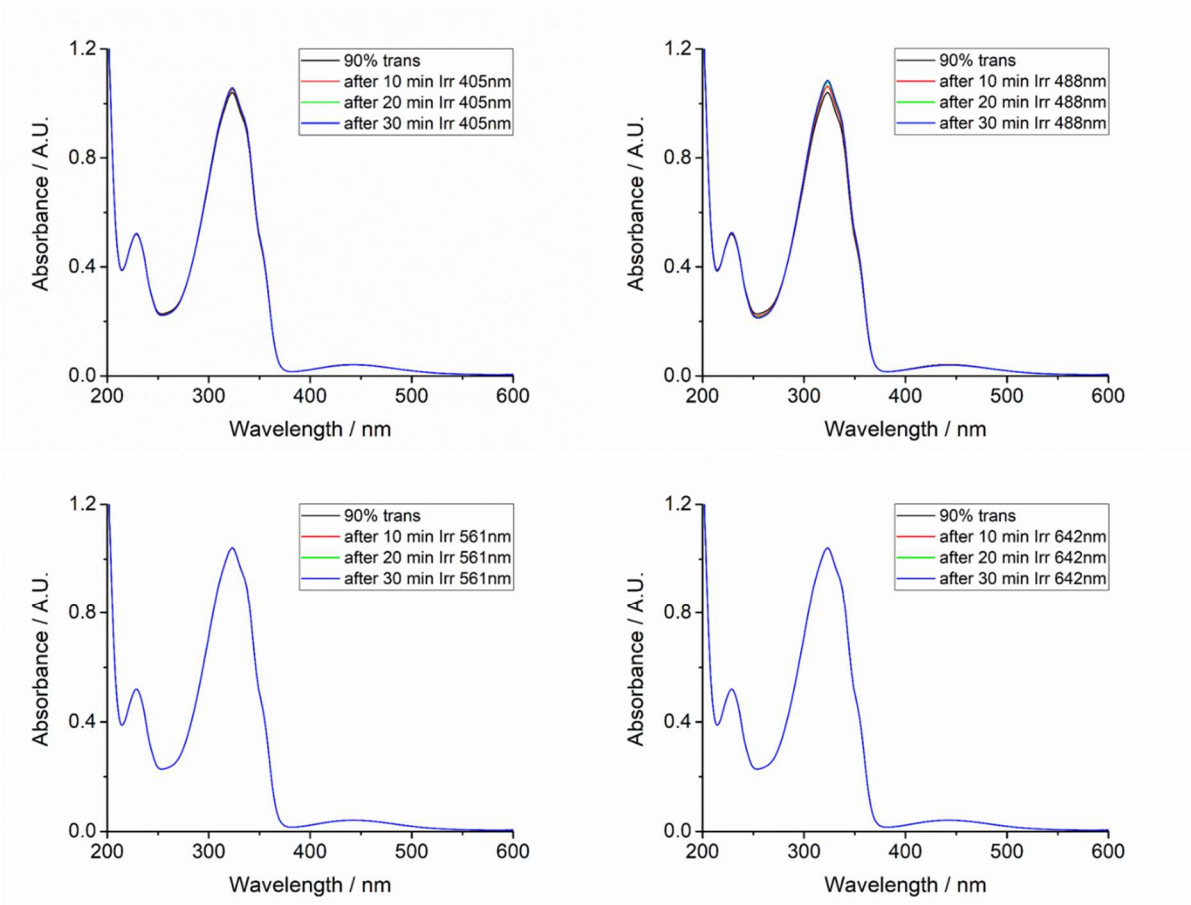

Fig. S9. UV-Vis absorption spectra of Azo in water:ethanol 7:3 solution after irradiation at the indicated wavelengths and times in a fluorimeter (see Table S2 for ratio of isomers).

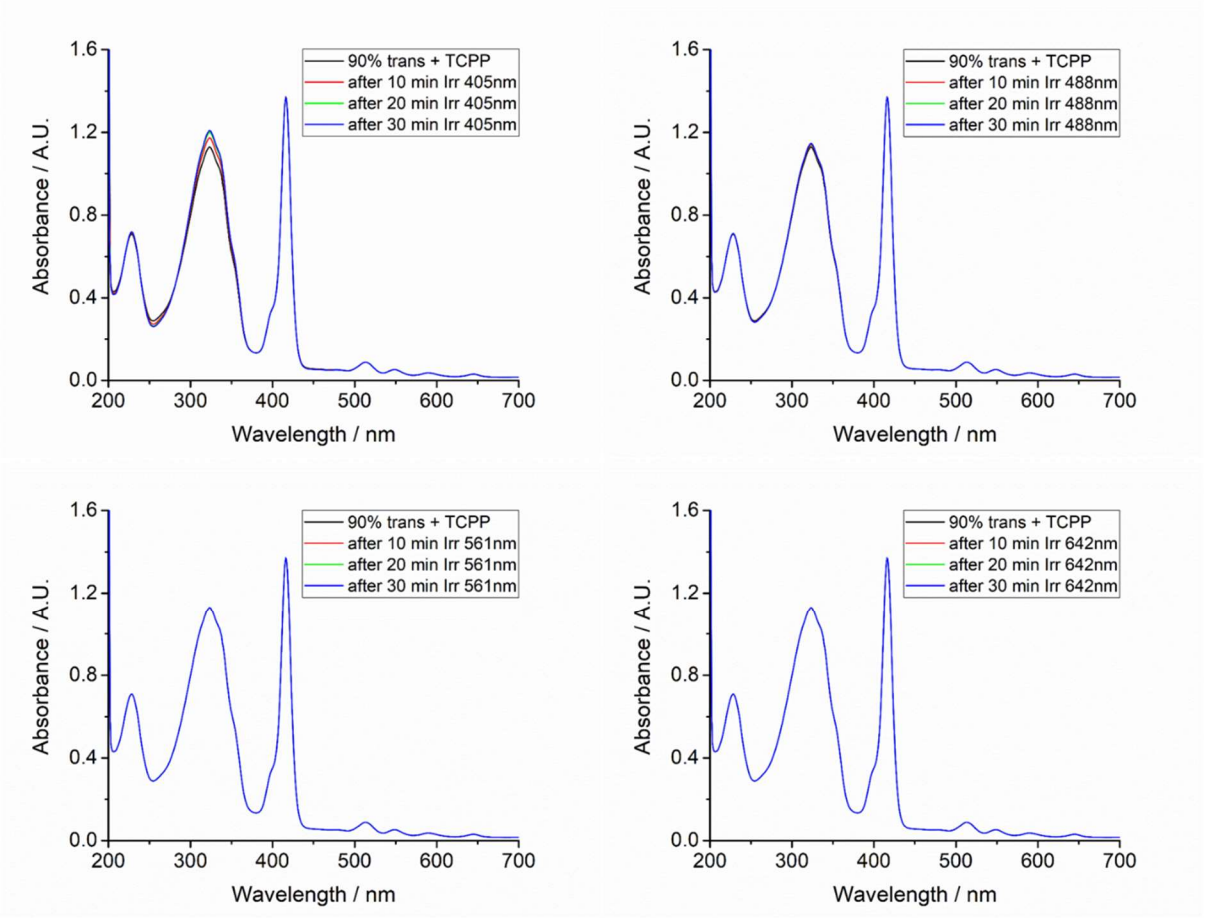

Fig. S10. UV-Vis absorption spectra of a solution of Azo and TCPP in water:ethanol 7:3 solution after irradiation at the indicated wavelengths and times in a fluorimeter (see Table S2 for ratio of isomers).

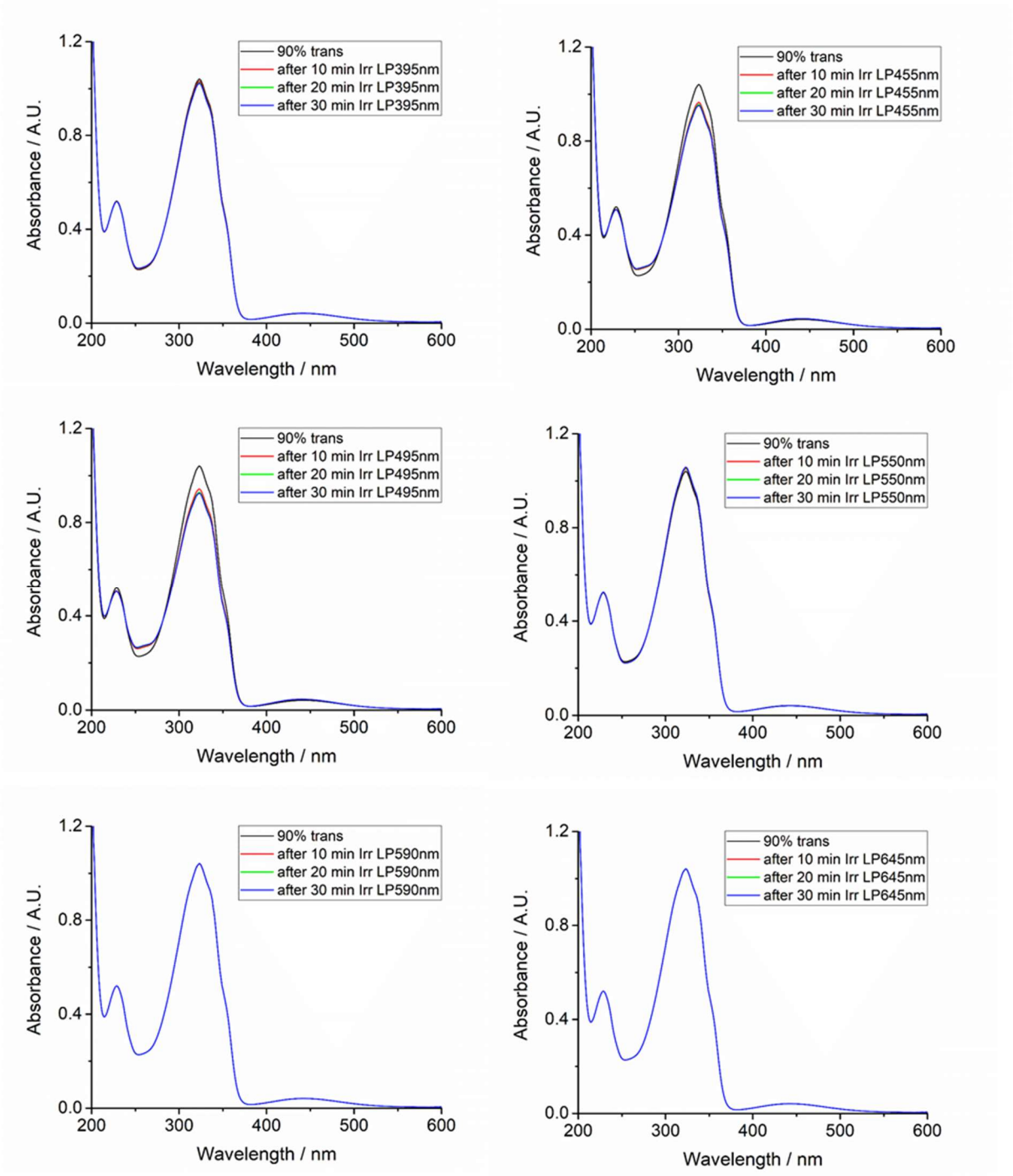

Fig. S11. UV-Vis absorption spectra of a solution of Azo in water:ethanol 7:3 solution after light irradiation after 30 minutes with a solar simulator at 300 mW/cm² equipped with different long-pass (LP) filters and a 10-mm thick water filter. (see Table S3 for ratio of isomers).

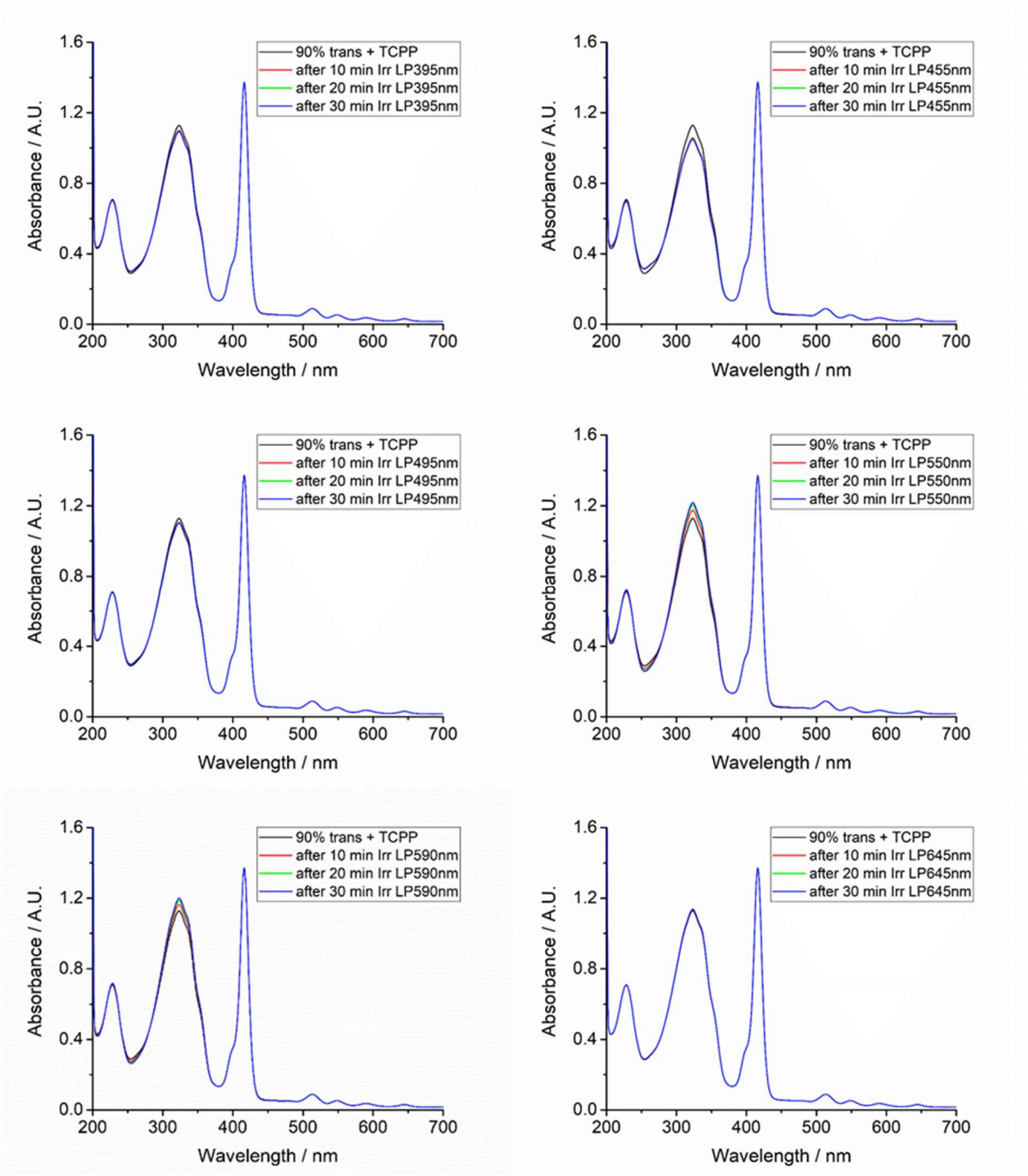

Fig. S12. UV-Vis absorption spectra of a solution of Azo and TCPP in water:ethanol 7:3 solution after light irradiation after 30 minutes with a solar simulator at 300 mW/cm² equipped with different long-pass (LP) filters and a 10-mm thick water filter. (see Table S3 for ratio of isomers).

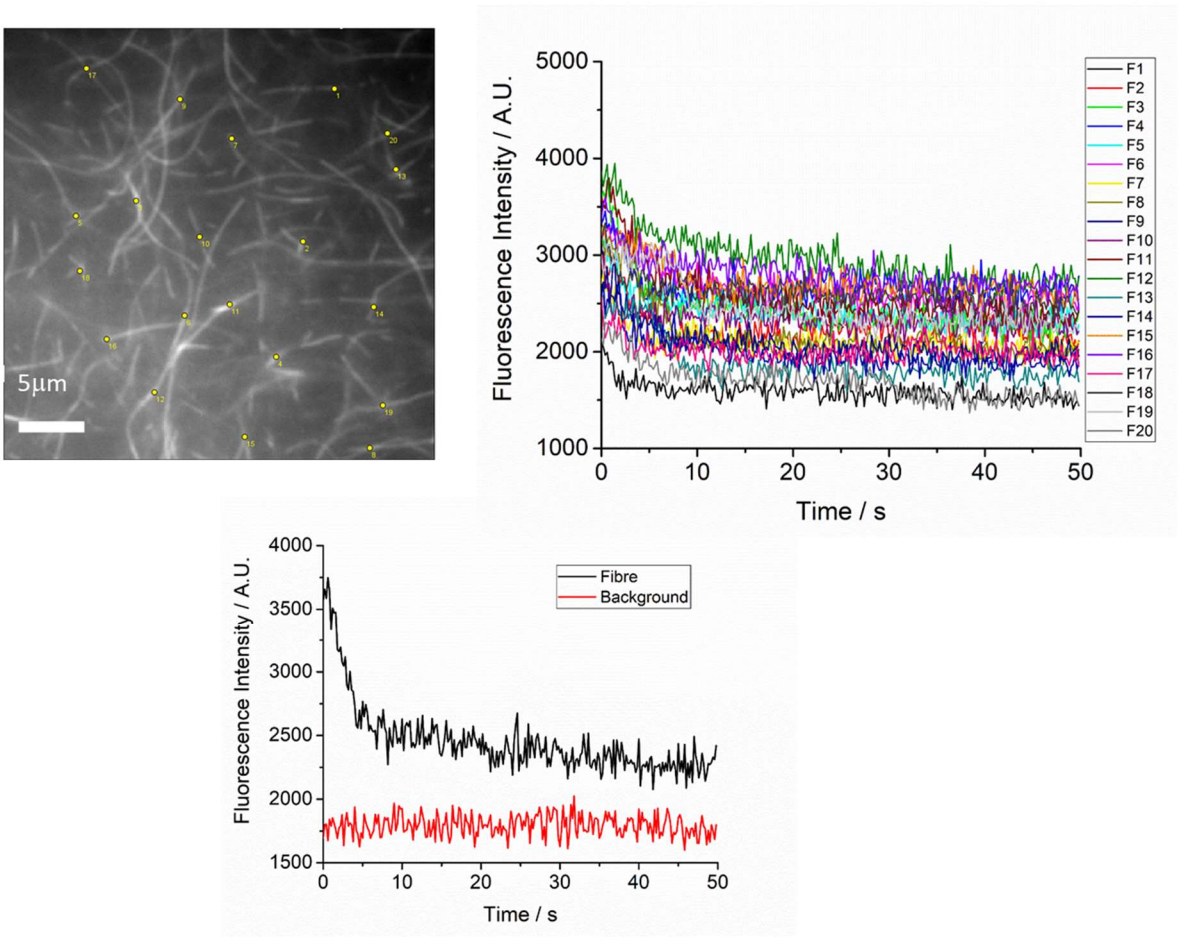

Figure S13. A TIRF micrograph (top left) showing Gel@TCPP@Azo in 5:5 water:ethanol with a starting *trans*:*cis* ratio of approximately 35:65 (prepared by irradiating the ethanol solution containing the Azo used for the preparation of the gel at 365 nm) corresponding to the start of Movie S13, and the points where the loss of fluorescence intensity was measured to produce the fluorescence intensity versus time plot (top right). A representative trace is compared with a background area (bottom). Scale bar represents 5 µm.

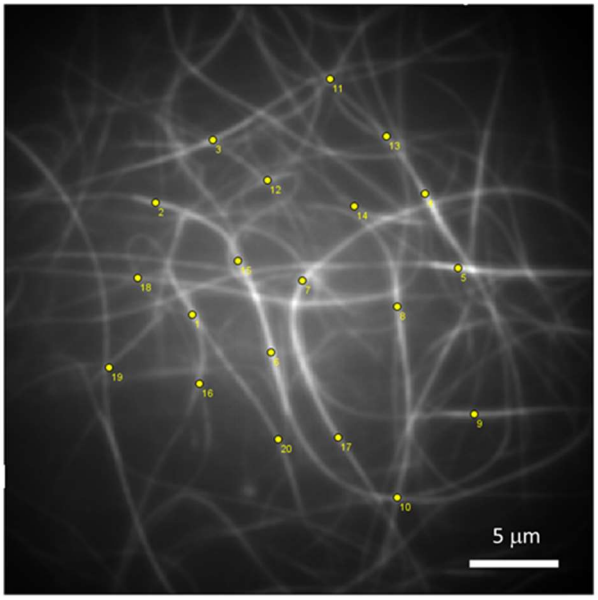

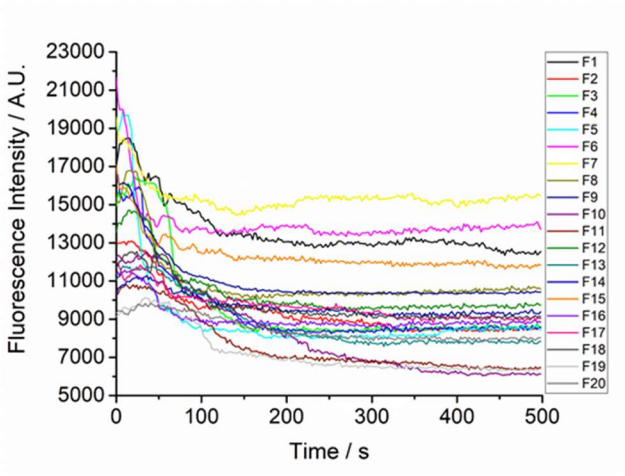

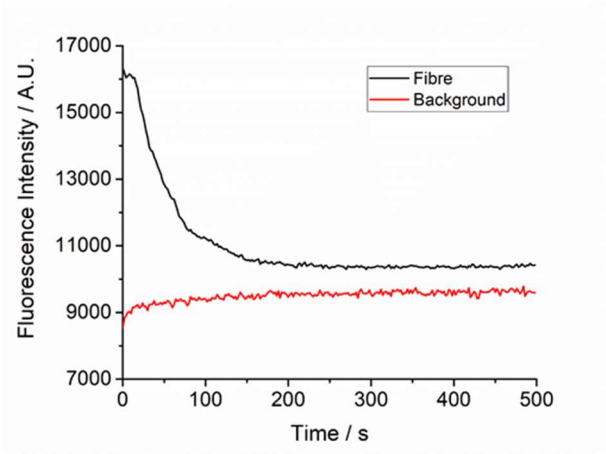

Figure S14. A TIRF micrograph (top) showing Gel@TCPP@Azo in 5:5 water:ethanol (where the starting *trans*:*cis* ratio is approximately 90:10) corresponding to the start of Movie S1, and the points where the loss of fluorescence intensity was measured to produce the fluorescence intensity versus time plot (middle). A representative trace is compared with a representative background area (bottom). Scale bar represent 5 mm.

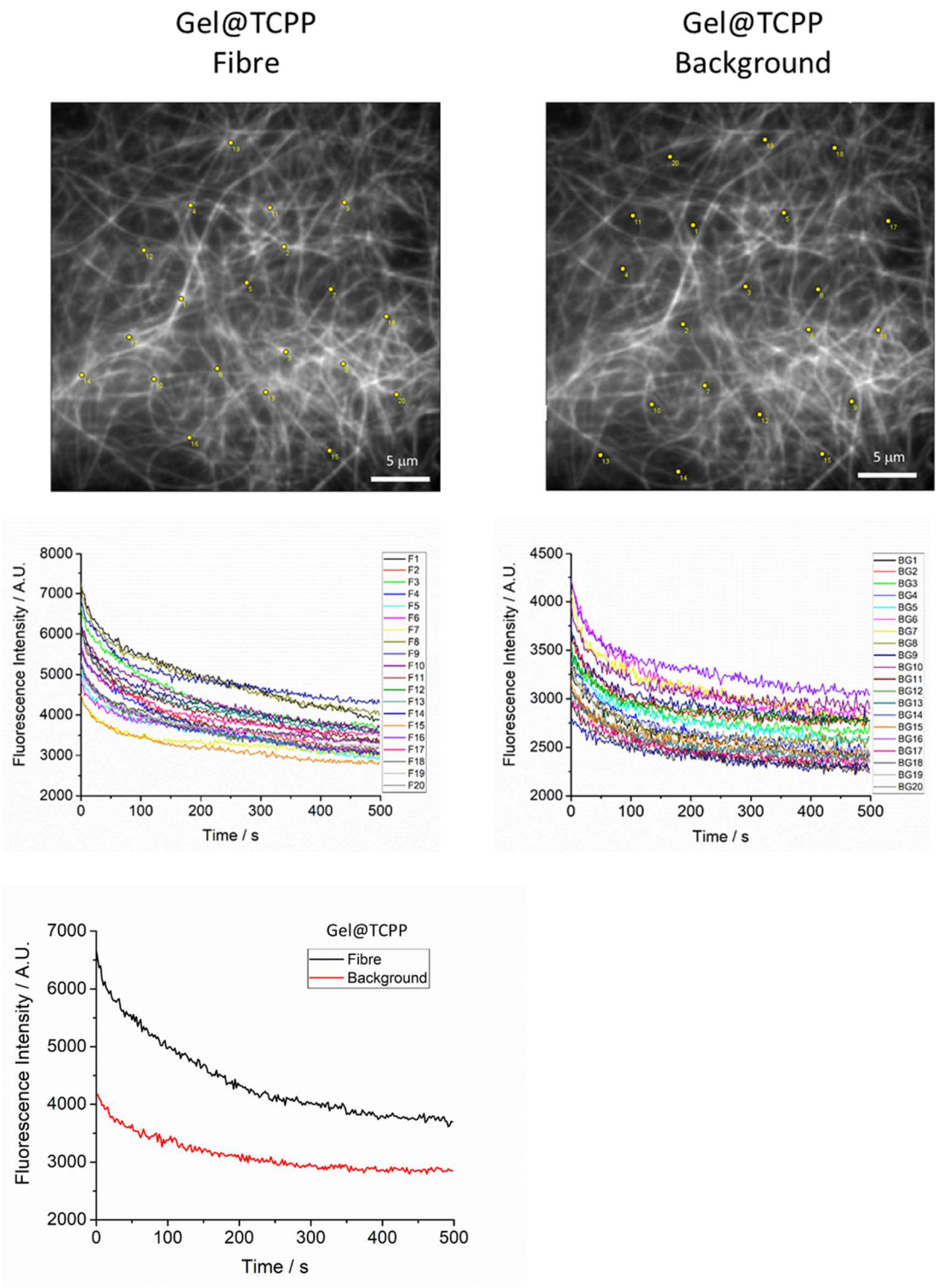

Figure S15. A TIRF micrograph (top) showing Gel@TCPP in 5:5 water: corresponding to the start of Movie S10, and the points where the loss of fluorescence intensity was measured to produce the fluorescence intensity versus time plots for fibres and background (middle). A representative trace is compared with a representative background area (bottom). Scale bar represent 5 □m.

Gel@TCPP

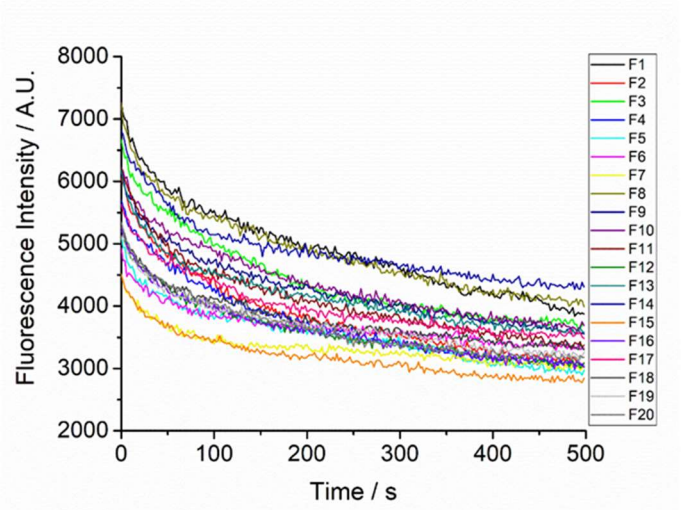

Gel@TCPP@Azo
Starting *trans:cis* 90:10

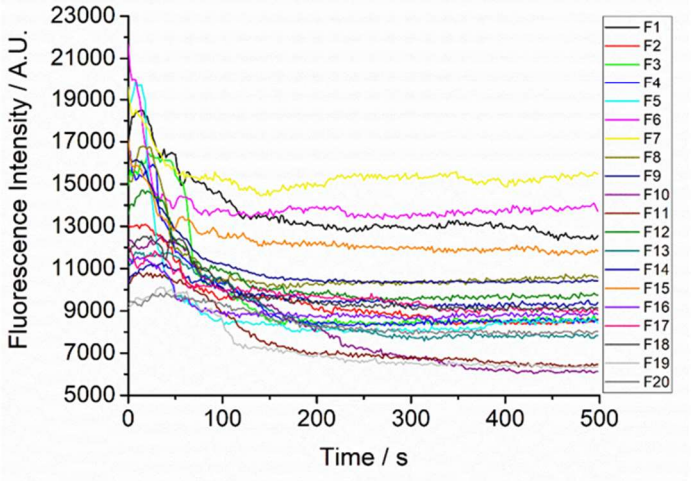

Gel@TCPP@Azo
Starting *trans:cis* 35:65

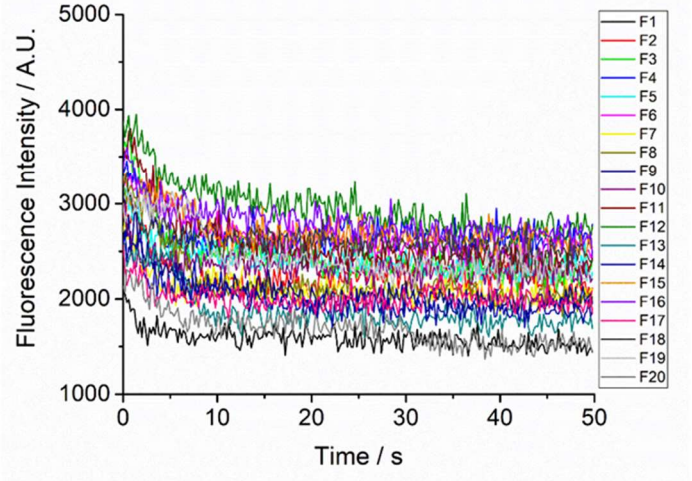

Figure S16. Comparison of the decreases in fluorescence in the fibres in Gel@TCPP, Gel@TCPP@Azo 90:10 *trans:cis* and Gel@TCPP@Azo 35:65 all in 5:5 water:ethanol under continuous TIRF irradiation at 405 nm.

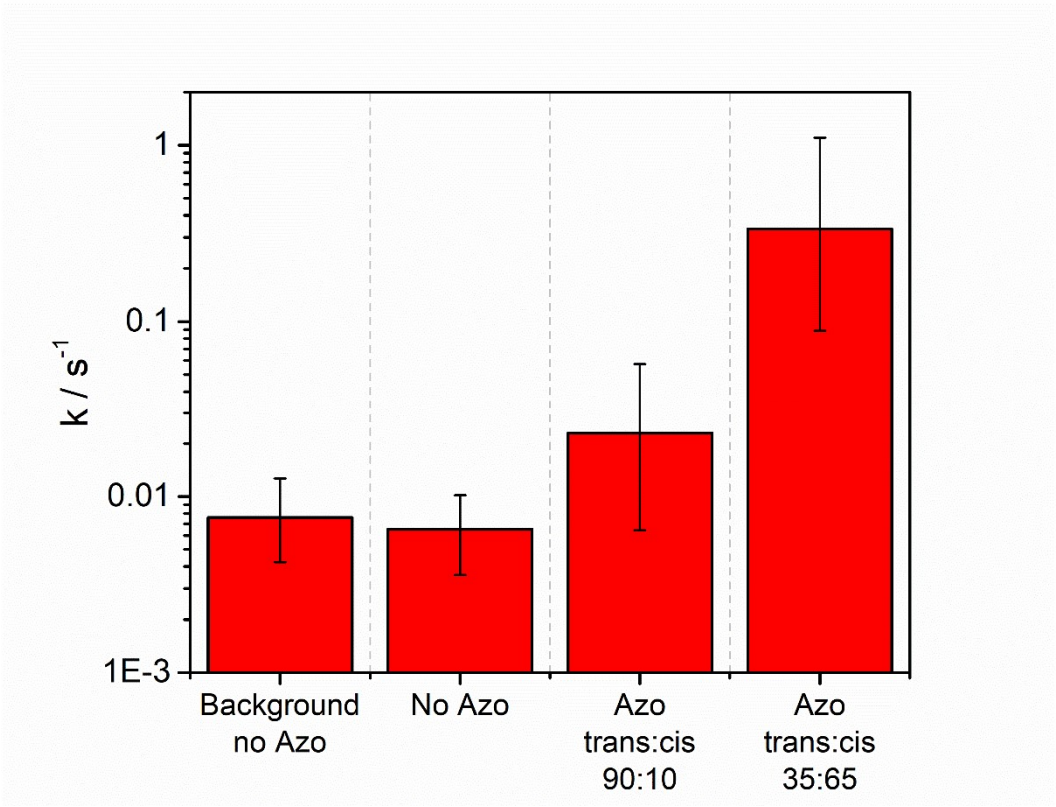

Figure S17. Comparison of the rate constants obtained from an exponential decay function fitting of the traces of time evolution of the fluorescence intensity on the fibres and background in the TIRF experiments under continuous TIRF irradiation at 405 nm for Gel@TCPP, Gel@TCPP@Azo 90:10 *trans*:*cis* and Gel@TCPP@Azo 35:65 all in 5:5 water:ethanol (taken from the data in Table S5).

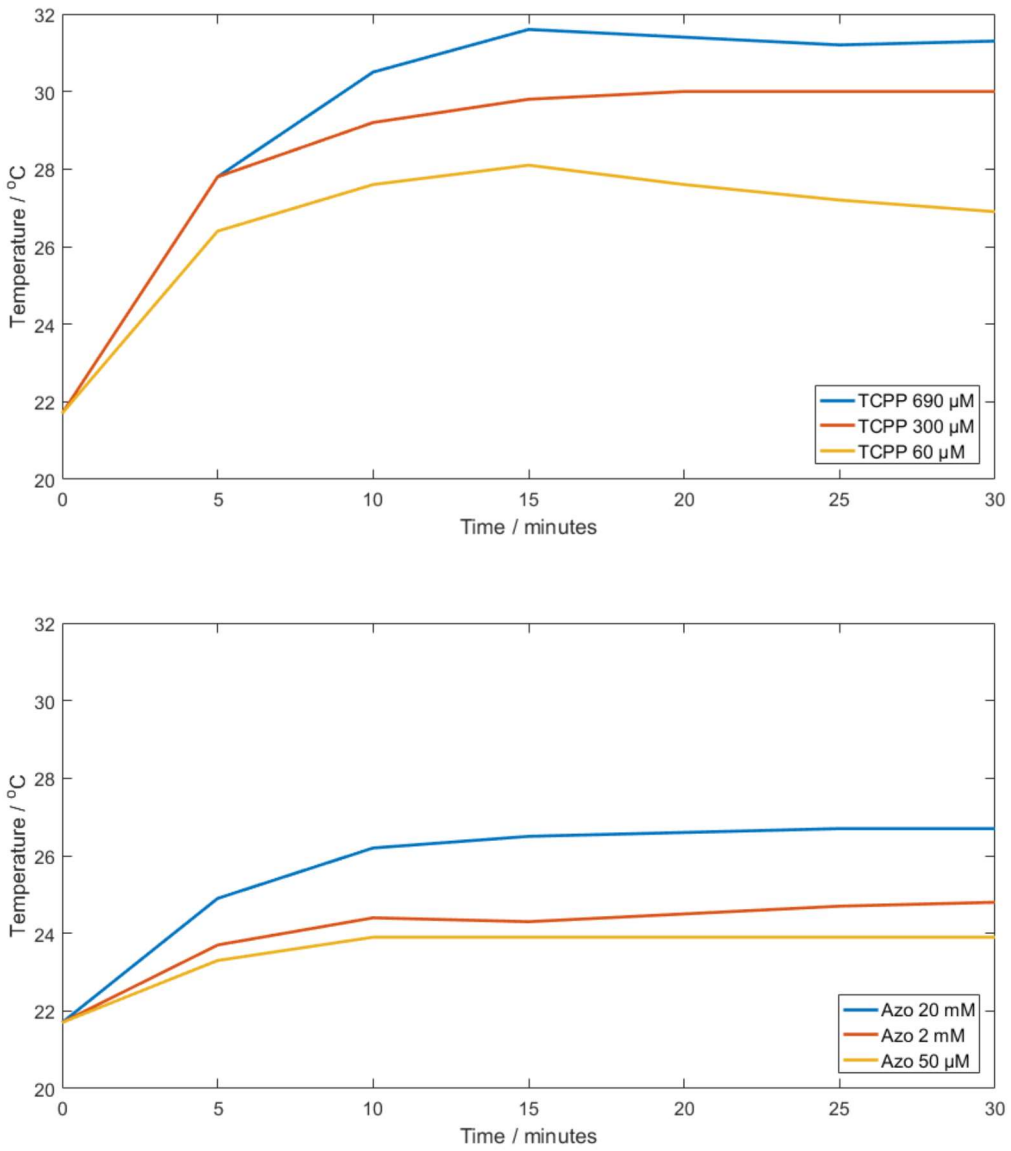

Figure S18. Photothermal effect of the sodium salt of TCPP in distilled water and of Azo in ethanol at varying concentrations under irradiation with a long pass 395 nm filter using a solar simulator (Power density 300 $mWcm^{-2}$). The measurements are corrected for an equivalent measurement using pure solvent to generate a background that has been removed from each point.

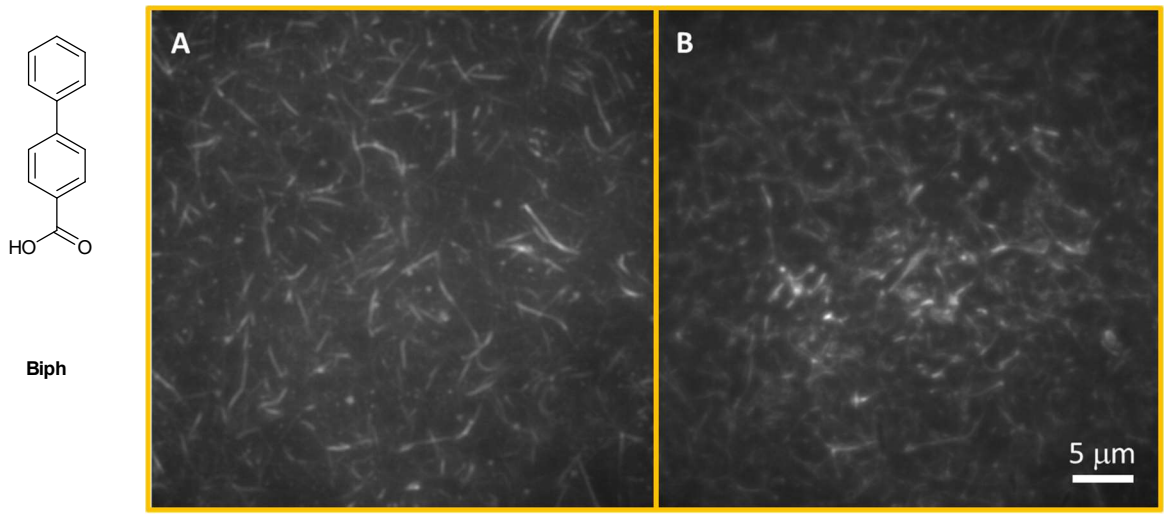

Figure S19. TIRF micrographs of the gel formed in 7:3 water:ethanol by a mixture containing 8 mM 1·2Br, 60 mM TCPP and 2 mM Biph (see structure above), taken from Movie S14. Image A shows the sample at the start of the irradiation and image B after 8.3 minutes irradiating at 405 nm. The formation of rings can be observed similarly to the gel where Azo is used in place of Biph, although the proportion of rings is qualitatively far lower in this case. Scale bar represents 5 mm.

Table S1. Storage modulus (*G'*), loss modulus (*G''*) and critical stress of the different gels obtained from stress sweep experiments as function of the incorporated guest and the water:ethanol ratio at 298 K.

Water:Ethanol	Sample	G' (Pa)	G'' (Pa)	Critical Stress (Pa) [a]
5:5	Gel	3440	610	129.6
	Gel@TCPP	6350	1180	130.4
	Gel@Azo	7450	1710	280.6
	Gel@TCPP@Azo	7050	1680	181.5
7:3	Gel	27000	5030	380.3
	Gel@TCPP	35500	5250	417.5
	Gel@Azo	26700	4350	420.3
	Gel@TCPP@Azo	27800	2600	392.3

[a] The critical stress is defined as the shear stress value at the cross-over point between storage and loss moduli.

Table S2. *Trans/cis* isomeric ratio of Azo and Azo+TCPP in water:ethanol 7:3 solution under light irradiation after 30 minutes at different wavelengths,[a] obtained from UV-Vis absorption spectra at 298 K. See Figures S9 S10 for spectra.

Sample	*trans/cis* ratio					
	Day-light	365 nm	405 nm	488 nm	561 nm	642 nm
Azo	90:10	0:100[b]	92:8	95:5	90:10	90:10
Azo@TCPP	90:10	0:100[b]	99:1	92:7	90:10	90:10

[a] Samples were irradiated using a fluorometer as light source, with excitation bandwidth of 8 nm.

[b] These reference values were obtained after 60 minutes of irradiation at the photostationary state.

Table S3. *Trans/cis* isomeric ratio obtained from UV-Vis absorption spectra of Azo and Azo+TCPP in water:ethanol 7:3 solution under light irradiation after 30 minutes with a solar simulator at 300 mW/cm² equipped with different long-pass (LP) filters and a 10-mm thick water filter. See Figures S11 S12 for spectra.

Sample	*trans/cis* ratio						
	Daylight	LP 395 nm	LP 455 nm	LP 495 nm	LP 550 nm	LP 590 nm	LP 645 nm
Azo	90:10	88:12	80:20	77:23	92:8	90:10	90:10
Azo@TCPP	90:10	86:14	81:19	87:13	100:0	98:2	91:9

Table S4. Photothermal effect of solutions and gel samples in water-ethanol ratio 5:5 and 7:3. The values reported represent the ΔT (in °C) recorded after irradiation for 30 minutes with a solar simulator (300 mW/cm², long-pass filter at 395 nm), when a steady state has been reached (typically after 10 minutes, see Figure S2).

Water:Ethanol ratio	**1·2Br**	**TCPP**		**Azo**		**TCPP@Azo**	
	Gel	*Sol*	*Gel*	*Sol*	*Gel*	*Sol*	*Gel*
5:5	4.3	5.3	8.0	4.5	7.0	6.3	7.3
7:3	2.8	5.6	8.0	4.1	4.9	7.3	10

Note: All values are corrected for the temperature increment recorded for the corresponding pure solvent mixture.

Table S5. Exponential decay rate constant of fluorescence intensity measured over time upon irradiation in Gel@TCPP (background and fibres), and Gel@TCPP@Azo *trans:cis* 90:10 and *trans:cis* 35:65 in water-ethanol 5:5 in the TIRF experiments with continuous irradiation at 405 nm.

Points	k (s^{-1})			
	Background Gel@TCPP	Fibres Gel@TCPP	Azo *trans:cis* 90:10	Azo *trans:cis* 35:65
1	0.00791 + 2.78E-04	0.00411 ± 1.75E-4	0.01739 ± 3.90E-4	0.7533 ± 0.117
2	0.00677 ± 3.30E-04	0.00686 ± 1.53E-4	0.01292 ± 5.31E-4	0.3555 ± 0.032
3	0.00624 ± 2.87E-04	0.00674 ± 1.04E-4	0.03492 ± 8.33E-4	0.2463 ± 0.013
4	0.00821 ± 2.60E-04	0.00602 ± 1.16E-4	0.01657 ± 3.82E-4	0.4724 ± 0.048
5	0.00811 ± 3.12E-04	0.00358 ± 2.43E-4	0.05289 ± 0.00128	0.2235 ± 0.021
6	0.00819 ± 1.92E-04	0.00758 ± 3.34E-4	0.05724 ± 0.00159	0.1243 ± 0.009
7	0.00599 ± 3.02E-04	0.01020 ± 4.38E-4	0.03888 ± 0.00188	0.4223 ± 0.044
8	0.00652 ± 4.16E-04	0.00504 ± 1.76E-4	0.04674 ± 0.00101	0.2063 ± 0.010
9	0.00564 ± 4.11E-04	0.00576 ± 1.82E-4	0.02319 ± 1.39E-4	0.2375 ± 0.016
10	0.00617 ± 4.02E-04	0.00520 ± 1.34E-4	0.00642 ± 1.42E-4	1.1050 ± 0.199
11	0.00827 ± 2.42E-04	0.00665 ± 1.91E-4	0.01269 ± 2.78E-4	0.1643 ± 0.008
12	0.00712 ± 4.38E-04	0.00631 ± 1.80E-4	0.01995 ± 3.75E-4	0.0885 ± 0.006
13	0.00931 ± 3.32E-04	0.00712 ± 2.53E-4	0.01065 ± 2.46E-4	0.3756 ± 0.030
14	0.00651 ± 3.57E-04	0.00853 ± 2.70E-4	0.01317 ± 3.40E-4	0.1287 ± 0.011
15	0.00424 ± 4.34E-04	0.00687 ± 2.49E-4	0.02258 ± 6.52E-4	0.3240 ± 0.039
16	0.00833 ± 3.43E-04	0.00623 ± 2.03E-4	0.03057 ± 9.10E-4	0.1089 ± 0.011
17	0.01265 ± 3.58E-04	0.00762 ± 1.62E-4	0.00766 ± 3.48E-4	0.3917 ± 0.067
18	0.00881 ± 3.59E-04	0.00707 ± 2.21E-4	0.01346 ± 4.46E-4	0.2845 ± 0.036
19	0.00776 ± 2.95E-04	0.00601 ± 2.39E-4	0.01322 ± 3.40E-4	0.4171 ± 0.041
20	0.00938 ± 3.09E-04	0.00678 ± 1.60E-4	0.00867 ± 2.96E-4	0.2935 ± 0.033

Table S6. Fluorescence intensity measurements before (BI) and after irradiation (AI) at 405 nm for the experiment reported in Movie S3 performed on Gel@TCPP@Azo in water-ethanol 5:5

Points	Fibres outside the irradiated area		% Variation	Fibres inside the irradiated area		% Variation	Background irradiated area		% Variation
	BI	AI		BI	AI		BI	AI	
1	2906	4504	+55.0	3767	2510	-33.4	1501	1628	+8.5
2	1974	3328	+68.6	5222	2946	-43.6	1455	1663	+14.3
3	3186	4437	+39.3	6281	2625	-58.2	1432	1595	+11.4
4	2777	3855	+38.8	5090	2366	-53.5	1799	1825	+1.4
5	2597	3754	+44.6	4543	2017	-55.6	1726	1917	+11.1
6	2905	4008	+38.0	4306	1794	-58.3	1711	1816	+6.1
7	2410	3600	+49.4	4880	2613	-46.5	1749	1870	+6.9
8	1681	2486	+47.9	5263	2302	-56.3	1655	1751	+5.8
9	2682	3281	+22.3	4240	2166	-48.9	1745	1753	+0.5
10	3591	4408	+22.8	4263	2016	-52.7	1796	1904	+6.0
11	1859	2869	+54.3	5136	2159	-58.0	1777	1904	+7.1
12	1756	2538	+44.5	4261	1950	-54.2	1808	1885	+4.3
13	2131	3000	+40.8	4041	1999	-50.5	1646	1751	+6.4
14	2021	2952	+46.1	8114	2399	-70.4	1500	1661	+10.7
15	2047	3470	+69.5	6397	2544	-60.2	1770	1914	+8.1
16	1700	2773	+63.1	3729	1918	-48.6	1663	1814	+9.1
17	2490	3448	+38.5	5929	2274	-61.6	1664	1769	+6.3
18	2214	3656	+65.1	5451	2537	-53.5	1938	2084	+7.5
19	2318	2915	+25.8	5152	2201	-57.3	1872	1963	+4.9
20	1985	2655	+33.8	5109	2277	-55.4	1759	1870	+6.3

21	3391	4206	+24.0	4259	2421	-43.2	1491	1575	+5.6
22	2062	2495	+21.0	5927	2615	-55.9	1847	1877	+1.6
23	1665	2776	+66.7	4873	2310	-52.6	1811	1944	+7.3
24	1348	2042	+51.5	5338	2480	-53.5	1853	1962	+5.9
25	2006	2440	+21.6	4408	2302	-47.8	1795	1970	+9.7
26	1065	1707	+60.3	5312	1708	-67.8	1859	2005	+7.9
27	1542	2316	+50.2	4652	2134	-54.1	1541	1685	+9.3
28	1208	2082	+72.4	4372	2956	-32.4	1383	1529	+10.6
29	1378	2246	+63.0	3781	2392	-36.7	1373	1483	+8.0
30	1594	2358	+47.9	3568	2328	-34.8	1396	1478	+5.9
31	1443	2105	+45.9	4619	2679	-42.0	1436	1572	+9.5
32	1940	2658	+37.0	3890	2257	-42.0	1526	1706	+11.8
33	1453	2067	+42.3	3742	2268	-39.4	1400	1551	+10.8
34	2252	2961	+31.5	4056	2225	-45.1	1665	1666	+0.1
35	1970	2730	+38.6	4668	2353	-49.6	1704	1765	+3.6
36	1696	2817	+66.1	5026	2197	-56.3	1542	1643	+6.5
37	1955	2776	+42.0	4970	2620	-47.3	1409	1513	+7.4
38	1555	2367	+52.2	4654	2600	-44.1	1683	1846	+9.7
39	1870	2857	+52.8	3803	2124	-44.1	1268	1375	+8.4
40	2010	2888	+43.7	4136	2453	-40.7	1314	1442	+9.7
41	2072	3189	+53.9	3750	2094	-44.2	1686	1708	+1.3
42	1764	2648	+50.1	4136	1983	-52.1	1634	1769	+8.3
43	1789	2692	+50.5	4135	2009	-51.4	1518	1598	+5.3
44	1207	1981	+64.1	3252	1699	-47.8	1710	1841	+7.7
45	1978	2619	+32.4	3900	2282	-41.5	1417	1530	+8.0
46	1943	2854	+46.9	3004	2019	-32.8	1418	1498	+5.6

47	1696	2527	+49.0	3013	1939	-35.6	1211	1390	+14.8
48	1997	2611	+30.7	3324	2002	-39.8	1221	1407	+15.2
49	1087	1764	+62.3	3528	2062	-41.6	1442	1544	+7.1
50	1672	2611	+56.2	2936	1986	-32.4	1307	1443	+10.4

Synthesis of naphthalimide labelled amphiphile 2.2Br

The overall synthetic route to the naphthalimide-containing compound **2**.2Br is shown in Scheme S1.

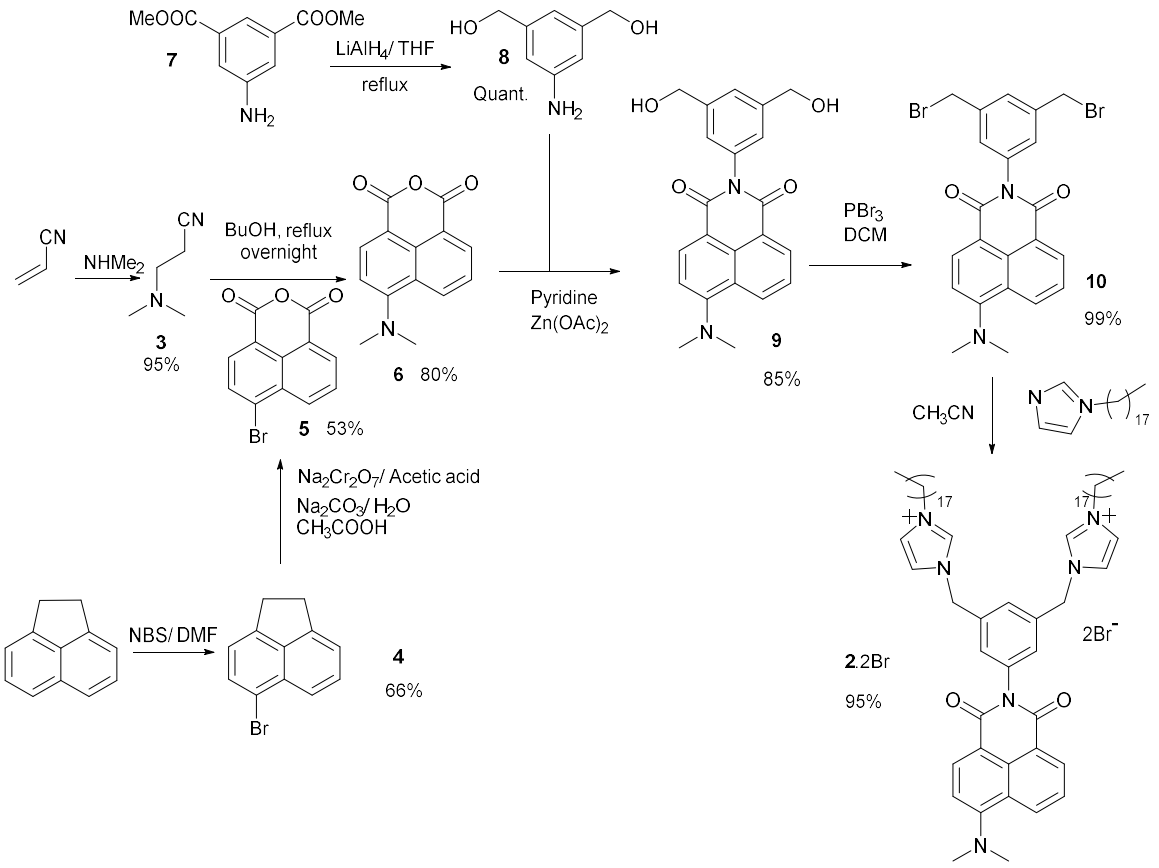

Scheme S1: Overall synthetic route to **2**.2Br.

General Characterisation Methods

NMR spectra were acquired on a Bruker AV400, Bruker AV(III)500 or Bruker DPX300 spectrometers and NMR spectra were recorded at room temperature. All chemical shifts are reported in δ parts per million (ppm), using the solvent residual signal as an internal standard and the coupling constant values (J) are reported in Hertz (Hz). ESI-MS were recorded using a Bruker micro-TOF II instrument. Infra-red spectra were recorded on a Bruker Tensor 27 instrument equipped with a Pike GladiATR attachment with a diamond crystal.

Synthesis of 3-dimethylaminopropionitrile (3) [1]

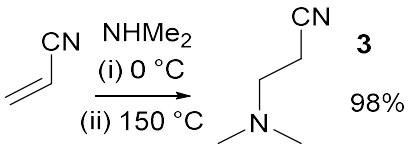

Scheme S2: Synthesis of ***3***.

Following a literature procedure,[1] acrylonitrile (6.5 ml, 0.1 mol) was added dropwise in an ice cold 40% aqueous solution of dimethyl amine (11.8 g, 0.105 mol) at 0°C under stirring condition for 3 hours (Scheme S2). After the addition, stirring was continued for 2 hours at 150°C. The product was extracted in chloroform. After removal of solvent, ***3*** was distilled out under vacuum (20 mmHg for 80 °C) as colourless liquid (9.6 g, 98% yield) that was used without further purification.

Synthesis of 5-bromo-1,2-dihydroacenaphthylene (4) [2]

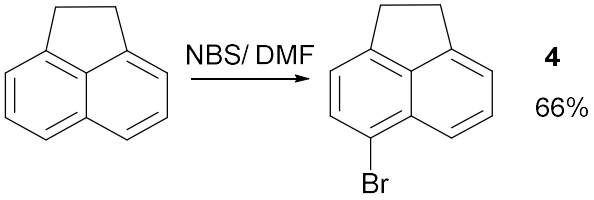

Scheme S3: Synthesis of **4**.

Adapting a literature protocol,[2] a suspension of 10 g (65 mmol) 1,2 dihydroacenaphthylene in 35 ml of DMF under continuous stirring the solution of 11.3 g (64 mmol) *N*-bromosuccinimide (NBS) in 35 ml of DMF was added drop by drop during 30 minutes (Scheme S3). After the addition of the solution was completed, the reaction mixture was stirred for another 2 hours at room temperature and then was poured into 1L of ice-water. Formed precipitate was separated by filtration and washed in the filter with ethanol. The product was purified by crystallization from methanol (10 g, 66% yield). ^{1}H NMR (500 MHz, DMSO-d_6) δ 7.70 (d, J = 7.3 Hz, 1H), 7.67 – 7.51 (m, 2H), 7.38 (d, J = 6.7 Hz, 1H), 7.25 – 7.12 (m, 1H), 3.41 – 3.31 (m, 2H), 3.28 (dt, J = 10.2, 3.4 Hz, 2H) ppm. ^{13}C NMR (126 MHz, DMSO-d_6) δ 146.85, 146.63, 140.21, 131.38, 130.53, 129.99, 121.30, 120.91, 120.89, 30.60, 29.88 ppm.

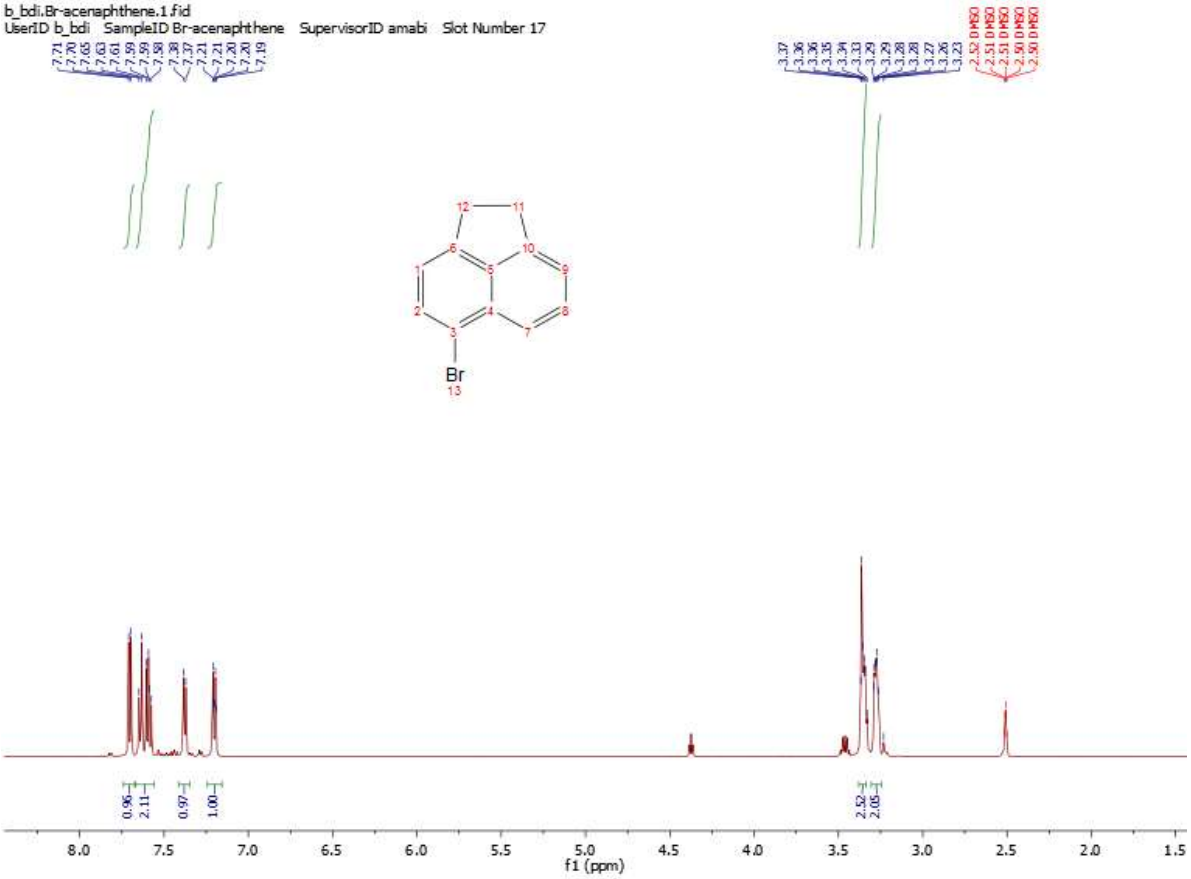
b_bdi.Br-acenaphthene.1.fid
UserID b_bdi SampleID Br-acenaphthene SupervisorID amabi Slot Number 17
7.71
7.70
7.65
7.63
7.61
7.59
7.59
7.58
7.38
7.37
7.21
7.21
7.20
7.20
7.19
3.37
3.36
3.36
3.35
3.34
3.33
3.29
3.29
3.28
3.28
3.27
3.26
3.23
2.52 DMSO
2.51 DMSO
2.51 DMSO
2.50 DMSO
2.50 DMSO
12
11
6
5
10
9
1
2
4
8
3
7
Br
13
0.96
2.11
0.97
1.00
2.52
2.05
8.0
7.5
7.0
6.5
6.0
5.5
5.0
4.5
4.0
3.5
3.0
2.5
2.0
1.5
f1 (ppm)

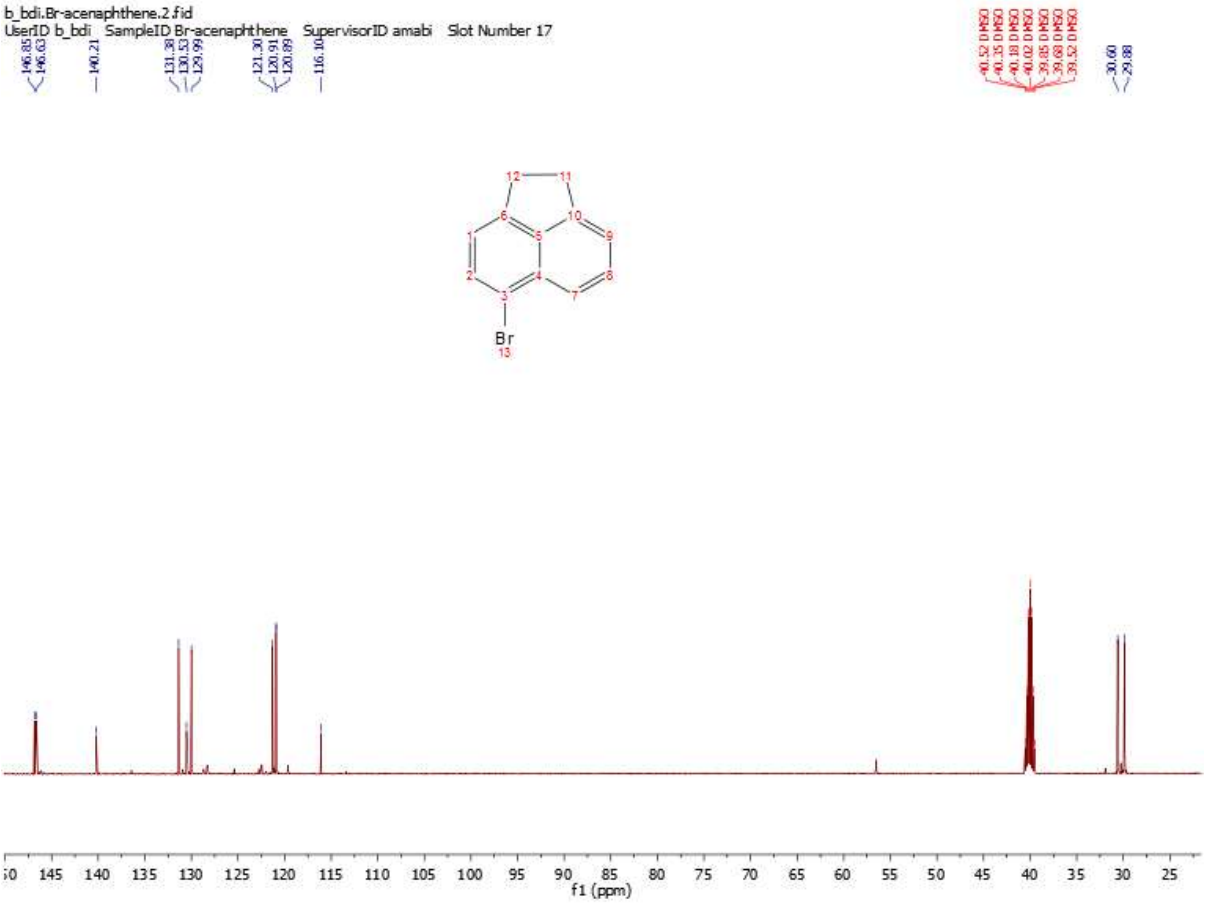
b_bdi.Br-acenaphthene.2.fid
UserID b_bdi SampleID Br-acenaphthene SupervisorID amabi Slot Number 17
146.85
146.63
140.21
131.38
130.53
129.99
121.30
120.91
120.89
116.10
40.52 DMSO
40.35 DMSO
40.18 DMSO
40.02 DMSO
39.85 DMSO
39.68 DMSO
39.52 DMSO
30.60
29.88
12
11
6
5
10
9
1
2
4
8
3
7
Br
13
145
140
135
130
125
120
115
110
105
100
95
90
85
80
75
70
65
60
55
50
45
40
35
30
25
f1 (ppm)

Synthesis of 6-bromo-1H,3H-benzo[de]isochromene-1,3-dione (5) [3]

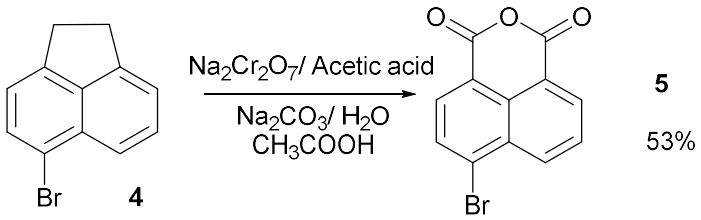

Scheme S4: Synthesis of ***5***.

A stirred mixture of 5-bromoacenapthene (**4**, 8 g, 34 mmol) and acetic acid (100 ml) was heated to 90 °C (Scheme S4) and of $Na_2Cr_2O_7.2H_2O$ (50 g, 0.17 mol) was added carefully (CAUTION, exothermic reaction) in small portions to keep temperature not higher than 90°C.[3] The reaction was then heated to reflux and kept at reflux for 5.5 hours. The reaction mixture was allowed to cool to room temperature and was poured into 750 ml of water. The precipitate formed was suspended in Na_2CO_3 (aq, 10%, 500 ml) and boiled for 1 hour. Cooling to room temperature gave a precipitate of 4-bromonaphthalic acid that was filtered, washed with water and dried. The anhydride ***5*** was formed during recrystallization from acetic acid. The product was obtained as grey solid (5 g, 53% yield). ^{1}H NMR (500 MHz, DMSO-d_6) δ 8.57 (dd, J = 8.1, 5.0 Hz, 2H), 8.33 (dd, J = 7.9, 1.5 Hz, 1H), 8.23 (dd, J = 7.7, 1.5 Hz, 1H), 8.01 (t, J = 7.8 Hz, 1H) ppm. ^{13}C NMR (126 MHz, DMSO-d_6) δ 160.67, 160.62, 134.15, 133.74, 133.04, 132.15, 130.92, 130.77, 130.41, 129.59, 120.21, 119.41 ppm.

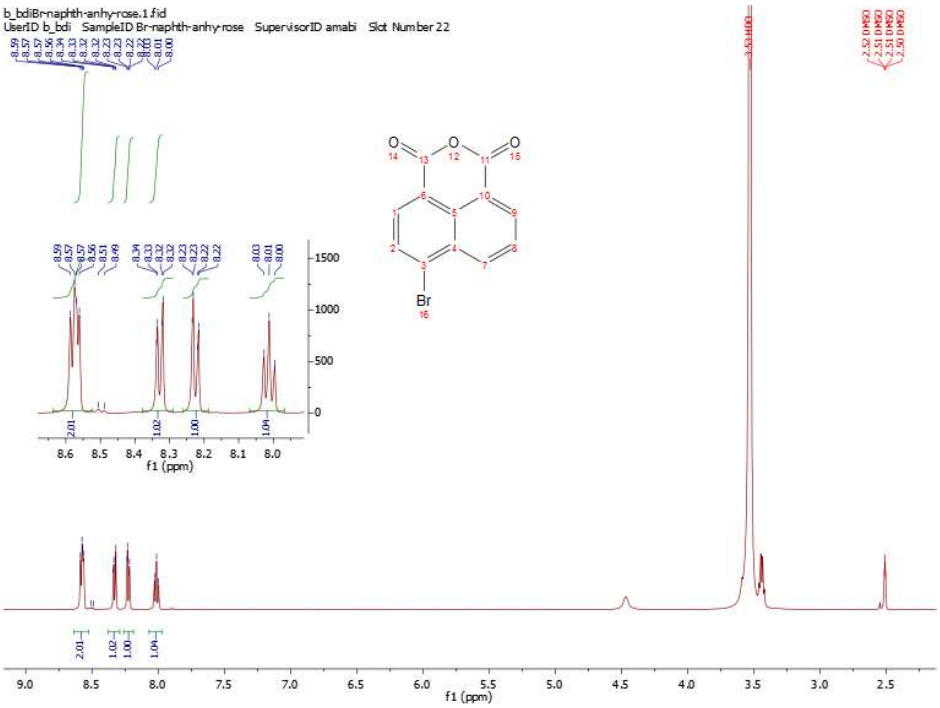

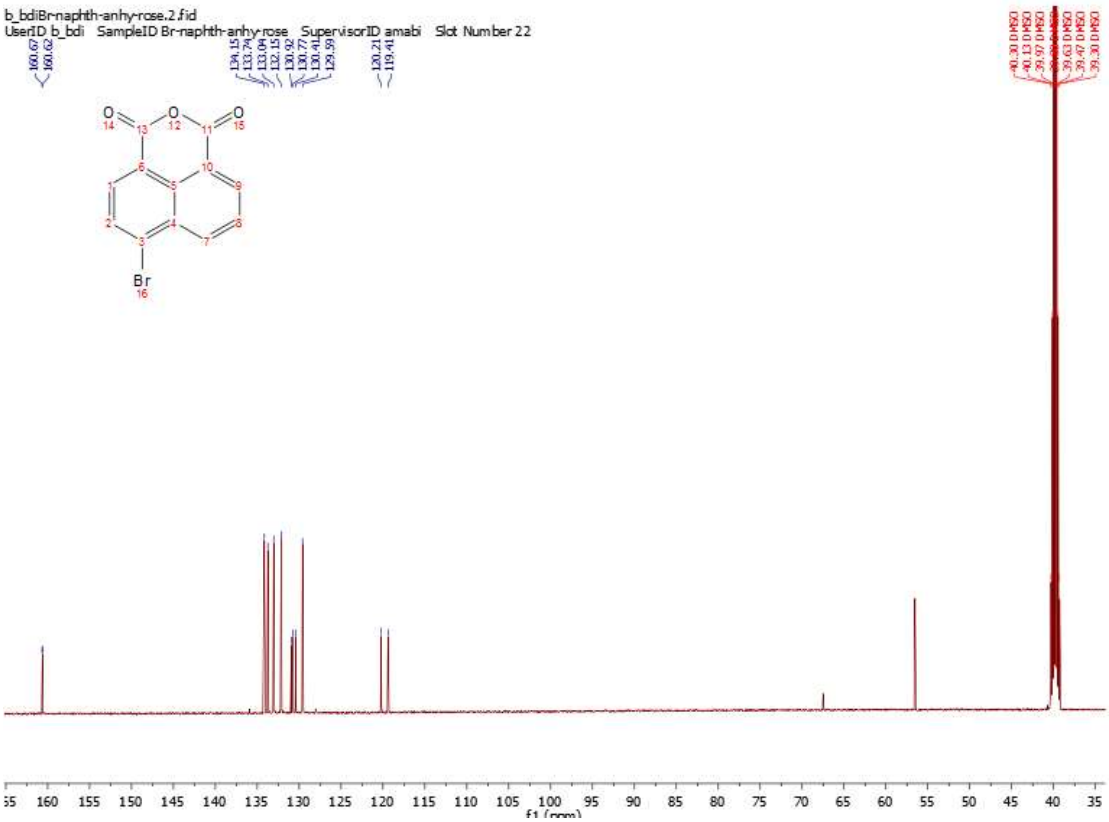
b_bdiBr-naphth-anhy-rose.2.fid
UserID b_bdi SampleID Br-naphth-anhy-rose SupervisorID amabi Slot Number 22
160.67
160.62
134.15
133.74
133.04
132.15
130.92
130.77
130.41
129.59
120.21
119.41
40.30 DMSO
40.13 DMSO
39.97 DMSO
39.80 DMSO
39.63 DMSO
39.47 DMSO
39.30 DMSO
O
O
O
Br
f1 (ppm)

Synthesis of 6-(dimethylamino)-1H,3H-benzo[de]isochromene-1,3-dione (6) [4]

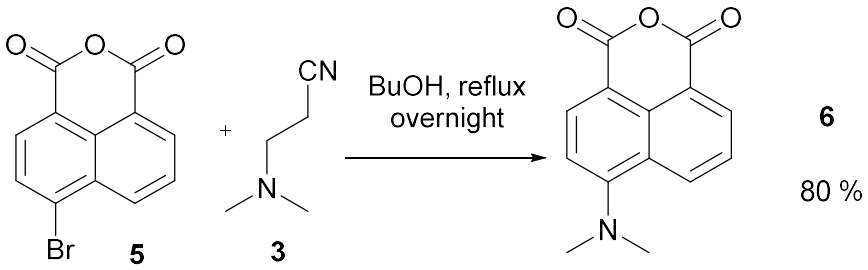

Scheme S5: Synthesis of **6**.

Using a modified protocol based on the literature,[4] a solution of 4-bromo-naphthalic anhydride (**5**, 2 g, 7.2 mmol) in *n*-butanol (100 ml) in a round-bottom flask equipped with reflux condenser (Scheme S5) was brought to reflux and 3.14 ml of 3-*N*,*N*-dimethylaminopropionotrile was added slowly. The reaction mixture was stirred at reflux overnight and cooled with an ice bath until the formation of yellow fluorescent precipitate. The solid was filtrated and washed with *n*-hexane to give the desired product **6** as a yellow solid (1.4 g, 80% yield). ^{1}H NMR (400 MHz, Chloroform-*d*) δ 8.53 (ddd, *J* = 22.4, 7.9, 1.2 Hz, 2H), 8.44 (d, *J* = 8.3 Hz, 1H), 7.69 (dd, *J* = 8.5, 7.3 Hz, 1H), 7.11 (d, *J* = 8.4 Hz, 1H), 3.20 (s, 6H) ppm. ^{13}C NMR (101 MHz, Chloroform-*d*) δ 161.66, 160.69, 157.89, 134.94, 124.95, 124.80, 119.16, 113.14, 109.34, 44.59 ppm.

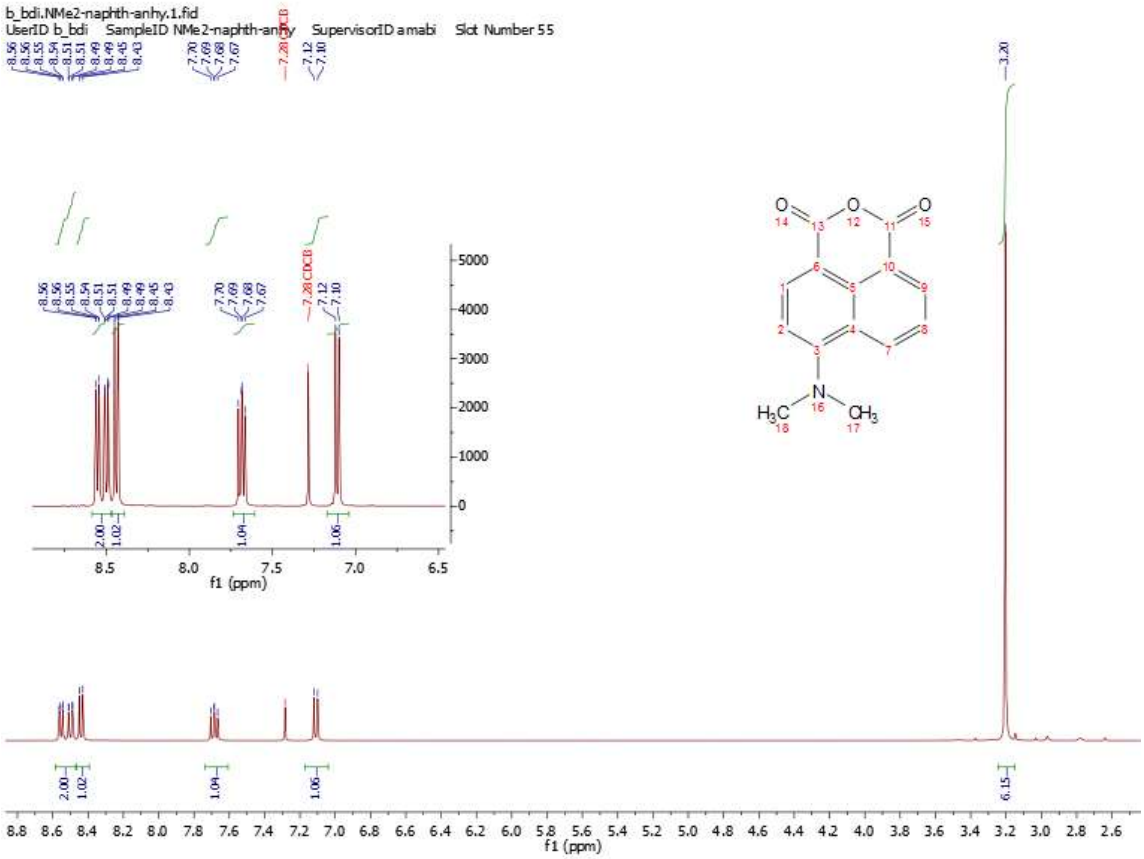

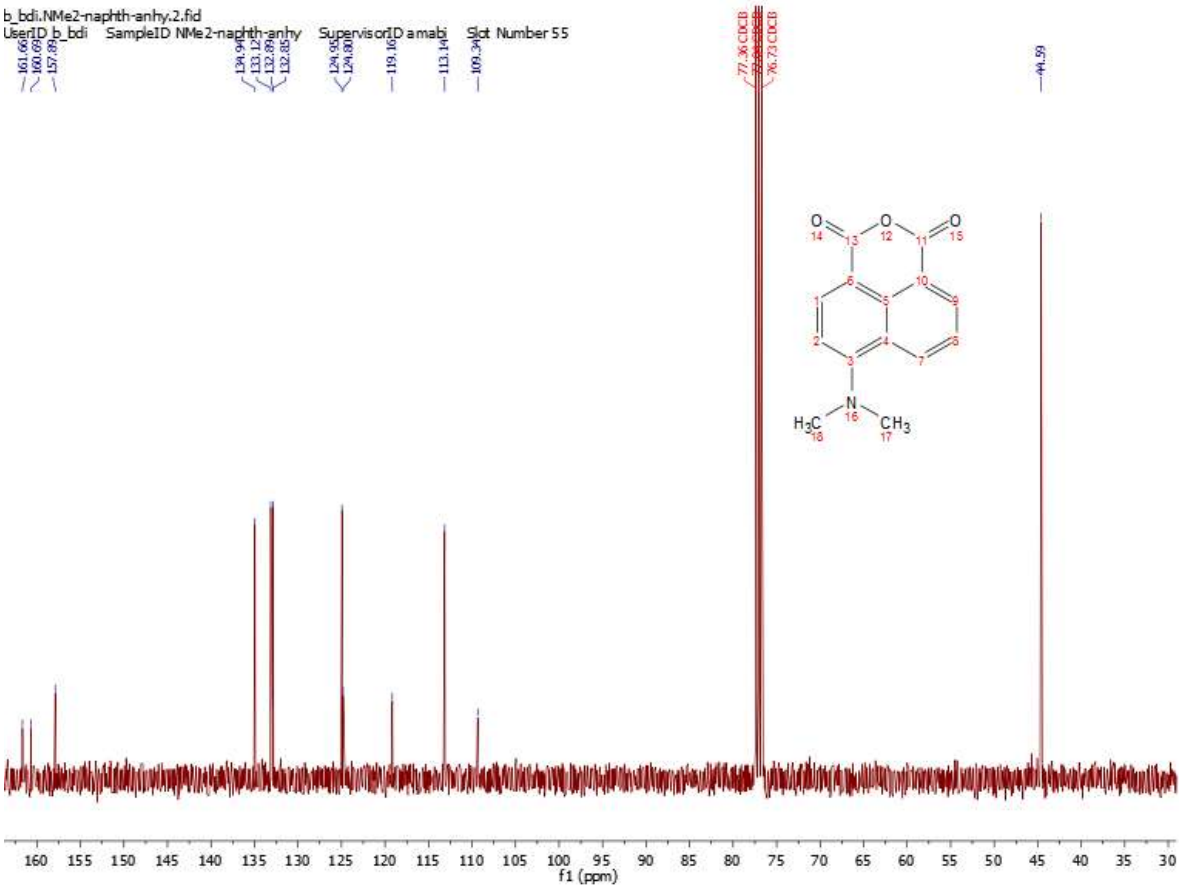

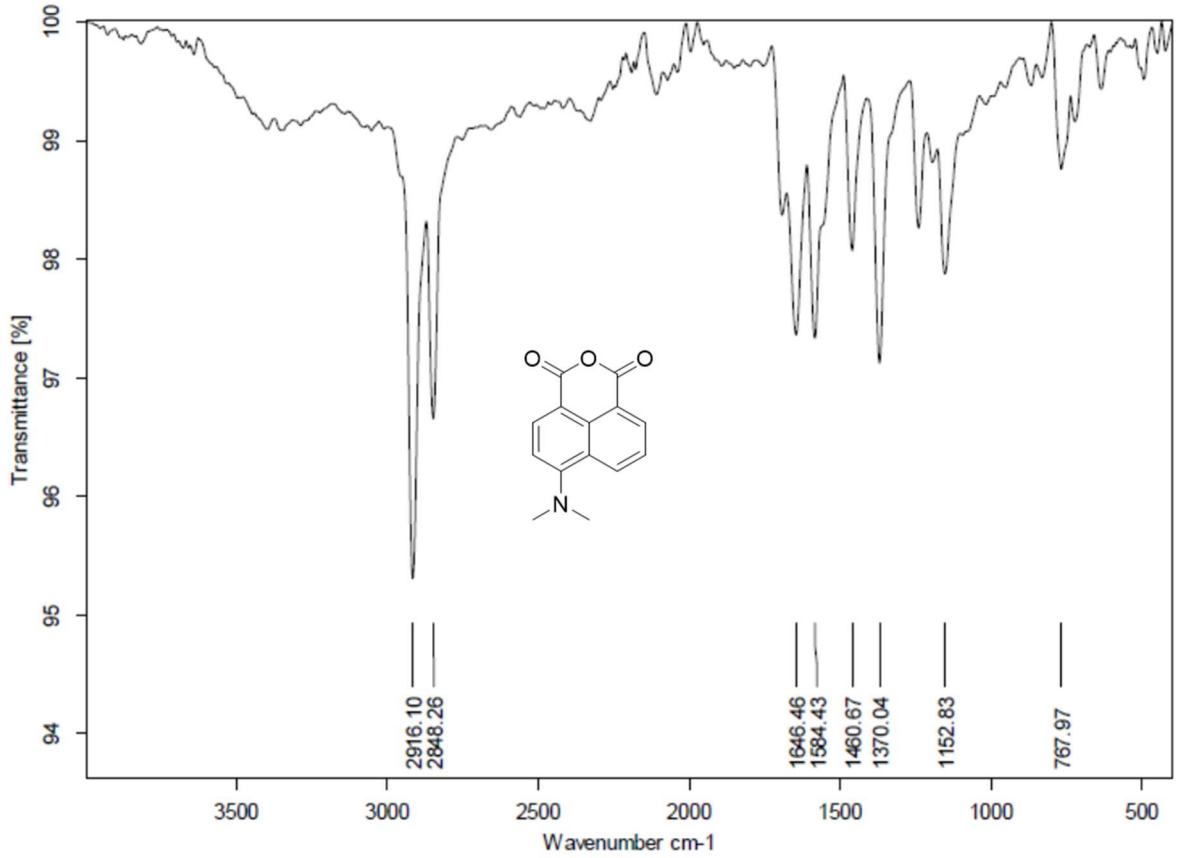

Synthesis of (5-amino-1,3-phenylene)dimethanol (8) *[adapted from reference 5]*

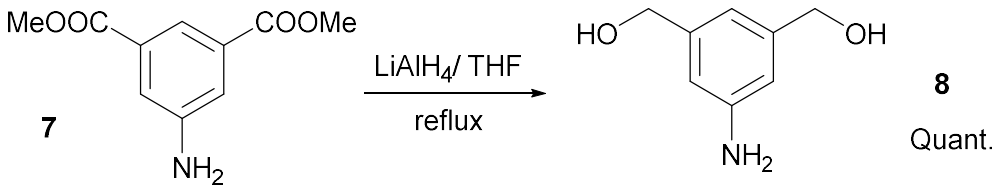

Scheme S6: Synthesis of **8**.

Using a modified literature procedure,[5] a solution of 5-amino-isophthalic acid dimethyl ester (**7**, 2 g, 9.57 mmol) in 20 ml anhydrous THF was slowly added into THF (100 ml) slurry of $LiAlH_4$ (2.2 g, 58 mmol) at 0°C under vigorous stirring (Scheme S6). After stirring at 0°C for 30 minutes, the mixture was allowed to reflux for 14 hours, at which point it was cooled to 0°C. Ethyl acetate (total 20 ml) was then slowly added into the greyish mixture under vigorous stirring to quench excess $LiAlH_4$ and then 15 ml of water was added to hydrolyse the alumina salt. A colour change from greyish to green then yellowish was observed. After stirring for another 1 hour, the resulting slurry was filtrated through a pad of silica gel using coarse frit and washed with several portion of THF (3 × 100 ml). Solvent removal of the combined filtrate and washings afforded a yellow-brownish crude compound. Further purification of **8** was achieved by recrystallization from THF/hexane (1.49 g, quantitative yield). ^{1}H NMR (500 MHz, DMSO-d_6) δ 6.41 (d, J = 3.7 Hz, 3H), 5.01 (br, J = 74.8 Hz, 4H), 4.33 (s, 4H) ppm. ^{13}C NMR (126 MHz, DMSO-d_6) δ 176.55, 148.71, 143.32, 112.90, 111.06, 25.46 ppm.

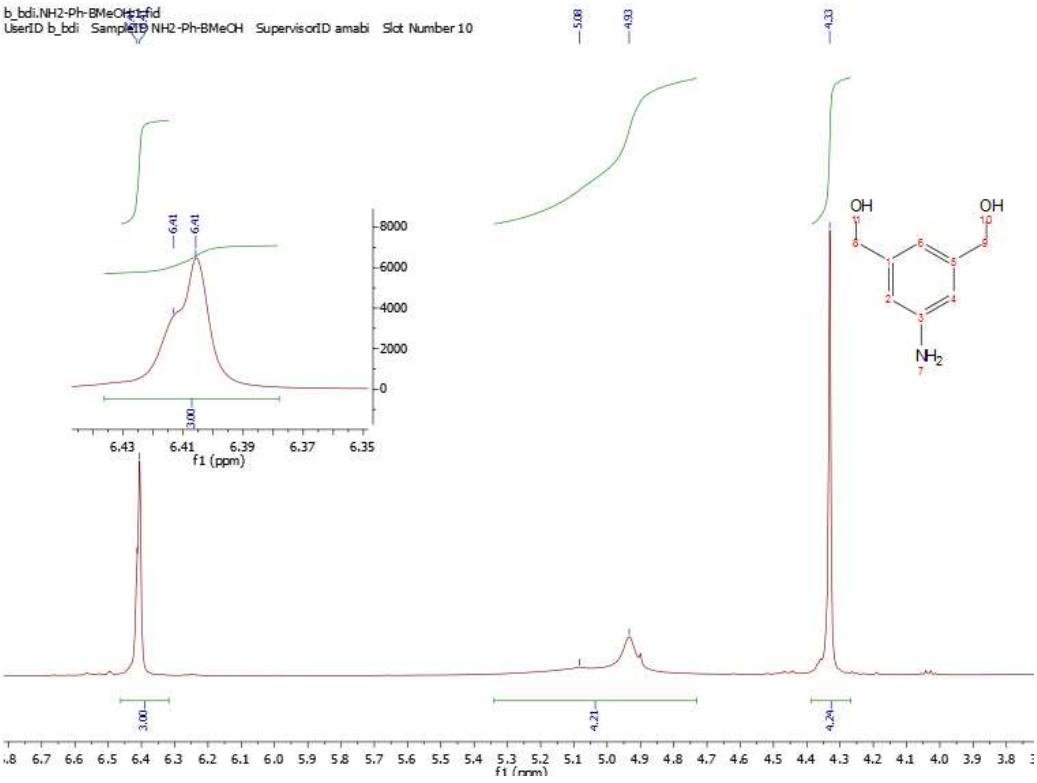

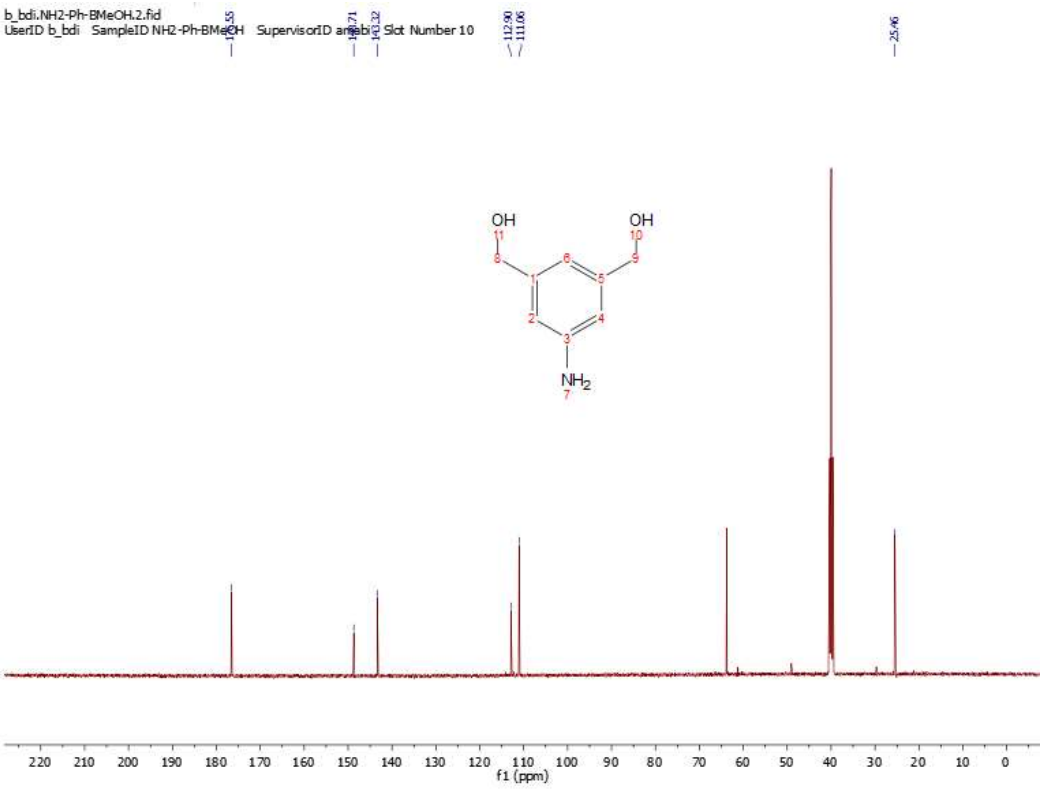
b_bdi.NH2-Ph-BMeOH.2.fid
UserID b_bdi SampleID NH2-Ph-BMeOH SupervisorID ambi Slot Number 10
OH
OH
NH2
f1 (ppm)

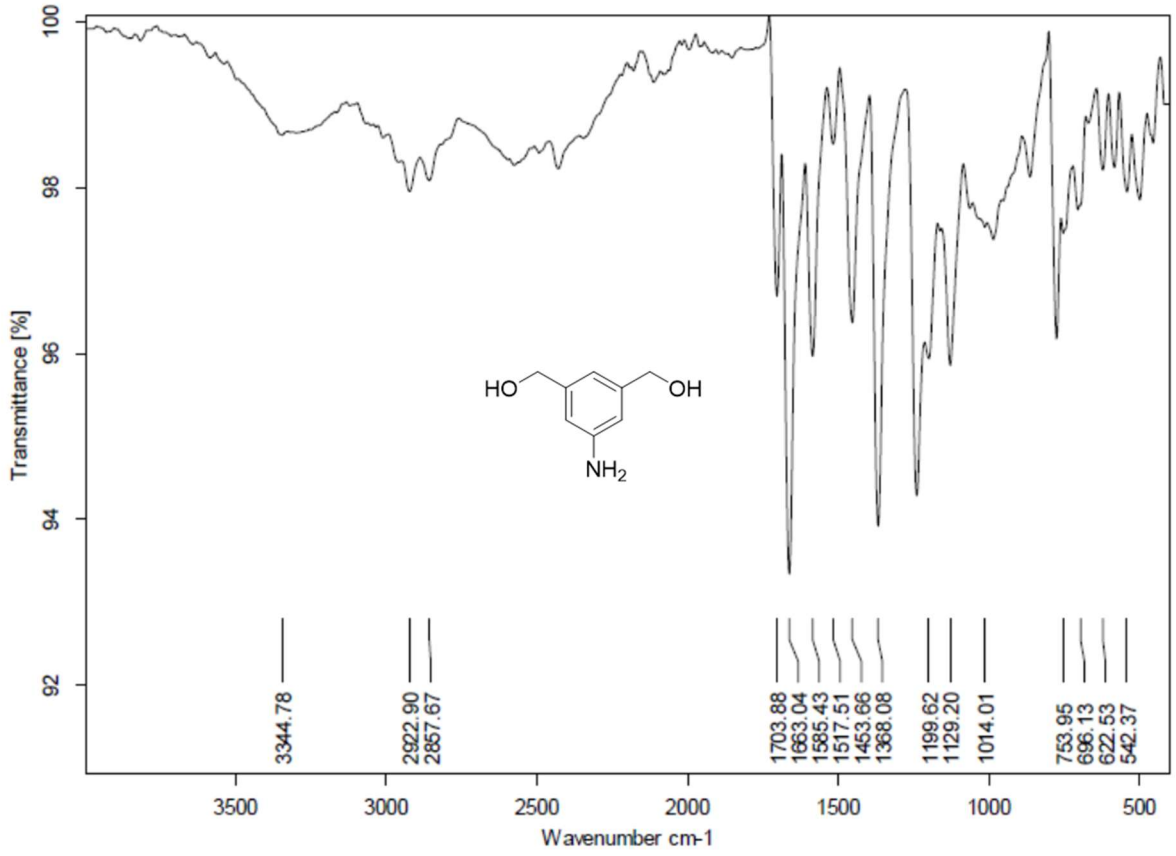
Transmittance [%]
Wavenumber cm-1
HO
OH
NH2
3344.78
2922.90
2857.67
1703.88
1663.04
1585.43
1517.51
1453.66
1368.08
1199.62
1129.20
1014.01
753.95
696.13
622.53
542.37

Synthesis of 2-(3,5-bis(hydroxymethyl)phenyl)-6-(dimethylamino)-1H-benzo[de]isoquinoline-1,3(2H)-dione (9)

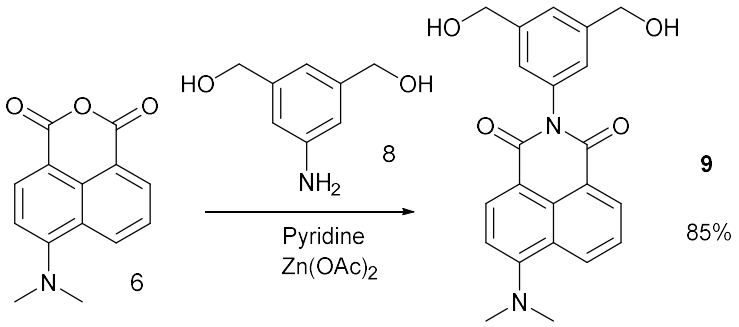

Scheme S7: Synthesis of **9**.

Using a procedure similar to that of a related compound,[6] a solution of (5-amino-1,3-phenylene_dimethanol) (8, 535 mg, 3.52 mmol), 4-*N*,*N*-dimethylamino-1,8naphthalic anhydride (**6**, 560 mg, 2.35 mmol) and $Zn(OAc)_2$ (475 mg, 0.6 mmol) in 10 ml pyridine was refluxed for 30 hours (Scheme S7). After the reaction seemed complete by TLC, the solvent was evaporated. The crude product was purified by column chromatography with DCM: EtOH 95:5 and affording the desirable product as yellow fluorescent solid (754 mg, 85% yield). ESI-MS $[M+H]^+$ 377.1494; calculated for $C_{22}H_{21}N_2O_4$ 377.1501 $[M+H]^+$;. ^{1}H NMR (500 MHz, DMSO-d_6) δ 8.49 (dd, J = 49.8, 7.9 Hz, 2H), 8.32 (d, J = 8.2 Hz, 1H), 7.76 (t, J = 7.9 Hz, 1H), 7.38 (s, 1H), 7.18 (d, J = 5.7 Hz, 3H), 5.32 (d, J = 5.8 Hz, 2H), 4.57 (d, J = 5.7 Hz, 4H), 3.11 (s, 6H) ppm. ^{13}C NMR (126 MHz, DMSO-d6) δ 164.36, 163.70, 157.13, 143.73, 136.38, 132.73, 132.11, 131.06, 130.51, 125.65, 125.48, 124.81, 124.47, 123.24, 114.14, 113.47, 63.07, 44.87 ppm.

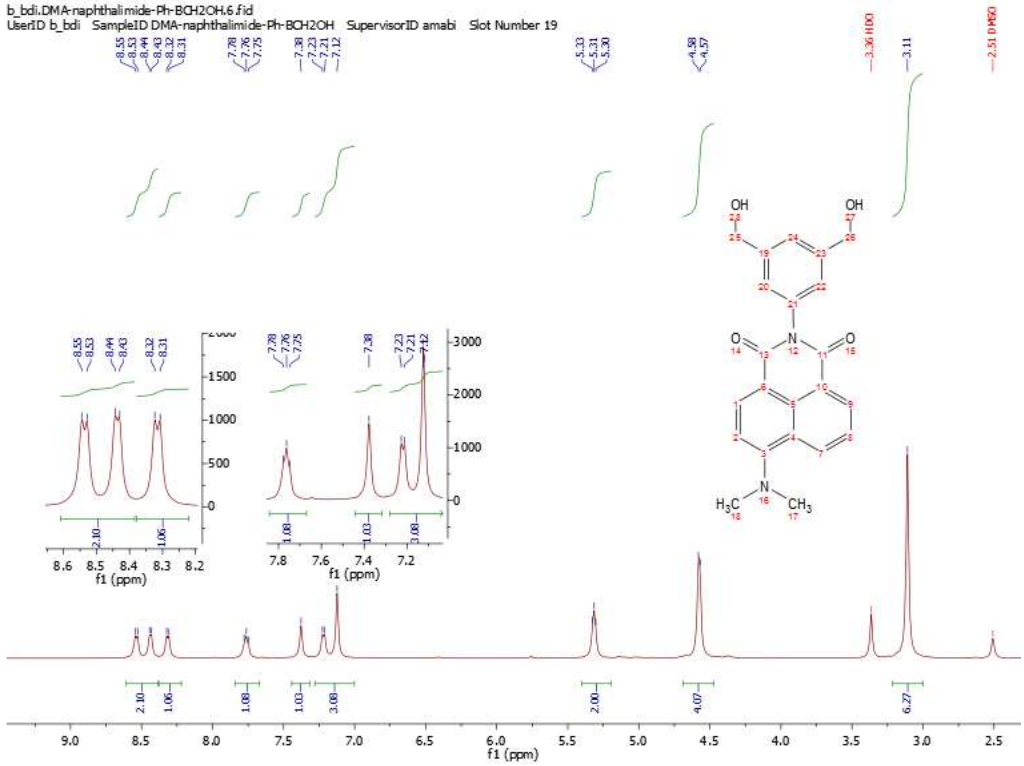

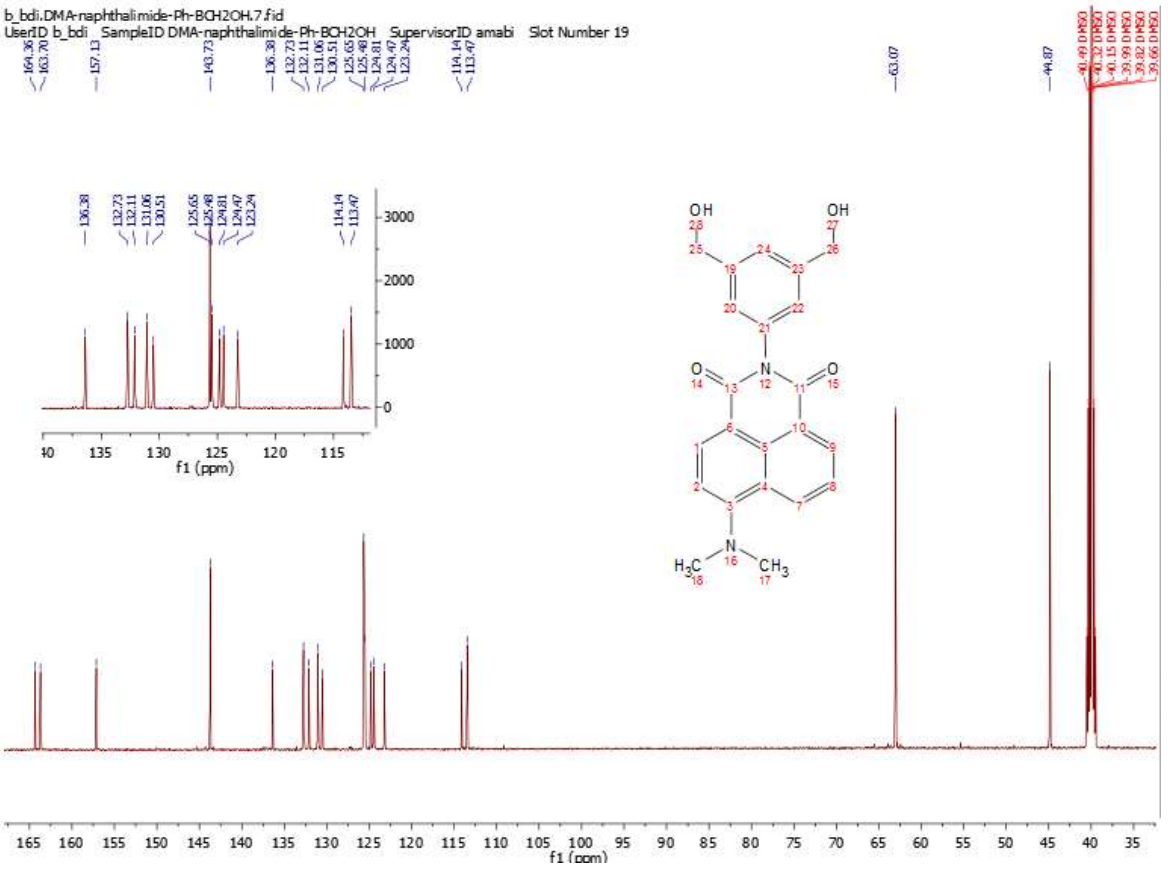

+MS, 0.6-0.8min #51-66

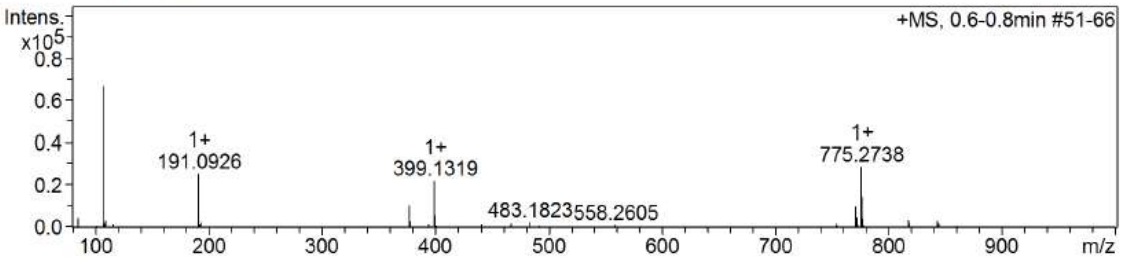

#	m/z	I %	
1	85.0590	6.7	
2	107.0415	100.0	
3	108.0436	2.8	
4	109.0376	4.7	
5	191.0926	38.2	
6	193.0888	3.8	
7	377.1494	15.9	M+H
8	378.1528	4.0	
9	399.1319	33.1	M+Na
10	400.1348	8.3	
11	483.1823	3.7	
12	753.2908	2.6	
13	770.3172	14.7	
14	771.3205	7.4	
15	775.2738	43.2	
16	776.2768	22.1	
17	777.2796	6.2	
18	817.2823	5.3	
19	818.2856	2.7	
20	843.2597	4.6	

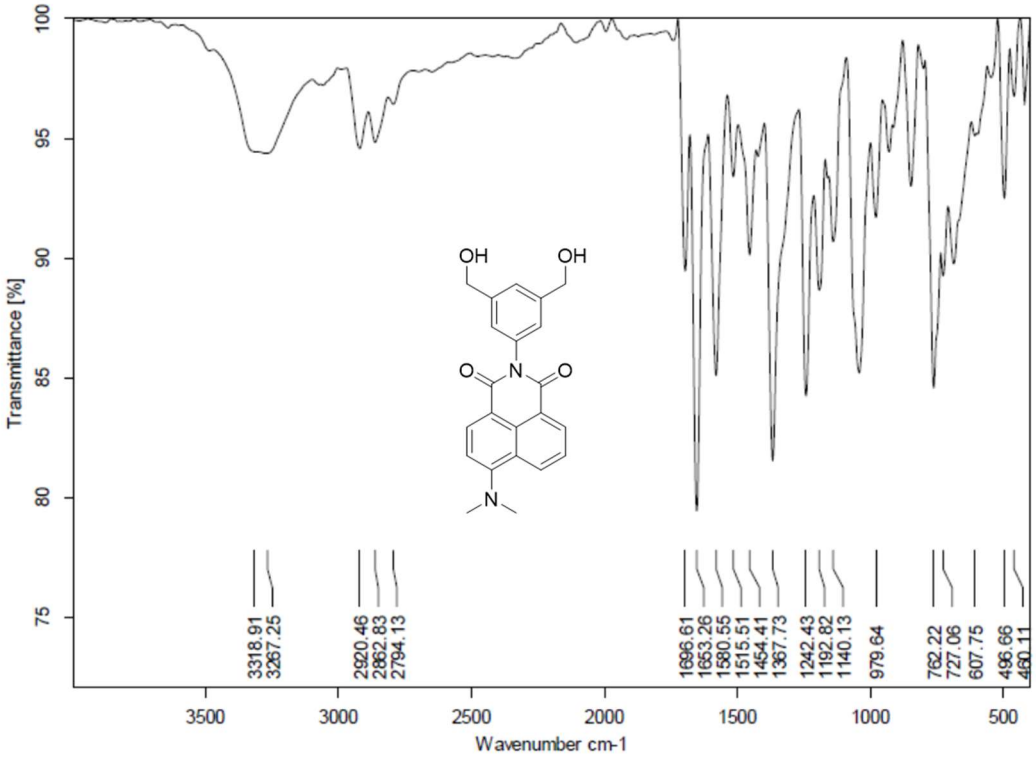
Transmittance [%]
100
95
90
85
80
75
3500
3000
2500
2000
1500
1000
500
Wavenumber cm-1
3318.91
3267.25
2920.46
2862.83
2794.13
1696.61
1653.26
1580.55
1515.51
1454.41
1367.73
1242.43
1192.82
1140.13
979.64
762.22
727.06
607.75
496.66
460.11
OH
OH
O
N
O
N

Synthesis of 2-(3,5-bis(bromomethyl)phenyl)-6-(dimethylamino)-1H-benzo[de]isoquinoline-1,3(2H)-dione (10)

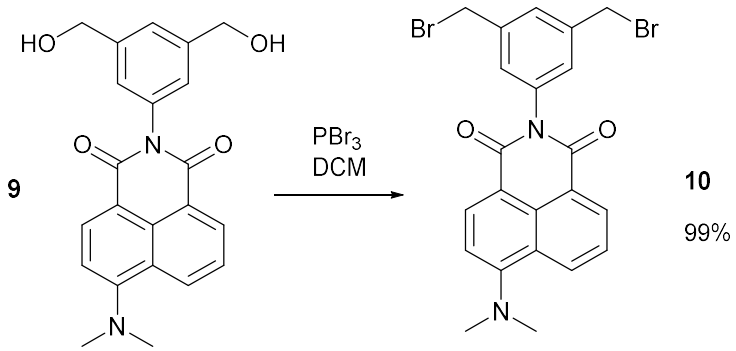

Scheme S8: Synthesis of **10**.

To a stirred solution of **9** (512 mg, 1.37 mmol) in anhydrous DCM (100 ml) at 0°C was added dropwise PBr_3 (172 µl, 1.83 mmol) (Scheme S8). The reaction was monitored by TLC analysis. The reaction was kept stirring at room temperature for two days (The starting material is not soluble in DCM, so the reaction was run for a long time). The reaction mixture was poured slowly into ice-water (50ml). The organic phase was washed with saturated $NaHCO_3$ (aq, 30ml ×2), 1M HCl (30 ml) and brine (30 ml×3), dried over anhydrous $MgSO_4$, filtered and concentrated by evaporation. The crude material was purified by column chromatography (DCM) affording the desired product **10** a light green fluorescent powder (710 mg, 99% yield). ESI-MS $[M+H]^+$ 500.9798; calculated for $C_{22}H_{19}Br_2N_2O_2$ 500.9813 $[M+H]^+$;. ^{1}H NMR (500 MHz, DMSO- d_6) δ 8.58 (dd, J = 8.6, 3.1 Hz, 1H), 8.47 (d, J = 7.2 Hz, 1H), 8.35 (d, J = 8.2 Hz, 1H), 7.80 (t, J = 7.9 Hz, 1H), 7.63 (s, 1H), 7.40 (s, 2H), 7.27 (t, J = 7.9 Hz, 1H), 4.77 (s, 4H), 3.13 (d, J = 2.8 Hz, 6H). ^{13}C NMR (126 MHz, DMSO- d_6) δ 164.30, 163.59, 157.25, 139.68, 137.09, 132.87, 132.36, 131.20, 130.35, 125.53, 124.79, 123.17, 113.50, 44.91, 33.83 ppm.

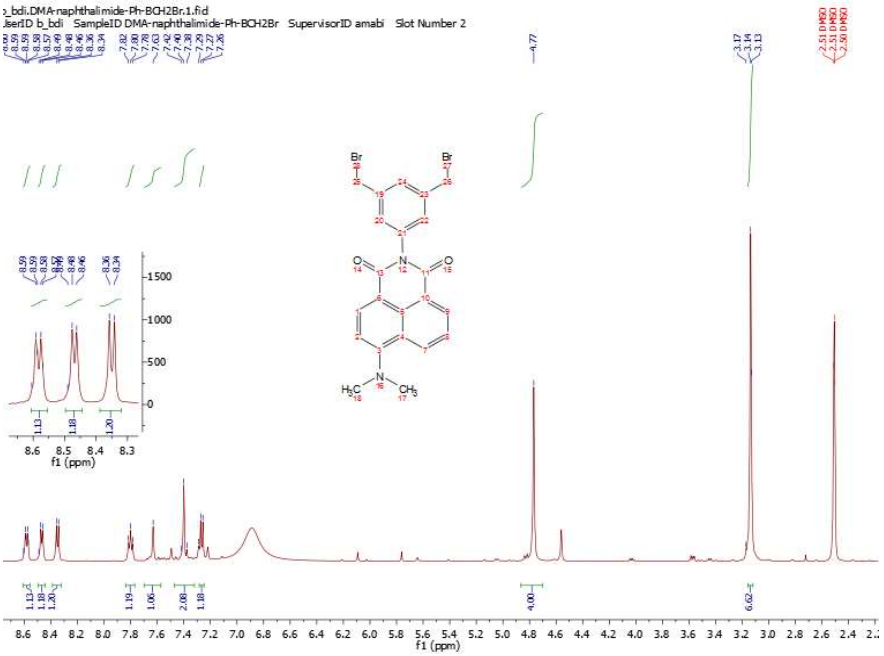
b_bdi.DMA-naphthalimide-Ph-BCH2Br.1.fid
UserID b_bdi SampleID DMA-naphthalimide-Ph-BCH2Br SupervisorID amabi Slot Number 2
f1 (ppm)

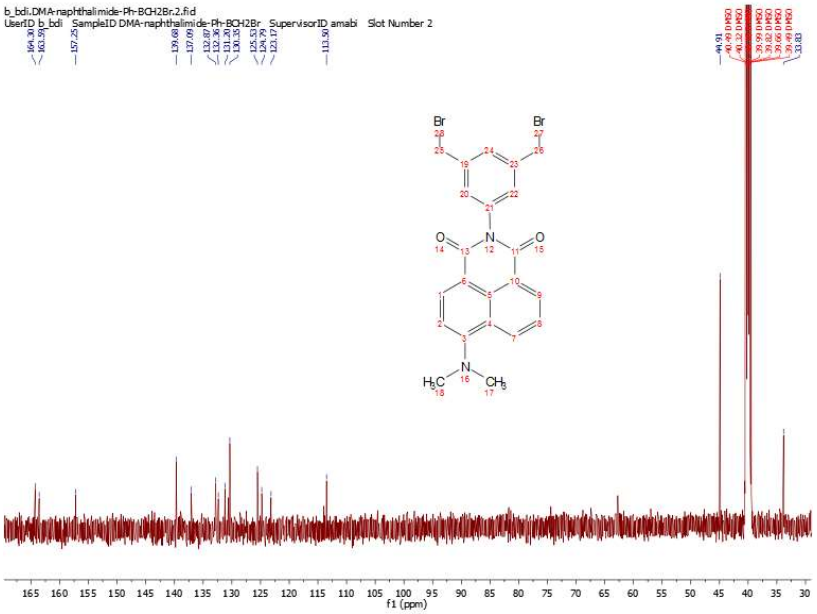
b_bdi.DMA-naphthalimide-Ph-BCH2Br.2.fid
UserID b_bdi SampleID DMA-naphthalimide-Ph-BCH2Br SupervisorID amabi Slot Number 2
f1 (ppm)

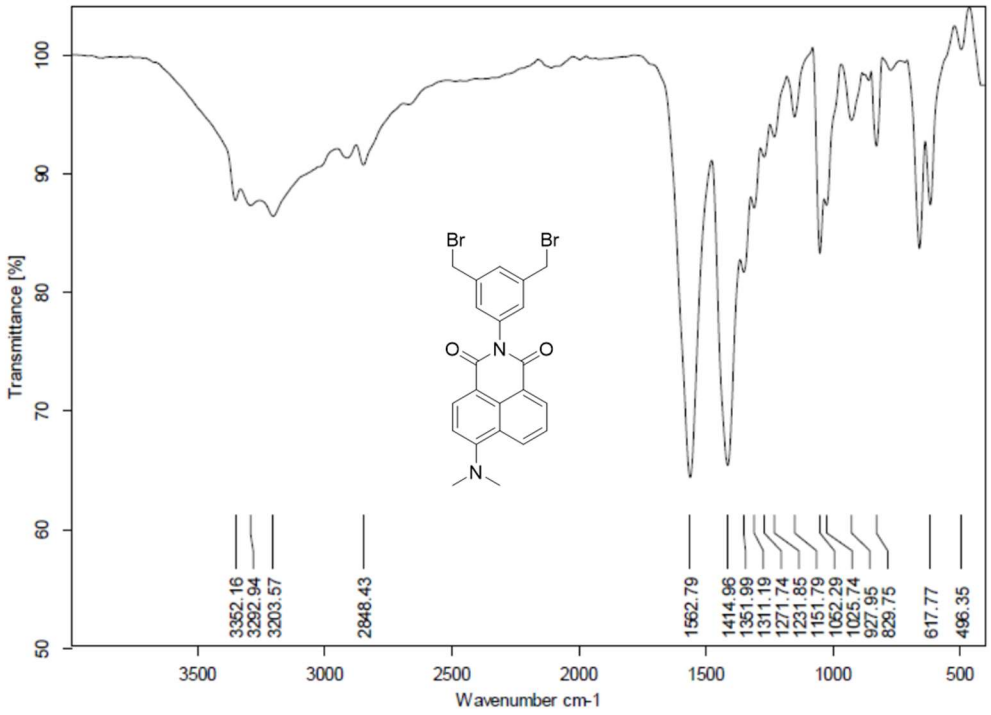

+MS, 0.6-0.8min #51-66

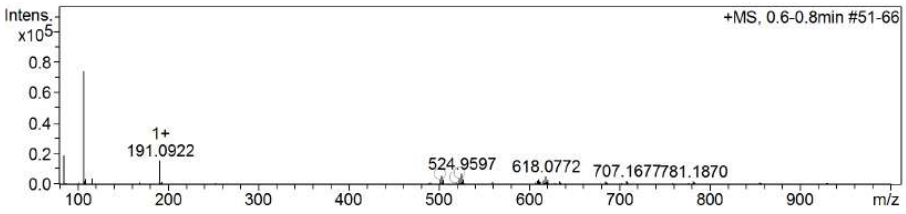

#	m/z	I %	
1	85.0586	25.9	
2	107.0412	100.0	
3	108.0432	2.9	
4	109.0374	4.9	
5	116.1075	5.2	
6	191.0922	21.0	
7	500.9798	4.0	⇦ M+H
8	502.9785	7.6	
9	504.9781	3.9	
10	522.9627	5.0	⇦ M+Na
11	524.9597	9.6	
12	526.9589	4.7	
13	609.0100	3.3	
14	610.1829	4.6	
15	611.1829	2.9	
16	616.0800	3.7	
17	618.0772	7.1	
18	620.0759	3.9	
19	633.1482	2.9	
20	707.1677	3.2	

Generate Molecular Formula Parameters

Charge	Tolerance	sigma limit	H/C Ratio	Electron Conf.	Nitrogen Rule	Chrom.BackGround	Calibration
+1	6 ppm	0.08	3 - 0	both	false	false	TRUE

Expected Formula C22 H18 Br2 N2 O2 **Adduct(s):** H, Na, NH4, C3H5N2, radical

#	meas. m/z	theo. m/z	|Err|[ppm]	Sigma	Formula	Adduct	Adduct Mass
1	500.9798	500.9808	1.90	0.0113	C22H19Br2N2O2	M+H	1.0078
1	522.9627	522.9627	0.00	0.0103	C22H18Br2N2NaO2	M+Na	22.9898
1	518.0066	518.0073	1.50	0.0513	C22H22Br2N3O2	M+H4N	18.0344

Note: Sigma fits < 0.05 indicates high probability of correct MF

Synthesis of 2.2Br

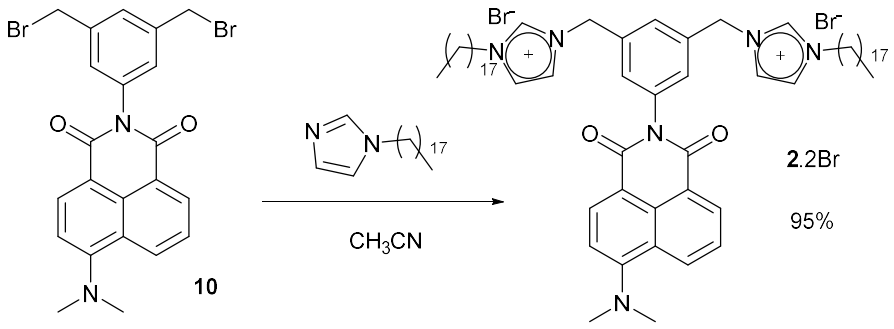

Scheme S9: Synthesis of **2**.2Br.

Compound **10** (720 mg, 1.43 mmol) and 1-octadecyl-1*H*-imidazole[7] (229 mg, 0.718 mmol) were dissolved in 50 ml of acetonitrile and the reaction mixture was kept under reflux overnight (Scheme S9). Then it was allowed to cool down to room temperature and the precipitated solid was collected by filtration and dried under vacuum. The final compound was obtained as yellow, fluorescent solid (910 mg, 95% yield). ESI-MS $[M\text{-}2Br]^{2+}$ 491.3647; calculated for $C_{64}H_{98}N_6O_2$ 491.3876 $[M\text{-}2Br]^{2+}$. ^{1}H NMR (400 MHz, DMSO- d_6) δ 9.44 (s, 2H), 8.60 (d, J = 8.6 Hz, 1H), 8.44 (d, J = 7.1 Hz, 1H), 8.32 (d, J = 8.3 Hz, 1H), 8.05–7.72 (m, 5H), 7.65 (s, 1H), 7.38 (s, 2H), 7.24 (d, J = 8.4 Hz, 1H), 5.55 (s, 4H), 4.19 (t, J = 7.1 Hz, 4H), 3.55–3.26 (m, 4H), 3.14 (s, 6H), 1.78 (h, J = 6.7 Hz, 4H), 1.30-1.10 (m, 56H), 0.85 (t, J = 6.7 Hz, 6H) ppm. ^{13}C NMR (126 MHz, $CDCl_3$) δ 164.61, 163.96, 157.48, 136.99 , 136.70, 136.06, 133.28, 131.95, 131.54, 130.65, 130.60, 130.33, 124.83, 123.01, 122.10, 113.80, 113.19, 51.81, 50.33, 44.75, 31.93, 30.16, 29.72, 29.67, 29.58, 29.44, 29.37, 29.07, 26.36, 22.70, 14.13 ppm.

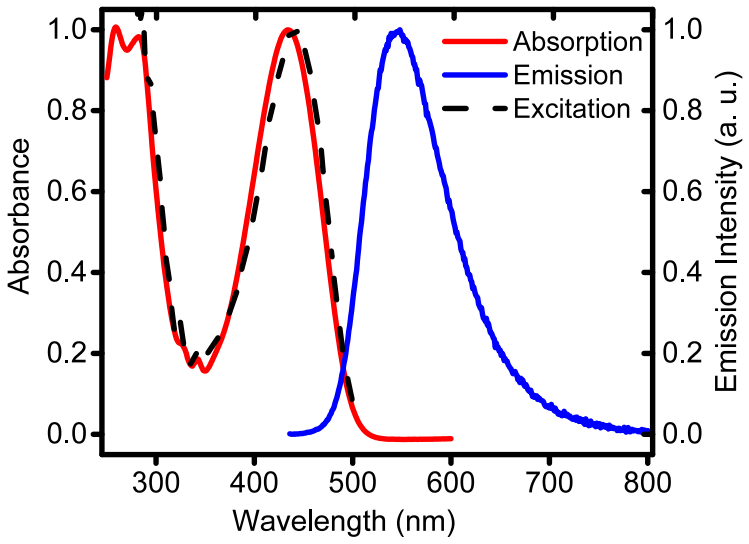

Spectra (indicated in graph) of **2**.2Br in MeOH at room temperature

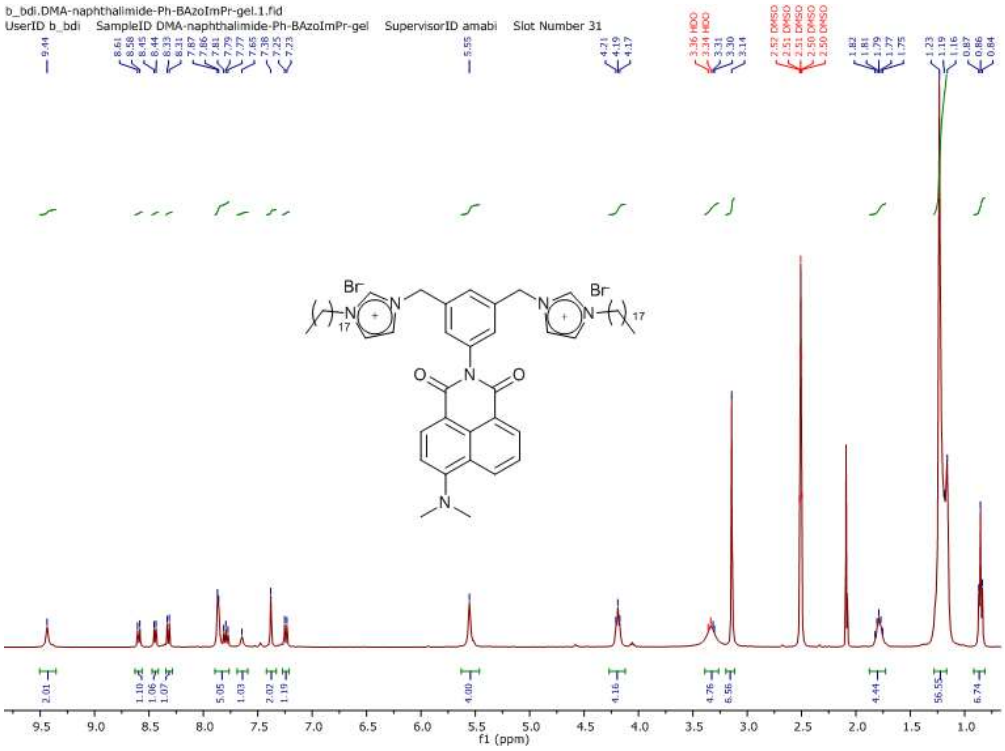

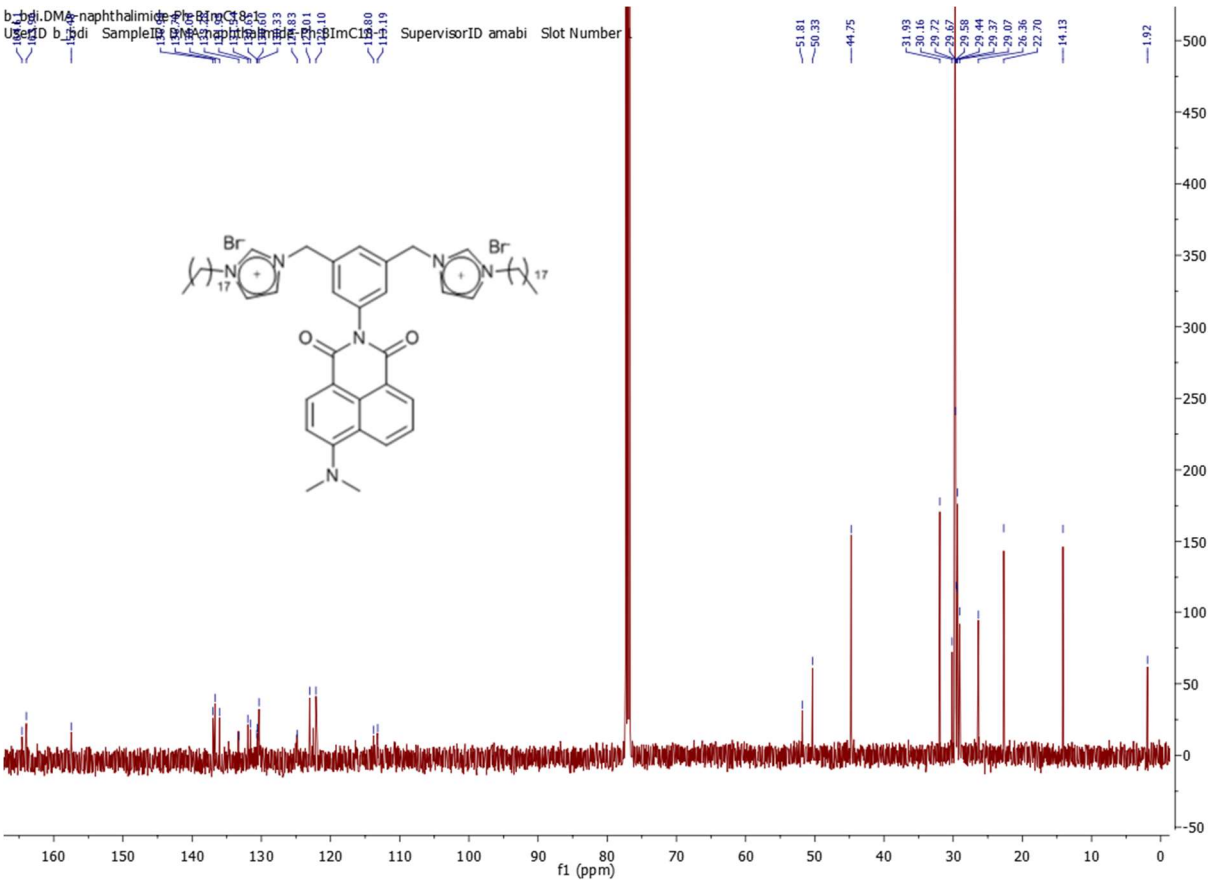

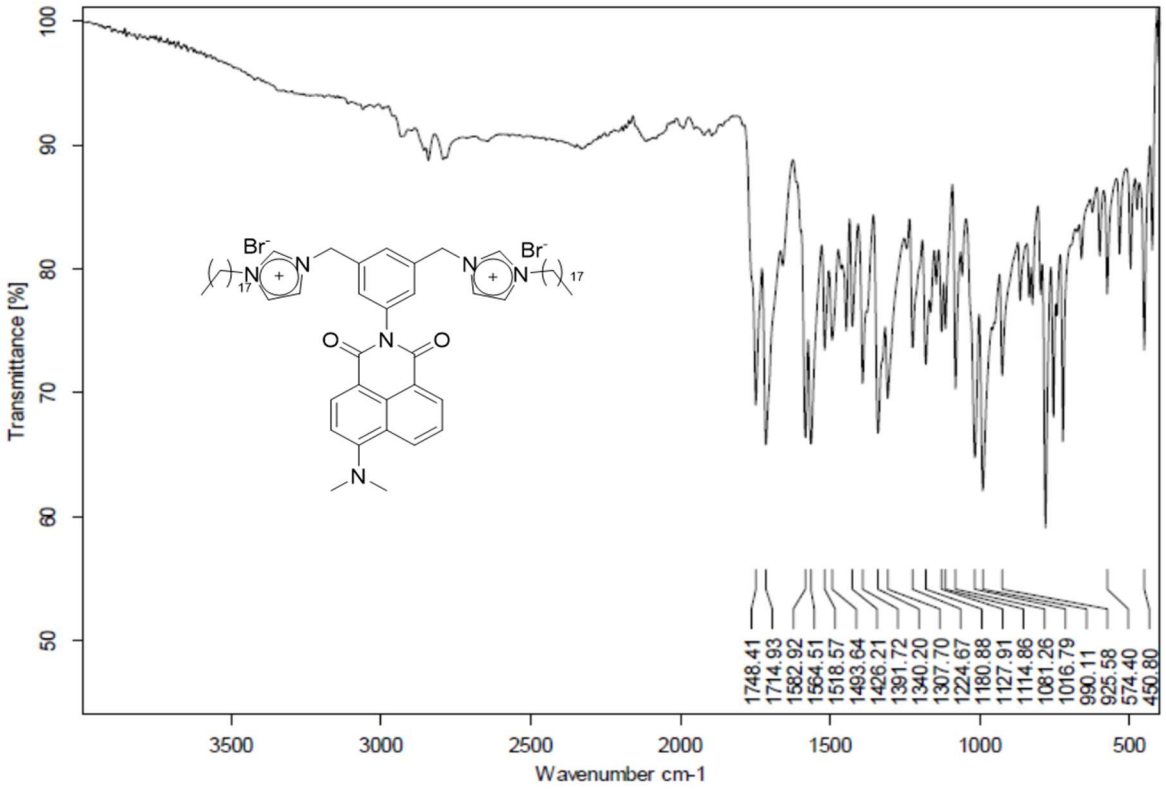

+MS, 0.7-0.9min #42-53

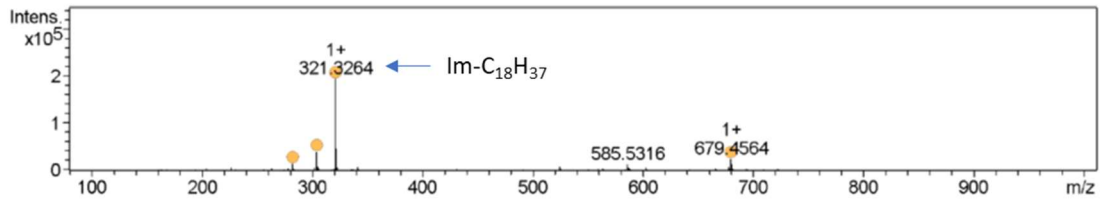

#	m/z	I %
1	226.1206	2.9
2	263.2116	2.4
3	278.2446	2.5
4	282.2792	6.9
5	302.2445	3.0
6	304.2622	20.4
7	305.2650	4.0
8	306.2747	2.6
9	321.3264	100.0
10	322.3297	24.1
11	323.3324	2.7
12	341.3507	3.6
13	524.4565	3.9
14	585.5316	6.8
15	586.5353	2.7
16	587.5462	2.5
17	602.5952	3.2
18	677.4405	3.8
19	679.4564	12.8
20	680.4592	6.4

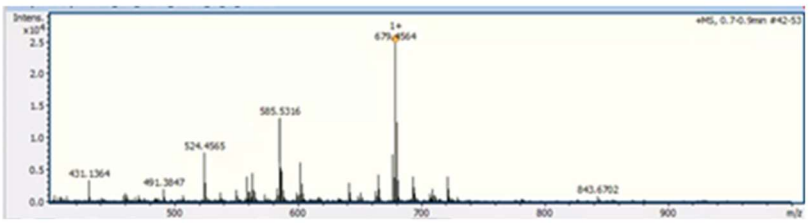

References:

33. S. Chatterjee and S. Ramakrishnan, A novel photodegradable hyperbranched polymeric photoresist. *Chem. Commun.* 49, 11041-11043 (2013).

34. K. Shomaya, D. Schmidt, M. Mahl and F. Würthner, Electron-poor bowl-shaped polycyclic aromatic dicarboximides: Synthesis, crystal structures, and optical and redox properties. *Org. Lett.* 19, 5328–5331 (2017).

35. P.A. Panchenko, A.N. Arkhipova, M.A. Zakharko, G. Jonusauskas, Y.V. Fedorov and O.A. Fedorova, Synthesis and spectral properties of fluorescent dyes based on 4-styryl-1,8-naphthalimide. *Russ. Chem. Bull.* 65, 2444–2451 (2016).

36. B.H. Rotstein, R. Mourtada, S.O. Kelley and A.K. Yudin, Solvatochromic reagents for multicomponent reactions and their utility in the development of cell-permeable macrocyclic peptide vectors. *Chem. Eur. J.* 17, 12257-12261 (2011).

37. L. Pocquet, N. Vologdin, G.F. Mangiatordi, I. Ciofini, O. Nicolotti, S. Thorimbert and M. Salmain, Supramolecular anchoring of NCN-pincer palladium complexes into a β-barrel protein host: molecular-docking and reactivity insights. *Eur. J. Inorg. Chem.* 3622- 3634 (2017).

38. X.Y. Zhu, H. Gao, W.Y. Zan, Y. Li, J.J Zhang. X.Y. Liu, X. Wei, F.C Qi, X.Y. Yao and H.X. Zhang, A rational designed thiols fluorescence probe: the positional isomer in PET. *Tetrahedron* 72, 2048-2056 (2016).

39. L. Casal-Dujat, M. Rodrigues, A. Yagüe, A.C. Calpena, D.B. Amabilino, J. González-Linares, M. Borràs, L. Pérez-García, Gemini imidazolium amphiphiles for the synthesis, stabilization, and drug delivery from gold nanoparticles, *Langmuir*, 28, 2368– 2381 (2012).

List of Micrograph Movies

Movie S1. TIRF video of an irradiation experiment performed on sample Gel@TCPP@Azo obtained in water-ethanol ratio 5:5. Real time 8.3 minutes, 20 frames per second (fps).

Movie S2. TIRF video of an irradiation experiment performed on sample Gel@TCPP@Azo obtained in water-ethanol ratio 7:3. Real time 8.3 minutes, 20 fps.

Movie S3. TIRF video of the central irradiation experiment performed on sample Gel@TCPP@Azo obtained in water-ethanol ratio 5:5. Real time 8.3 minutes, 20 fps.

Movie S4. TIRF video of the central irradiation experiment performed on sample Gel@TCPP@Azo obtained in water-ethanol ratio 6:4. Real time 8.3 minutes, 20 fps.

Movie S5. Video of an irradiation experiment performed on sample Gel@TCPP@Azo 5:5 using light at 405 nm. Real time 8.3 minutes, 20 fps.

Movie S6. Video of the irradiation experiment performed on sample Gel@TCPP@Azo 5:5 using light at 488 nm. Real time 5 minutes, 10 fps.

Movie S7. Video of the irradiation experiment performed on sample Gel@TCPP@Azo 5:5 using light at 561 nm. Real time 8.3 minutes, 20 fps.

Movie S8. Video of the irradiation experiment performed on sample Gel@TCPP@Azo 5:5 using light at 642 nm. Real time 8.2 minutes, 20 fps.

Movie S9. SRRF video of the irradiation experiment performed on sample Gel@TCPP@Azo obtained in water-ethanol ratio 7:3. Real time 1.7 minutes, 10 fps.

Movie S10. TIRF video of the irradiation experiment performed on sample Gel@TCPP obtained in water-ethanol ratio 5:5. Real time 8.3 minutes, 10 fps.

Movie S11. TIRF video of the irradiation experiment performed on sample Gel@TCPP obtained in water-ethanol ratio 7:3. Real time 1.7 minutes, 10 fps.

Movie S12. TIRF video of the irradiation experiment performed on sample Gel@TCPP@AzoH (prepared from the sodium salt of TCPP but with no additional base to deprotonate the Azo compound) obtained in water-ethanol ratio 5:5. Real time 8.3 minutes, 10 fps.

Movie S13. TIRF video of an irradiation experiment performed on sample Gel@TCPP@Azo in 5:5 water:ethanol with a starting *trans*:*cis* ratio of approximately 35:65 (prepared by irradiating the ethanol stock solution containing the Azo used for the preparation of the gel at 365 nm). Real time 50 seconds, 5 fps.

Movie S14. TIRF video of the irradiation experiment performed on sample Gel@TCPP@Biph obtained in water-ethanol ratio 7:3. Real time 8.3 minutes, 20 fps.

Movie S15. TIRF video of an irradiation experiment performed on sample Gel@TCPP@Azo in 5:5 water:ethanol with a starting *trans*:*cis* ratio of approximately 35:65 (prepared by irradiating the ethanol stock solution containing the Azo used for the preparation of the gel at 365 nm). Real time 120 seconds, 10 fps.

Movie S16. TIRF video of an irradiation experiment performed on sample Gel@TCPP@Azo obtained in water-ethanol ratio 5:5. Real time 8.3 minutes, 20 fps.

Movie S17. TIRF video of an irradiation experiment performed on sample Gel@TCPP@Azo obtained in water-ethanol ratio 7:3. Real time 8.3 minutes, 10 fps.